Investigating the impact of Caspase-8 and Connexin-43 on metastasis and tumour aggressiveness in human ovarian cancer using an orthotopic mouse model

Inaugural Dissertation
submitted to the
Faculty of Veterinary Medicine
in partial fulfilment of the requirements
for the PhD-Degree
of the Faculties of Veterinary Medicine and Medicine
of the Justus Liebig University Giessen

by
Seyed Mohsen Aberoumandi
of
(Hamedan,Iran)

Giessen (2024)

From the

Institute for Veterinary Anatomy, Histology and Embryology

Director / Chairman

Prof. Dr. Dr. Stefan Arnhold

First Reviewer/ Supervisor: **Prof. Dr. Christine Wrenzycki**

Second Reviewer: **Prof. Dr. Jennifer Schön**

Second Supervisor and additional Committee Member: **PD Dr. Mourad Sanhaji**

Vice-Chair/ Co-supervisor: **Prof. Dr. Rajkumar Savai**

Chair: **Prof. Dr. Norbert Weissmann**

Date of Doctoral Defense: **29 October 2025**

Erklärung

Ich erkläre: Ich habe die vorgelegte Thesis selbständig, ohne unerlaubte fremde Hilfe und nur mit den Hilfen angefertigt, die ich in der Thesis angegeben habe. Alle Textstellen, die wörtlich oder sinngemäß aus veröffentlichten oder nicht veröffentlichten Schriften entnommen sind, und alle Angaben, die auf mündlichen Auskünften beruhen, sind als solche kenntlich gemacht. Bei den von mir durchgeführten und in der Thesis erwähnten Untersuchungen habe ich die Grundsätze guter wissenschaftlicher Praxis, wie sie in der ‚Satzung der Justus Liebig Universität Gießen zur Sicherung guter wissenschaftlicher Praxis' niedergelegt sind, eingehalten.

List of Abbreviations

Abbreviation	Definition
2D	2-Dimensional
3D	3-Dimensional
53BP1	P53-Binding Protein 1
ABD buffer	Antibody Dilution Buffer
ADGRG1	Adhesion G Protein-Coupled Receptor G1
AJCC	American Joint Committee on Cancer
Apaf-1	Apoptotic Protease Activating Factor-1
APTES	3-aminopropyltriethoxysilane
ASC	American Cancer Society
ATP	Adenosine Triphosphate
BAK	Bcl-2 Antagonist or Killer
BAX	Bcl-2 Associated X Protein
BCA	Bi-Cinchonine
BCL-2	B-Cell Lymphoma-2
BLI	Bioluminescence imaging
BID	BH3-Interacting Domain Death Agonist
tBID	Truncated BH3-Interacting Domain Death Agonist
BIK	Bcl-2 Interacting Killer
BRCA	Breast Cancer
BRCA1/2	Breast Cancer Gene 1/2
BSA	Bovine Serum Albumin
BSO	Bilateral Salpingo-Oophorectomy
CA125	Cancer Antigen 125
CDH4	Cadherin 4
CDH15	Cadherin 15
CARD	Caspase Recruitment Domain
CAS9	CRISPR-Associated Protein 9
CASP8	Caspase-8
CDC42BPA	CDC42 binding protein kinase alpha
CO2	Carbon Dioxide
CRISPR	Clustered Regularly Interspaced Short Palindromic Repeats
CX43	Connexin-43
DD	Death Domain
DDT	4,4′-Dichlorodiphenyl Richloroethane
DED	Death Effector Domain
DEGs	Differentially Expressed Genes
DISC	Death-Inducing Signalling Complex
DMEM	Dulbecco’s Minimum Essential Medium
DMSO	Dimethyl Sulfoxide
DNA	Deoxyribonucleic Acid
DR4/DR5	Death Receptor 4 / Death Receptor 5
DSBs	DNA Double-Strand Breaks
ECL	Enhanced Chemiluminescence
EDTA	Ethylene Diamine Tetraacetic Acid
EOC	Epithelial Ovarian Cancer
EMT	Epithelial-to-Mesenchymal Transition

ERK1/2	Extracellular Signal-Regulated Kinase 1/2
FADD	Fas-Associated Death Domain
FasR	Fas Receptor (APO-1 / CD95)
FFPE	Formalin's-fixed paraffin embedded
FIGO	International Federation of Gynaecology and Obstetrics
GC	Guanine and Cytosine
GFRA1	GDNF Family Receptor Alpha 1
GEO	Gene Expression Omnibus
GnRH	Gonadotropin-Releasing Hormone
GO	Gene Ontology
GJA1	Gap junction Alpha 1
GJIC	Gap junction intercellular communication
H&E	Haematoxylins and Eosin
HE4	Human Epididymis Protein 4
HGSOC	High-Grade Serous Ovarian Cancer
HISAT2	Hierarchical indexing for spliced alignment of transcripts
IHC	Immunohistochemical Analysis
ITGB8	Integrin Subunit Beta 8
KO	Knock Out
IVIS	In Vivo Imaging System
IP	Intraperitoneal
LAMB3	Laminin Subunit Beta 3
LGSOC	Low-Grade Serous Ovarian Cancer
Luc	Luciferase
mAb	Monoclonal Antibody
MMP9	Matrix Metallopeptidase 9
MOMP	Mitochondrial Outer Membrane Permeabilisation
mTOR	Mammalian Target of Rapamycin
NAC	Neoadjuvant Chemotherapy
NCKAP1L	NCK associated protein 1 like
OC	Ovarian Cancer
OVCAR	Ovarian Carcinoma
P/S	Penicillin–Streptomycin
PARP	Poly (ADP-Ribose) Polymerase
PD-1	Programmed Cell Death Protein 1
PD-L1	Programmed Death-Ligand 1
PFS	Progression-Free Survival
PlGF-1/2	Placental Growth Factor 1 and 2
RLU	Relative Luminescence Units
RT	Room Temperature
SDS-PAGE	Sodium Dodecyl Sulfate–Polyacrylamide Gel Electrophoresis
siRNA	Small Interfering RNA
sgRNA	Small guided RNA
S1PR1	Sphingosine-1-Phosphate Receptor 1
SOC	Serous Ovarian Cancer
TBS	Tris-Buffer Solution
TEMED	Tetramethyl Ethylenediamine
TME	Tumour Microenvironment

TNF-R	Tumour Necrosis Factor Receptor
TNFα	Tumour Necrosis Factor Alpha
TNM	Tumour, Node, Metastasis Classification
TP53	Tumour Protein P53
TPA	12-O-Tetradecanoyl Phorbol-13-Acetate
TRADD	TNF-R Associated Death Domain
TRAIL-R	TNF-Related Apoptosis-Inducing Ligand Receptor
VEGF	Vascular Endothelial Growth Factor
VEGFR	Vascular Endothelial Growth Factor Receptor
WT	Wild Type

Abstract in English

Ovarian carcinoma is the leading cause of mortality among gynaecological malignancies, primarily due to late-stage diagnosis and the presence of metastatic disease. As most patients present with advanced tumours, an improved understanding of the molecular mechanisms driving tumour progression, metastasis, and therapeutic resistance is required for the development of targeted therapies. Caspase-8 (CASP8), a key regulator of apoptosis, and Connexin-43 (CX43), a gap-junction protein implicated in cell-cell communication and metastasis, have emerged as potential therapeutic targets in ovarian cancer. This PhD project aimed to investigate the functional roles of CASP8 and CX43 in ovarian cancer progression, metastasis, and response to chemotherapy using clinically relevant in vivo and in vitro models. High-grade serous ovarian cancer cell lines (OVCAR8 and OVCAR3) were engineered using CRISPR-Cas9 to generate CASP8 and/or CX43 knockout (KO) models for analysis in an orthotopic mouse model and complementary in vitro assays. In vivo, luciferase-labelled OVCAR8 KO:CASP8 cells exhibited significantly enhanced tumour growth and widespread organ dissemination compared with OVCAR8 WT, highlighting a tumour-suppressive role for CASP8. In vitro, CASP8-deficient cells displayed increased resistance to carboplatin and paclitaxel, with reduced chemotherapy-induced apoptosis relative to WT cells. Immunodetection studies revealed increased CX43 expression following CASP8 loss, suggesting functional crosstalk between these proteins. Functional assays demonstrated that CASP8 depletion enhanced invasion in OVCAR3 cells, while co-depletion of CASP8 and CX43 attenuated this phenotype; however, combined KO increased migratory capacity. Overall, these findings reveal a complex, context-dependent interaction between CASP8 and CX43 in regulating ovarian cancer invasion, migration, and therapeutic response, supporting their potential relevance as targets for improved treatment strategies.

Zusammenfassung auf Deutsch

Das Ovarialkarzinom ist die häufigste Todesursache unter den gynäkologischen Malignomen, was in erster Linie auf die späte Diagnosestellung und das Vorliegen metastatischer Erkrankungen zurückzuführen ist. Da sich die Mehrzahl der Patientinnen mit fortgeschrittenen Tumoren vorstellt, ist ein verbessertes Verständnis der molekularen Mechanismen, die das Tumorwachstum, die Metastasierung und die therapeutische Resistenz antreiben, für die Entwicklung zielgerichteter Therapien erforderlich. Caspase-8 (CASP8), ein zentraler Regulator der Apoptose, und Connexin-43 (CX43), ein Gap-Junction-Protein, das an der Zell-Zell-Kommunikation und Metastasierung beteiligt ist, haben sich als potenzielle therapeutische Zielstrukturen beim Ovarialkarzinom herauskristallisiert. Ziel dieser Promotionsarbeit war es, die funktionellen Rollen von CASP8 und CX43 bei der Progression des Ovarialkarzinoms, der Metastasierung und der Chemotherapieantwort unter Verwendung klinisch relevanter in-vivo- und in-vitro-Modelle zu untersuchen. Hochgradig seröse Ovarialkarzinom-Zelllinien (OVCAR8 und OVCAR3) wurden mittels CRISPR-Cas9-Technologie genetisch modifiziert, um CASP8- und/oder CX43-Knockout-(KO-)Modelle für Analysen in einem orthotopen Mausmodell sowie ergänzenden in-vitro-Assays zu erzeugen. In vivo zeigten luciferase-markierte OVCAR8 KO:CASP8Zellen im Vergleich zu OVCAR8 WT ein signifikant verstärktes Tumorwachstum sowie eine ausgeprägte multiorgane Dissemination, was auf eine tumorsuppressive Rolle von CASP8 hindeutet. In vitro wiesen CASP8-defiziente Zellen eine erhöhte Resistenz gegenüber Carboplatin und Paclitaxel auf, begleitet von einer verminderten chemotherapieinduzierten Apoptose im Vergleich zu WT-Zellen. Immunodetektionsstudien zeigten eine erhöhte CX43-Expression nach Verlust von CASP8, was auf eine funktionelle Wechselwirkung zwischen diesen Proteinen hin. Funktionelle Assays ergaben, dass die Depletion von CASP8 die Invasivität OVCAR3-Zellen erhöhte, während die gleichzeitige Depletion von CASP8 und CX43 diesen Phänotyp abschwächte; hingegen führte der kombinierte Knockout zu einer gesteigerten Migrationsfähigkeit. Zusammenfassend zeigen diese Ergebnisse eine komplexe, kontextabhängige Interaktion zwischen CASP8 und CX43 bei der Regulation von Invasion, Migration und Therapieansprechen des Ovarialkarzinoms und unterstreichen deren potenzielle Bedeutung als Zielstrukturen für verbesserte therapeutische Strategien.

Table of Contents

1. Introduction

1.1 Overview of Ovarian Cancer

Ovarian cancer (OC) is the most lethal cancer among women, ranking fourth among all fatal diseases in women, this underscores the urgent need for curative treatment options (Chandra *et al.*, 2019). The lack of effective diagnostic approaches often leads to delayed detection, with most patients being diagnosed at an advanced stage. Advanced ovarian cancer is characterised by the dissemination of disease throughout the abdomen and beyond. Survival rates vary considerably between countries, with the global 5-year survival rate for advanced ovarian cancer estimated at approximately 50% (DeSantis *et al.*, 2019).

1.2 Staging of Ovarian Cancer

Ovarian cancer is a highly heterogeneous disease, necessitating precise staging and grading of the tumour to enable selection of the most appropriate treatment for each patient (Garrido *et al.*, 2021). The staging of ovarian cancer is based on standardised systems developed by the International Federation of Gynecology and Obstetrics (FIGO), the American Joint Committee on Cancer (AJCC), and the tumour, node, and metastasis (TNM) classification, which together provide essential information for determining prognosis and guiding therapeutic strategies. The TNM system takes into account anatomical location and pathological characteristics, where T stands for tumour size and local growth (T0–T4), N denotes lymph node metastases (N0–N3), and M describes distant metastases (M0–M1). The FIGO considers metastasis to lymph nodes and extra-abdominal organs as metastatic disease, although it also classifies ovarian, fallopian tube and peritoneal cancer as primary tumour sites. Depending on the tumour size, location and metastases, the FIGO classifies ovarian cancer in stages I to IV (Table 1), which correspond to the TNM classification (Telloni, 2017; Berek *et al.*, 2021).

Table 1: Staging of ovarian cancer using the AJCC and FIGO system.

Stage	Description
I	The cancer is limited to one (IA) or both (IB) ovaries. The cancer is present in one or both ovaries and is present on the outer surface of at least one of the ovaries. Alternatively, the tumour may have ruptured (IC).
II	A tumour may involve one or both ovaries (outside) or the uterus or fallopian tubes (classified as IIA) with a pelvic extension (IIB).
III	The cancer is found in one or both ovaries and has spread to abdominal organs and/or lymph nodes, where microscopic tumour deposits may be observed (IIIA) or small (<2cm) deposits of tumour on abdominal peritoneal surfaces (IIIB). Cancer has spread to pelvic or retroperitoneal abdominal lymph nodes, where deposits may be visible and larger (>2 cm) within the abdomen (IIIC).
IV	The cancer has metastasised to organs outside of the abdominal cavity, including the lungs, liver and others.

1.3 Histopathologic Classification of Ovarian Cancer

It is estimated that nearly 90% of cases of ovarian cancer have an epithelial origin (Wang *et al.*, 2022). Four histological subgroups of epithelial ovarian cancer (EOC) have been identified, namely serous, endometrioid, mucinous and clear cell carcinomas. Serous ovarian cancer (SOC), which is the most prevalent subgroup, accounting for about 70% of epithelial ovarian cancers, is distinguished into high-grade (HGSOC) and low-grade (LGSOC) forms. The majority of cases are high-grade, predominantly affecting elderly women, and have a high mortality rate. Genetic changes are frequent in HGSOC, primarily manifested as breast cancer (BRCA) and tumour protein P53 (TP53) deletion or mutation. Only 2% of patients meet the criteria for LGSOC. These are often younger women with a 50% chance of survival after 10–

12 years (Wang *et al.*, 2022). Mucinous and clear cell carcinomas also tend to present at a younger age. The other areas where the ovarian cancer is developed are the germ cells and stroma (Garrido *et al.*, 2021).

Several factors make ovarian cancer a difficult disease to treat effectively. The complexity of these cancers comes from the microenvironment, which is affected by changes in genetic factors. The degree of complexity also varies according to changes in epigenetic factors. Understanding the tumour microenvironment (TME) is key to diagnosis, treatment selection, and patient survival. The microenvironment varies for different types of ovarian carcinomas, with changes in gene expression leading to different tumour markers. The tumour markers play a crucial role in the development of targeted therapies (Bast, Hennessy and Mills, 2009).

1.4 Risk Factors for Ovarian Cancer

A large cohort study demonstrated that approximately 20% of women exhibited an inherited genetic mutation associated with a higher risk of developing ovarian cancer. Women with a strong family history of ovarian cancer or a BRCA mutation should be considered at a higher risk of ovarian cancer (Alsop *et al.*, 2012).
The risk of ovarian cancer in women with breast cancer type 1 (BRCA1) mutation is increased by 63%, and in breast cancer type 2 (BRCA2) mutations by 27%, respectively. Furthermore, age (over 50 years) is a significant factor influencing ovarian cancer risk, as are vaginal infections and endometriosis which play important roles in the development of ovarian cancer (Alsop *et al.*, 2012; Walker, Jacobson and Sobel, 2019).

1.5 Diagnosis of Ovarian Cancer

The combination of non-specific early symptoms, the anatomical location of the ovaries, the lack of effective screening methods and the biological behaviour of ovarian cancer contribute to the frequent diagnosis of the disease at an advanced stage. Tumour markers are significant in the development of targeted therapies. Biomarkers are categorised into four distinct groups: diagnostic, prognostic, predictive

and response. The most commonly used biomarkers are Cancer Antigen 125 (CA125), Human Epididymis Protein 4 (HE4), and mesothelin, which are often used in combination (Bandiera *et al.*, 2013).

1.6 Current Therapies for Epithelial Ovarian Cancer

The treatment of ovarian cancer typically involves a combination of surgical, chemotherapeutic, targeted and in some cases, radiotherapeutic interventions. The specific treatment plan is determined by the stage and type of ovarian cancer, as well as the patient's overall health and preferences.

1.6.1 Debulking Surgeries

The surgical approach may include:

- Total Hysterectomy: Removal of the uterus.
- Bilateral Salpingo-Oophorectomy (BSO): Removal of both ovaries and fallopian tubes.
- Omentectomy: Removal of the omentum, a fatty layer covering the abdominal organs, where ovarian cancer often spreads.
- Lymph Node Dissection: Removal of lymph nodes in the pelvic and para-aortic areas to check for cancer spread.
- Cytoreductive Surgery: For advanced stages, surgery aims to remove as much of the tumour mass as possible and sometimes the surgeon will need to remove a piece of colon to debulk the cancer properly (Falzone *et al.*, 2021).

1.6.2 First-Line Chemotherapy

Following surgery, patients are typically administered drug therapy. The standard treatment comprises a platinum compound, typically carboplatin and a taxane, usually paclitaxel. The combination of carboplatin and paclitaxel demonstrated comparable efficacy to cisplatin and paclitaxel, although with significantly reduced toxicity (Kampan *et al.*, 2015; Garrido *et al.*, 2021). Carboplatin functions as an alkylating agent, resulting in the cross-linking of DNA strands. This process inhibits DNA, RNA, and protein synthesis, as well as the triggering of programmed cell death, predominantly in rapidly dividing cells. Paclitaxel stabilises cellular microtubules and inhibits the

formation of the mitotic spindle, thereby inducing apoptotic cell death through a variety of apoptotic mechanisms in multiple cell types (Kampan *et al.*, 2015; Jaunky *et al.*, 2021). The initial treatment regimen comprises the administration of intravenous platinum/taxane every three weeks for a total of six cycles. The same compounds are typically administered to patients with stage III/IV ovarian cancer undergoing neoadjuvant chemotherapy (NAC) protocols for three cycles, followed by debulking surgery and a further three cycles of platinum/taxane (Ledermann, 2018). The intravenous systemic route of administration is the preferred option, although several studies have also proposed intraperitoneal administration. However, in terms of progression-free survival (PFS), this did not improve results (Chambers *et al.*, 2019).

The stage and histological subtype of EOC are crucial factors in determining the most appropriate treatment for individual patients. The efficacy of therapeutic interventions is significantly reduced when the disease is diagnosed at an advanced stage (Figure 1). The American Cancer Society's (ASC) guideline development recommends optimal debulking as the initial treatment for stage I invasive epithelial ovarian cancers. Adjuvant chemotherapy is recommended based on grading. Stage IA and IB do not require further treatment. Stage II cancers are treated with debulking, carboplatin, and paclitaxel. Stage III may require targeted therapy. Stage IV cancers spread to distant organs and require surgery, first-line therapy and targeted therapy (Figure 1, Oronsky *et al.*, 2017).

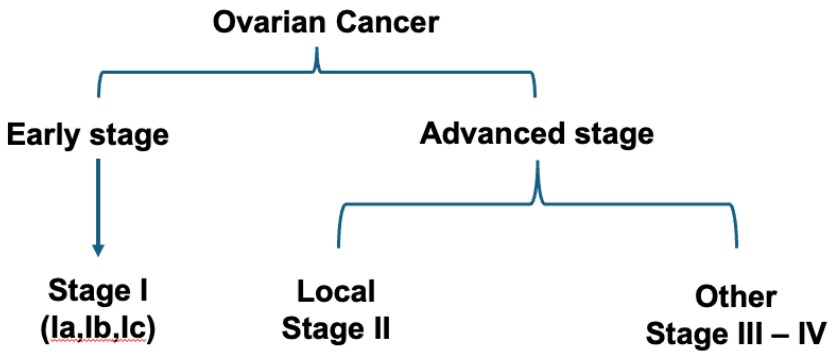

Figure 1: Simplified staging of ovarian cancer (adapted from Oronsky *et al.*, 2017).

Approximately 80% of patients respond to the initial therapy. However, almost all of these patients experience local or distant tumour recurrence within the next 15 to 18 months (Oronsky *et al.*, 2017). In such cases, a second surgery may be required, followed by chemotherapy, which is chosen depending on the previous treatment, response to it and how fast the tumour recurred. A high recurrence rate is frequently associated with a low response to the first-line therapy, which is linked to platinum resistance. This accounts for approximately 15% of cases. Despite responding to the therapy, these patients relapse within the next six months. There are also tumours that progress during therapy or relapse within one month. These are considered to be platinum refractory. Patients who relapse more than six months after initial therapy are classified as platinum-sensitive (Kim *et al.*, 2012).

In conclusion, the current therapeutic approaches are inadequate for the treatment of advanced ovarian cancer. A significant proportion of patients (80%) experience tumour recurrence, while 90% exhibit chemoresistance or high toxicity. Consequently, there is a pressing need to develop novel therapeutic strategies with the aim of improving overall survival rates.

1.6.3 Targeted Drug Therapy for Ovarian Cancer

The improved prognosis for epithelial ovarian cancer is largely attributed to the introduction of new biological agents. Enhanced understanding of ovarian cancer biology has led to identify multiple molecular targets, including growth factor receptors, signal transduction pathways, cell cycle regulators and angiogenic mechanisms. However, this section will now cover two primary molecular targeted agents used in treating ovarian cancer: the anti-VEGF antibody bevacizumab (Bevacizumab gamma, Avastin) and the PARP inhibitor olaparib.

1.6.4 PARP Inhibitors

The poly (ADP-ribose) polymerases (PARPs) constitute a vast family of multifunctional enzymes. PARP-1, the most prevalent isoform, is essential for the repair of DNA single-strand breaks by base excision repair. The suppression of PARPs results in the accumulation of DNA single-strand breaks, which subsequently give rise to DNA double-strand breaks at replication forks. In normal cells, double-strand breaks are

repaired by the error-free homologous recombination double-stranded DNA repair pathway, which includes critical components such as the tumour-suppressor proteins BRCA1 and BRCA2. In the absence of either BRCA1 or BRCA2, these lesions are unable to be repaired efficiently, resulting in cell cycle arrest and cell death. Nevertheless, an alternative to non-homologous end-joining exists for the repair of double-strand breaks (Itamochi, 2010; Kim *et al.*, 2012).

Olaparib (Lynparza), Niraparib (Zejula), Rucaparib (Rubraca) and Talazoparib (Talzenna) are poly (ADP-ribose) polymerase (PARP) inhibitors that are currently in use. These drugs have been approved for the treatment of epithelial ovarian cancer (EOC) in patients with mutations of BRCA1/2 or other genes, whose mutation/inactivation leads to homologous recombination deficiency (Kim *et al.*, 2012). The revelation of the epigenetic mechanism of the BRCA1/2 germline mutation, as well as its relationship with ovarian cancer in 5-10% of cases, gave rise to the therapeutic idea of synthetic lethality. In fact, in patients with a BRCA mutation, PARP inhibition causes unrepaired DNA single- and double-strand breaks, which eventually lead to cell death (Fong *et al.*, 2009).

1.6.5 Bevacizumab (Bevacizumab gamma, Avastin)

Angiogenesis, defined as the formation of new blood vessels from pre-existing vasculature, is a fundamental process that underpins tumour growth, invasion, and metastasis. The orchestration of angiogenesis is regulated by several growth factor receptor-mediated signalling pathways (Itamochi, 2010). Among these, the vascular endothelial growth factor (VEGF) family and their corresponding receptors (VEGFRs) play a central role in mediating tumour angiogenesis, constituting a pivotal signalling axis in this context. The mammalian VEGF family comprises seven structurally related glycoproteins: VEGF-A (commonly referred to as VEGF), VEGF-B, VEGF-C, VEGF-D, VEGF-E, and placental growth factors 1 and 2 (PlGF-1 and PlGF-2). Collectively, these factors coordinate the complex processes involved in neovascularisation, thereby facilitating tumour progression and dissemination (Hicklin and Ellis, 2005).

It is often observed that overexpression of VEGF is present in a variety of solid tumours, and that this is associated with an increased risk of metastatic disease and a poor prognosis in a number of different malignancies, including ovarian cancer

(Kerbel, 2008). Furthermore, it has recently been discovered that coexpression of VEGF and VEGF receptor 2 (VEGFR2) is present in both ovarian cancer cells and ovarian tumour tissues (Guo *et al.*, 2010). Consequently, the VEGF signalling pathways are regarded as promising therapeutic targets for the treatment of ovarian cancer patients.

Two main strategies are used to inhibit the VEGF signalling pathway: blocking the VEGF ligand itself with monoclonal antibodies or soluble receptor constructs and targeting the VEGFR using tyrosine kinase inhibitors or receptor-specific antibodies. Among these, bevacizumab (Avastin), a monoclonal antibody that binds directly to the VEGF ligand, is the most widely studied and used in clinical practice (Raspollini *et al.*, 2005).

In conclusion, molecular biology has led to the creation of innovative targeted therapies for ovarian cancer. Among these, angiogenesis inhibitors show the most promise, especially as maintenance therapy alongside standard chemotherapy. However, more research is needed on how antiangiogenic drugs interact with traditional cytotoxic treatments. Other targeted agents, such as PARP and mammalian target of rapamycin (mTOR) inhibitors, also hold potential. Ovarian cancer remains difficult to treat because of its biological heterogeneity and the absence of a single dominant molecular pathway that can be universally targeted (Itamochi, 2010; Garrido *et al.*, 2021).

1.6.6 Hormone Therapy

Ovarian cancer is a hormone-responsive malignancy in some cases, with steroid hormones and their receptors playing a critical role in disease progression. While hormone therapy offers a low-toxicity treatment option for advanced or recurrent ovarian cancer, current evidence regarding its efficacy remains inconclusive. This is primarily due to limitations such as small study populations, heterogeneity in ovarian cancer pathology, variable hormone receptor expression, and a lack of reliable molecular markers (Li *et al.*, 2021).

The main hormone therapies used for ovarian cancer are anti-estrogens (Li et al., 2021), CYP19A1 (aromatase, estrogen synthetase) inhibitors (Borella et al., 2023) and Gonadotropin-Releasing Hormone (GnRH) agonists (Halperin *et al.*, 2003; Borella *et al.*, 2023).

1.6.7 Immunotherapy

Immuno-oncology is founded on the principle that cancer cells can evade immune surveillance by establishing an immunosuppressive microenvironment, thereby promoting tumour progression. According to the immunoediting theory, most tumour cells possess immunogenic properties, making them suitable targets for immune-based therapies. Immunotherapies, ranging from tumour antigen-based vaccines to adoptive transfer of anti-tumour T cells, represent a promising and diverse set of strategies for cancer treatment.

Despite significant advances in immunotherapy and its demonstrated efficacy across various tumour types, ovarian cancer-particularly EOCs exhibits only a modest response to these treatments. EOCs are considered immunogenic tumours, as they can elicit spontaneous anti-tumour immune responses detectable both within the tumour microenvironment and the surrounding tissues. However, the effectiveness of immunotherapy in ovarian cancer is limited by several factors that can suppress or impede the patient's immune response, including tumour heterogeneity, the immunosuppressive tumour microenvironment, and variable expression of immune-related markers (Kostova *et al.*, 2021). In recent years, a new characteristic of tumours, TME, has emerged as a critical component in our knowledge of the illness. There are intricate interactions between the tumour and the surrounding area, influencing protein expressions, cell metabolism and multiple signal pathways, resulting in apoptosis resistance, tumour growth, metastatic, invasive cell behaviour and a pro-tumourigenic immune response (Hagemann *et al.*, 2006; Kostova *et al.*, 2021a).

Immunotherapy for cancer utilises three primary approaches: active immunotherapy, passive immunotherapy, and immunomodulation. Active immunotherapy aims to stimulate the patient's own immune system to recognise and attack tumour cells,

thereby generating long-lasting immunological memory. In contrast, passive immunotherapy involves the direct administration of immune components, such as antibodies or immune cells, to induce an immediate anti-tumour effect. Immunomodulation refers to a range of therapies that enhance or regulate the immune system's response, particularly those that do not fit neatly into the active or passive categories (Longoria and Eskander, 2015). Key strategies for ovarian cancer immunotherapy include checkpoint blockade agents, vaccines, adoptive cell transfer and combination therapies.

In recent years, immune checkpoint inhibitors have emerged as the most widely used treatment for ovarian cancer. These agents modulate immune responses by targeting regulatory pathways-such as CTLA-4, PD-1, and PD-L1-that are critical for maintaining self-tolerance and preventing autoimmunity. By inhibiting these checkpoints, immune checkpoint inhibitors enhance the immune system’s ability to recognize and eliminate cancer cells while minimizing damage to normal tissues. This approach represents a significant advance in ovarian cancer therapy, shifting the focus from hormonal manipulation to immune modulation for improved clinical outcomes (Siminiak *et al.*, 2022). Currently, combination therapies with immune checkpoint inhibitors and radiotherapy, anti-angiogenic drugs, PARP inhibitors and chemotherapy are being tested (Garrido *et al.*, 2021). Some of these combinations (such as Nivolumab and Pembrolizumab; Pembrolizumab with Cisplatin and Gemcitabine; Nivolumab and Ipilimumab) are showing PFS and better or additive anti-tumour drug activity. The combination of immune checkpoint inhibitors with PARP inhibitors may be particularly beneficial, as PARP inhibitors increase the production of chemokines, recruiting T-cells and tumour cells, thereby increasing the expression of PD-L1. Furthermore, clinical trials have shown that ovarian cancer patients without BRCA mutations may become sensitive to PARP inhibitors after adding immune checkpoint inhibitors to their treatment (Palaia *et al.*, 2020; Yang *et al.*, 2020).

In summary, targeted therapies have emerged as crucial tools in the treatment of ovarian cancer, particularly in addressing the challenge of platinum resistance. These therapies are designed to target specific features of cancer cells that promote growth and survival.

1.7 Apoptosis

The phenomenon of apoptosis, or programmed cell death, was first described by Kerr et al. in the 1970s. This process is an essential mechanism by which the body eliminates excessive, damaged, or harmful cells (Elmore, 2007). Apoptosis is a normal process occurring during development and ageing, as well as in the maintenance of cell populations within tissues. It also occurs as a defensive mechanism, for example during immune responses or when cells are damaged by disease or harmful agents (Elmore, 2007).

1.7.1 The Morphology of Apoptosis

The morphological changes that occur during apoptosis have been characterised using light and electron microscopy (Häcker, 2000). During the initial stages of apoptosis, cell shrinkage and pyknosis can be observed under a light microscope. The cells decrease in size, the cytoplasm becomes denser, and the organelles become more tightly packed. Pyknosis results from chromatin condensation and represents the most characteristic feature of apoptosis. On histological examination with Haematoxylin and Eosin staining, apoptosis is observed to involve single cells or small clusters of cells. Apoptotic cells appear as round or oval masses with dark eosinophilic cytoplasm and dense purple nuclear chromatin fragments (Häcker, 2000; Elmore, 2007).

1.7.2 Mechanisms of Apoptosis

The identification of apoptotic processes is critically important for elucidating the aetiology of disorders caused by defective apoptosis. This knowledge may facilitate the development of novel pharmaceutical agents targeting specific apoptotic pathways or genes. In mammals, two principal apoptotic pathways have been identified: the extrinsic system (mediated by death receptors) and the intrinsic pathway (mediated by mitochondria (Goldar *et al.*, 2015).

Caspases are a family of cysteine proteases that are one of the primary executioners of programmed cell death (apoptosis) in cells. Currently, over a dozen members of this

family have been detected in almost every mammalian cell and are highly evolutionarily conserved (Peter and Krammer, 2003). Although not all members directly induce apoptosis, those that do are classified into two categories: initiator caspases, including caspases 2, 8, 9, and 10, and effector (executioner) caspases, comprising caspases 3, 6, and 7 (Kurokawa and Kornbluth, 2009). Initiator caspases possess long pro-domains, termed the caspase recruitment domain (CARD) for caspases 2 and 9, or the death effector domain (DED) for caspases 8 and 10 (Kurokawa and Kornbluth, 2009).

1.7.3 Extrinsic Apoptotic Pathway

The extrinsic apoptotic pathway is initiated by the binding of death receptors such as FasR (APO-1/CD95), TNF-related apoptosis-inducing ligand receptors (TRAIL-RI/DR4 and TRAIL-RII/DR5), or tumour necrosis factor receptor (TNF-R) to their respective ligands FasL, TRAIL, or TNFα (Figure 2). These receptors belong to the TNF receptor superfamily, which currently comprises 29 members, with FasR being the most extensively studied. It consists of extracellular, transmembrane, and cytoplasmic domains (Peter and Krammer, 2003).

Upon stimulation, FasR recruits and binds to the adaptor protein Fas-associated death domain (FADD), as both the cytoplasmic fragment of FasR and FADD contain a C-terminal protein–protein interacting death domain (DD), leading to the formation of the death-inducing signalling complex (DISC). Subsequently, pro-Caspases-8 or -10 are recruited to the DISC, where they bind to FADD via their N-terminal DED, thereby activating them as active Caspases-8 or -10 (hereinafter Caspases-8 and -10, Figure 2). While TRAIL-R activates caspases-8 and -10 similarly to FasR, TNF-R initially recruits the adaptor protein TNF-R-associated death domain (TRADD, Peter and Krammer, 2003; Elmore, 2007).

TRADD can recruit FADD to create the DISC, which activates caspases such as FasR and TRAIL-R. Subsequently, Caspases-8 or -10 can cleave pro-Caspase-3 to activate Caspase-3 (hereinafter caspase-3), the primary apoptotic effector in cells (Muzio *et al.*, 1998).

1.7.4 Intrinsic Apoptotic Pathway

The intrinsic apoptotic pathway, also known as the mitochondrial pathway, is a fundamental mechanism by which cells initiate programmed cell death in response to internal stressors such as DNA damage, oxidative stress, or nutrient deprivation (Elmore, 2007). Upon activation by cellular stress, pro-apoptotic proteins Bax and Bak oligomerise and integrate into the mitochondrial outer membrane, resulting in mitochondrial outer membrane permeabilisation (MOMP). This permeabilisation enables the release of cytochrome c from the mitochondrial intermembrane space into the cytosol. Once in the cytosol, cytochrome c associates with apoptotic protease activating factor-1 (Apaf-1), ultimately leading to the formation of the apoptosome and the activation of caspases. These caspases orchestrate the orderly dismantling of cellular components, culminating in cell death (Peña-Blanco and García-Sáez, 2018).

Apoptosome assembly, a multiprotein complex formed by cytochrome c and Apaf-1, represents a pivotal event in the intrinsic apoptotic pathway. Upon formation, the apoptosome recruits and activates pro-caspase-9, converting it into active caspase-9. This initiates a proteolytic cascade, in which caspase-9 activates downstream effector caspases, including caspases-3, -6, and -7 (Figure 2). These effector caspases execute the apoptosis phase by cleaving key cellular substrates, ultimately producing hallmark apoptotic features, including DNA fragmentation, chromatin condensation, and cellular shrinkage (Elmore, 2007; Jeong and Seol, 2008).

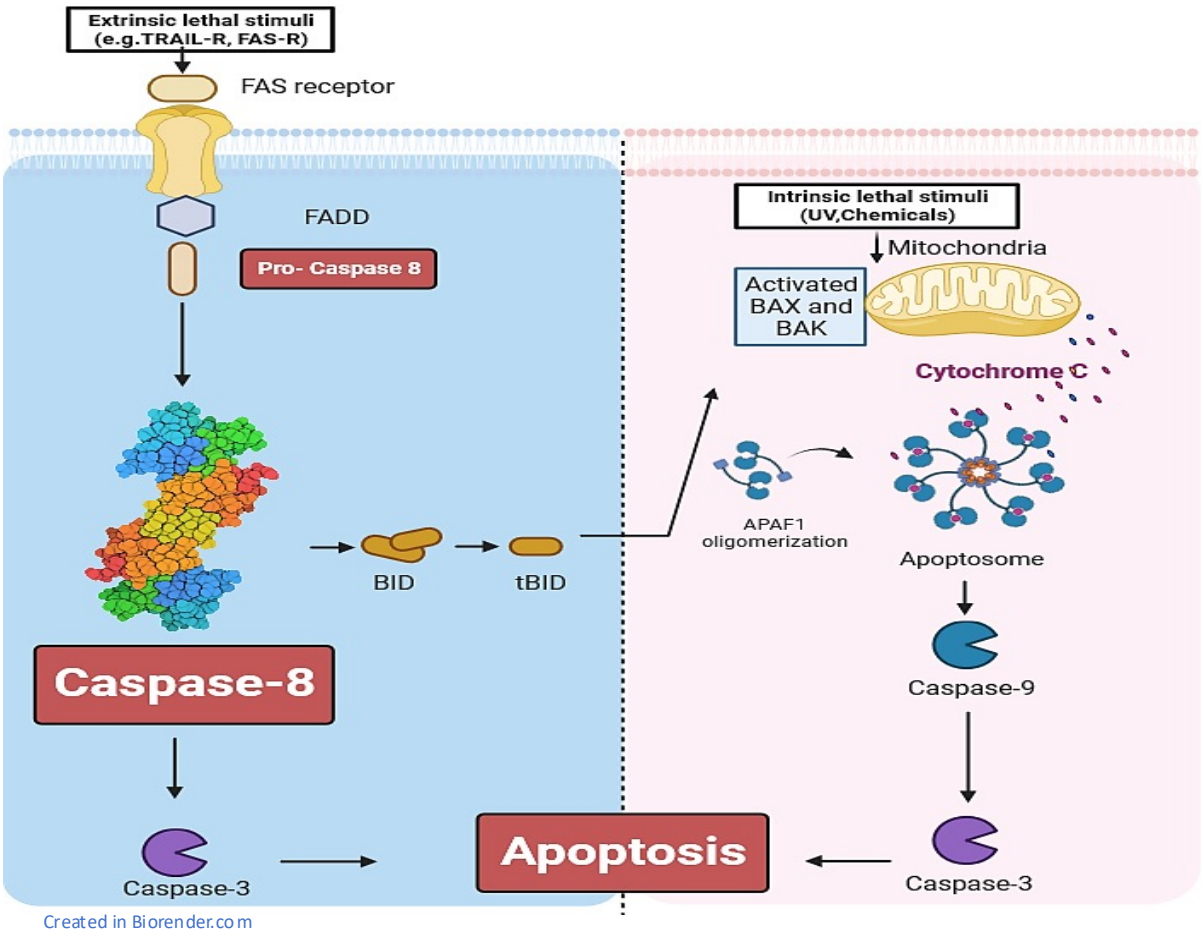

Figure 2: Overview of extrinsic and intrinsic apoptotic pathways. Apoptosis is a programmed cell death mechanism that can be triggered through two pathways: extrinsic and intrinsic. The extrinsic pathway begins with external signals binding to death receptors on the cell surface (i.e. FAS receptor), activating a caspase cascade that leads to cell death. In contrast, the intrinsic pathway is initiated from within the cell due to stress signals, causing mitochondria to release pro-apoptotic proteins, such as SMAC and cytochrome C, that activate caspases, resulting in apoptosis. Both pathways are of significant importance in maintaining cellular homeostasis and eliminating damaged or unwanted cells (Elmore, 2007).

1.7.5 Caspase-8

Caspase-8 (CASP8) is an aspartate-specific cysteine protease that plays a pivotal role in both apoptosis and immune responses. Caspases are categorised based on their

function:caspases-2, -3, -6, -7, -8, -9 and -10 primarily mediate apoptosis, while caspases-1, -4, -5, -8, and -12 are involved in immunological processes. Apoptotic caspases are further divided into initiator (caspases-2, -8, -9, and -10) and effector/executor (caspases-3, -6, and -7) groups (Kostova *et al.*, 2021b). Initiator caspases are activated in response to cellular stress signals, such as death receptor activation, inflammation, or DNA damage, through recruitment into multiprotein complexes. Once activated, initiator caspases cleave and activate effector caspases, which in turn execute apoptosis by targeting specific cellular substrates, thereby orchestrating the controlled dismantling of the cell (Mandal *et al.*, 2020).

CASP8 is most commonly associated with its apoptotic functions. However, over the past few decades, CASP8 has been identified as a central node in multiple signalling pathways, with a role in a range of non-apoptotic processes. Tumours with dysregulated expression of CASP8 have been shown to exhibit increased aggressiveness, invasiveness and chemoresistance (Mandal *et al.*, 2020).

1.7.6 Apoptotic Functions of Caspase-8

Caspase-8, like other members of the caspase family, is synthesised as a single inactive zymogen (pro-Caspase-8). It is the primary activator of the extrinsic apoptotic pathway, but under certain circumstances, it can also activate the intrinsic apoptotic pathway (Kostova *et al.*, 2021).

The primary downstream target of active CASP8 is pro-caspase-3. Type I cells are those in which CASP8 alone activates Caspase-3; type II cells require further activation of the intrinsic pathway for apoptosis. CASP8 in type II cells bridges the gap between the extrinsic and intrinsic apoptotic pathways by cleaving BH3-interacting domain death agonist (BID) to truncated BID (tBID), which activates the intrinsic pathway and intensifies the apoptotic signal (Figure 2, Kostova *et al.*, 2021a).

1.7.7 Non-Apoptotic Functions of Caspase-8

CASP8 is well-known for its role in initiating apoptosis through the extrinsic pathway. However, it also has several non-apoptotic functions, including regulating cell proliferation, differentiation, autophagy, anoikis, pyroptosis, inhibition of necroptosis, cell migration, metastasis, embryonic development, NFκB activation, immune cell homeostasis, inflammatory response and cytokine release (Mandal *et al.*, 2020; Kostova *et al.*, 2021).

CASP8 is activated in the late luteal phase in healthy ovaries, contributing to luteal cell apoptosis. Its expression also increases around eight weeks of pregnancy, suggesting a role in ovarian remodeling during early gestation. Deletion of CASP8 in embryonic mouse models resulted in significant mortality due to multiple abnormalities in several physiological systems (Bejarano, Rodríguez and Pariente, 2018; Kostova *et al.*, 2021).

CASP8 expression levels and epigenetic changes exhibits considerable variation in normal ovaries, primary and metastatic ovarian cancers (Kostova *et al.*, 2021). CASP8 expression is approximately 25-fold higher in metastases, with 20% more promoter methylation than in the main tumour or healthy ovaries. The substantial promoter methylation results in the inactivation of CASP8, implying that metastases express high quantities of inactivated CASP8 and benefit from its non-apoptotic properties. In this context, enhanced apoptosis resistance, elevated proliferation, and modifications in metastatic protein expression may confer advantages to metastases (Varfolomeev *et al.*, 1998).

Neuroendocrine tumours, which include neuroblastomas and small cell lung carcinomas, as well as brain tumours such as glioblastoma and medulloblastoma frequently exhibit loss of CASP8 expression. Similarly, cancers of mesodermal and endodermal origin, including those of the liver, breast, prostate, ovary, lymph nodes, retina, stomach and bones, also frequently exhibit lost CASP8 expression (Mandal *et al.*, 2020). There is clear evidence of a causal relationship between the presence of the gene and the onset of pathogenesis in most cases, with the exception of neuroblastoma and gastric adenocarcinoma, where genetic alterations frequently lead to the deletion of the CASP8 gene. This has been linked to the establishment of

metastasis and involvement in the late stages of carcinogenesis, respectively (Soung *et al.*, 2005).

Cancer cells employ several strategies to evade apoptosis, including inhibition of CASP8-dependent apoptosis through allelic loss or deletion, as well as somatic missense and frameshift mutations, which have all been linked to genetic changes in gastric adenocarcinoma, colorectal cancer and hepatocellular carcinoma. These modifications lead to apoptosis inhibition by producing a shortened mutant CASP8 isoform or a dominant-negative variant (Fulda, 2009; Mandal *et al.*, 2020).

Mandal et al. demonstrated that higher rates of invasion and migration occur in cervical cancer cells when CASP8 is lost. CASP8 affects invasion and metastases through various mechanisms (Mandal *et al.*, 2022). Mandal et al. discovered a unique method by which CASP8 controls the transcription of genes linked to cell invasion and migration (Mandal *et al.*, 2022). CASP8 directly inhibits CDK9 activity by direct contact. When CASP8 is reduced, CDK9 is more phosphorylated and activated. This can then facilitate the activation of the transcription machinery and change the expression of many proteins linked to invasion and migration, including TGM2 and stomatin (Mandal *et al.*, 2022).

It has been demonstrated that patients with ovarian cancer who exhibit low CASP8 expression have a poor prognosis. The RNA Polymerase II-containing transcriptional elongation complex demonstrated a distinct composition in CASP8-negative HGSOC cells, which enhanced transcriptional activity. In addition to demonstrating decreased sensitivity to paclitaxel and carboplatin, CASP8 mutant cells also exhibit enhanced BRD4 expression and CDK9 activity (Gasimli *et al.*, 2023).

In three separate gene expression datasets of ovarian tumours, low CASP8 expression was linked to a worse overall survival. Conversely, ovarian cancer subtypes with robust T-cell infiltration and improved overall prognosis showed significantly higher levels of CASP8 expression, indicating that CASP8 expression accelerated chemotherapy-induced cell death (Hernandez *et al.*, 2015). The reduction of CASP8 expression resulted in the downregulation of NF-κB signalling, the stabilisation of Receptor-interacting serine/threonine-protein kinase 1 (RIPK1), and

the acceleration of necroptotic cell death, despite the perishing of CASP8 high cancer cells by apoptosis (Hernandez *et al.*, 2015).

In summary, CASP8 is a critical regulator of apoptosis, and its loss or dysfunction significantly impairs the ability of cancer cells to undergo programmed cell death. Recent research has uncovered a variety of genetic, epigenetic, and post-translational mechanisms that contribute to CASP8 inactivation in human cancers. Gaining a deeper molecular understanding of these regulatory processes will be essential for developing targeted therapies aimed at restoring CASP8 expression and function.

1.8 Connexin-43 as a Gap Junction Protein

Gap junctions (GJ) are clusters of intercellular channels composed of two hexameric hemi-channels, which are spaced approximately 2-4 nm apart on adjacent cells (See Figure 3 for more details). Connexin proteins serve as the fundamental components of these channels, which are comprised of three intracellular domains: the N- and C-terminal domains, a cytoplasmic loop, and four transmembrane domains (Hervé *et al.*, 2007). GJs enable the bidirectional exchange of small hydrophilic molecules with a molecular weight of less than 1200 daltons. These include ions (Ca^{2+}, K^{+} and HCO^{-}_{3}), secondary messengers (inositol 3-phosphate and cAMP), reactive oxygen species, small molecules (glucose, amino acids, nucleotides, ATP and NAD+), peptides and microRNAs (Kutova, Pospelov and Balalaeva, 2023; Mizdrak *et al.*, 2024). Furthermore, connexins facilitate the formation of functional channels at the non-junctional areas of the plasma membrane. These channels, known as hemichannels, facilitate communication between the intracellular and extracellular environments, which is crucial for the regulation of autocrine and paracrine signalling (Sáez and Leybaert, 2014). The human connexin protein family comprises 21 members, of which the most extensively studied is Connexin-43 (CX43) encoded by gap junction alpha 1(GJA1) gene (Mizdrak *et al.*, 2024).

A

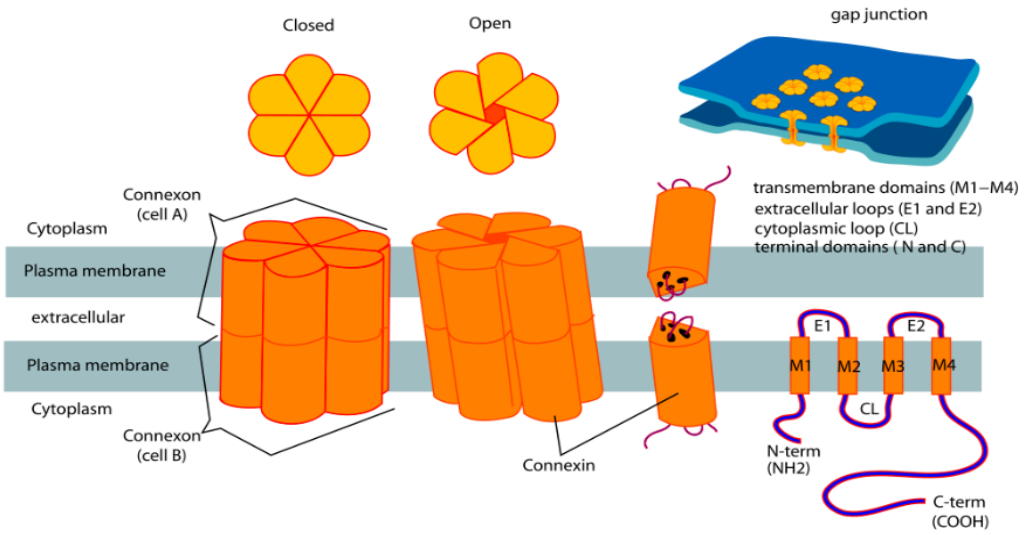

B

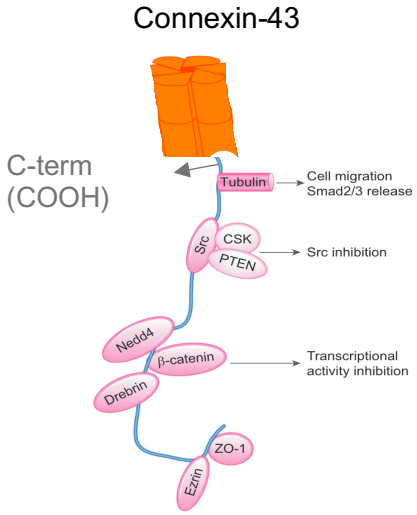

Figure 3: See next page for caption.

Figure 3: Schematic structure of connexins and isoform Connexin-43. (A) A connexon, also known as a connexin hemichannel, is a complex of six connexin proteins that forms the channel of a gap junction between the cytoplasm of two neighbouring cells. This channel allows ions and signalling molecules to flow bidirectionally. Each connexin molecule is composed of several key domains: four transmembrane segments (M1–M4) that span the cell membrane, two extracellular loops (EL1 and EL2) that are involved in docking between hemichannels, and one cytoplasmic loop (CL) between M2 and M3. N-terminal and C-terminal domains are also located in the cytoplasm (Image modified from Mariana Ruiz, WIKIPEDIA). **(B)** The interaction between connexins and proteins that influence tumour migration and growth is a key area of research. The following proteins have been identified as interacting with specific connexin regions and may represent potential targets for therapeutic intervention. Cell migration is regulated by the interaction between tubulin and CX43 (Aasen *et al.*, 2019). Other cytoskeleton-associated proteins, including vinculin, cadherins, catenins, ZO-1, and drebrin, have also been linked to similar processes. Furthermore, CX43 has been shown to oppose the tubulin Smad2/3 association, leading to Smad2/3 release (Aasen *et al.*, 2019, Image modified from Aasen *et al.*, 2019).

1.8.1 The Roles of Connexin-43 in the Ovary

Given that Connexin-43 and Connexin-37 are the most abundant connexins in the ovaries of numerous species (Kordowitzki *et al.*, 2021), their role in the female gonad has been extensively explored, leading to the description of several functions for these gap junction proteins (Aasen *et al.*, 2019; Kordowitzki *et al.*, 2021; Ackert *et al.*, 2001).

1.8.2 Folliculogenesis and Oogenesis

CX43 is essential for the development of ovarian follicles. It forms gap junctions in granulosa cells, facilitating direct cell-to-cell communication. This communication is crucial for nutrient and signal exchange, as well as follicular maturation. Proper function of CX43 ensures the synchronised development of follicles, leading to the maturation of a dominant follicle ready for ovulation (Aasen *et al.*, 2016). The role of the gap junctions in follicular development was demonstrated by generating mice that

lacked different connexin isoforms. The ovaries of prenatal CX43 knockout (KO) animals were excised and allowed to grow further in vitro, in organ culture or in vivo, under the kidney capsule of wild-type (WT) mice, in order to avoid postnatal mortality. The development of oocytes was impeded, and folliculogenesis in CX43-deficient ovaries did not advance beyond the primary follicle stage in both experimental settings (Ackert *et al.*, 2001).

1.8.3 Regulatory Role of CX43 in Apoptosis

In more detail, it was demonstrated that CX43 functions as a survival factor and its expression was negatively correlated with cell death (Lin *et al.*, 2003). In female mice with acute hyperglycaemia and chronic diabetes, there was a reduction in ovarian CX43 expression and an increase in apoptotic follicles. The findings of this study indicate that apoptosis and a reduction in CX43 expression are related, suggesting that the ovarian follicle may also be subject to these interactions (Chang, Dale and Moley, 2005). This hypothesis provides an explanation for the observation that the ovaries of CX43 KO females have fewer oocytes and more primordial germ cells that are undergoing apoptosis (Gershon, Plaks and Dekel, 2008). The expression of CX43 in pancreatic cancer cells was found to induce apoptosis and growth inhibition. This tumour-suppressive role was observed to be independent of the canonical gap junction pathway. CX43 was identified as a mitochondrial protein that translocates to the mitochondria during apoptosis. It has been demonstrated that CX43 functions with Bax to initiate the mitochondrial apoptotic pathway (Sun *et al.*, 2012).

1.8.4 CX43-Mediated Gap Junction Dependent Functions

It has been demonstrated that gap junction intercellular communication (GJIC) is elevated when CX43 is overexpressed and reduced when it is knocked down (Pollmann *et al.*, 2005; Li, Zhou and Donahue, 2008). In instances where changes in CX43 expression directly altered GJIC, contradictory roles for CX43 were observed in the carcinogenesis process (Shao *et al.*, 2005). A study utilising the HBL100 cell line, which exhibits primary tumour characteristics, demonstrated that CX43 overexpression enhanced the process of diapedesis (Pollmann *et al.*, 2005). Conversely, overexpression of CX43 was demonstrated to inhibit cell invasion in a separate study utilising a cell line with basal-like properties (MDA-MB231-MET, Li,

Zhou and Donahue, 2008). In the CX43 knockdown investigation, a cell line with basal-like properties (Hs578T) exhibited increased migration and proliferation (Shao *et al.*, 2005).

The impact of modifying GJ formation and CX43 expression on CX43-mediated gap junction-dependent functions was assessed in a further series of studies. A study indicated that GJ formation could be inhibited by carbenoxolone, while CX43 expression may be reduced by RNA interference in order to decrease cancer cell extravasation. Furthermore, the study demonstrated that the expression of the metastatic gene twist resulted in an increase in GJIC and a decrease in extravasation. This is consistent with previous findings that have shown that twist is associated with an increase in CX43 expression (Stoletov *et al.*, 2013).

A considerable body of evidence indicates that primary breast cancer tumours exhibit reduced expression of CX43. It is conceivable that the absence of GJ expression in early tumour cells represents a necessary condition for cells to physically separate from one another (Stoletov *et al.*, 2013). This may facilitate the local cell invasion of the surrounding stroma and vascular tissue during tumour growth, which are preliminary stages of the metastatic process (Naus and Laird, 2010). Conversely, it was demonstrated that established breast cancer and melanoma metastatic lesions exhibited elevated levels of CX43 (Elzarrad *et al.*, 2008). This indicates that connexins may be implicated in the later stages of metastatic processes, such as vascular penetration and tissue colonisation (Elzarrad *et al.*, 2008).

1.8.5 CX43-Mediated Gap Junction Independent Functions

In addition to its role in GJIC, CX43 has been shown to modulate the tumour-suppressive characteristics of several malignant cell types, including cervical (Johnstone *et al.*, 2010) and prostate cancers (Fukushima *et al.*, 2007). Furthermore, it has been demonstrated that CX43 functions independently of GJ formation in the context of breast cancer in the basal-like cell line MDA-MB-231 (Shao *et al.*, 2005). This results in a reduction in the angiogenic molecule thrombospondin-1 in a two-dimensional (2D) model and a reduction in migration, angiogenesis, and epithelial-to-mesenchymal transition (EMT) in a three-dimensional (3D) model (McLachlan *et al.*,

2006). It is proposed that CX43 can regulate key molecules such as α- and β-catenin and the pro-apoptotic protein Bak through mechanisms independent of GJIC. Notably, antiangiogenic agents like quercetin and genistein were found to increase CX43 expression and inhibit proliferation in MDA-MB-231 breast cancer cells without enhancing GJIC, further supporting a GJIC-independent role for CX43 in controlling cell growth (Conklin, 2007). In light of these findings, it can be concluded that CX43 can inhibit tumour-promoting agents such as 12-O-tetradecanoyl phorbol-13-acetate (TPA) and 4,4′-dichlorodiphenyltrichloroethane (DDT), which inhibit GJIC contributing to alterations in cell proliferation and transformation (Conklin *et al.*, 2007).

MicroRNAs (miRNAs) binds to the 3´-UTR (3- untranslated region) of mRNA to regulate protein expression. Prior research has demonstrated that miRNA may be involved in a variety of biological processes, including the development of embryos, inflammation, metastasis, and tumour formation (Jin *et al.*, 2013). Furthermore, evidence indicates that miRNA, including miR-195 and miR-24, facilitate both cell proliferation and glioma formation. In human tumours, connexin mRNA expression is often reduced (though occasionally elevated). Multiple mechanisms, including transcription factor activity and epigenetic silencing through histone acetylation and promoter methylation, represent potential therapeutic targets for connexin (Jin *et al.*, 2013). The transfection of miR-125b has been demonstrated to downregulate the expression of PARP and Caspase-3 in U87 cells. This effect may be mediated by its downstream targets, including CX43, as evidenced by the luciferase assay (Murphy *et al.*, 2016; Aasen *et al.*, 2019).

The C-terminal of CX43 regulates cell migration by promoting the interaction between tubulin and CX43 (Aasen *et al.*, 2019). Additionally, other cytoskeleton-associated proteins, including vinculin, cadherins, catenins, ZO-1, and drebrin, have been demonstrated to play a role in analogous processes (Dai *et al.*, 2007; Aasen *et al.*, 2019). Moreover, CX43 may act to oppose the tubulin-Smad2/3 interaction, which results in the release of Smad2/3. In order to promote c-Src inhibition, CX43 binds to both c-Src and its endogenous inhibitors, phosphatase and tensin homolog (González-Sánchez *et al.*, 2016). CX43 has also been observed to inhibit β-catenin's

transcriptional activity in the nucleus, where it controls the expression of genes that promote cell malignancy, through its interaction with β-catenin (Aasen *et al.*, 2019).

1.8.6 Complex Roles of Connexins in Cancer

The substantial body of experimental data indicates that, due to their pro- and anti-tumourigenic properties, connexins may play a causative role in the aetiology of cancer. Consequently, the dual role of the connexins, with a particular focus on CX43, is reviewed in the following section (Bonacquisti and Nguyen, 2019).

1.8.7 Connexins as Tumour Suppressors (Anti-Tumourigenic)

In a seminal ex vivo study conducted over half a century ago, Loewenstein and Kanno postulated that GJIC controls cancer growth by demonstrating the loss of electrical connectivity in rat liver tumours (Loewenstein *et al.*,1966). Since that time, a number of connexin knockout mouse models, most notably, CX43 (breast and lung) and CX26 (breast), have provided evidence in favour of the theory that connexins have tumour-suppressive roles (Aasen *et al.*, 2016). The reduction in connexin expression observed in tumours is the result of a number of processes, including transcriptional and epigenetic regulation, which occur at the transcriptional level (Sirnes *et al.*, 2011). It is possible that microRNAs targeting connexins are responsible for the post-transcriptional inhibition of connexin expression (Jin *et al.*, 2013; Aasen *et al.*, 2019).

The ectopic expression of connexins in cancer cells frequently results in the partial restoration of growth control. This finding supports the theory that connexins may function as tumour suppressors (Zhang *et al.*, 2001). Conversely, the experimental elimination of connexins may result in more aggressive cancer cell behaviour (Shao *et al.*, 2005). In addition to their role in regulating cell growth, connexins possess the capacity to either facilitate or impede the process of apoptosis in cells (Rodríguez-Sinovas *et al.*, 2021). These effects may result from the intercellular transfer of life or death signals, such as Ca^{2+}, IP3 and cAMP, which are mediated through gap junctions (Aasen *et al.*, 2016, 2019). Moreover, pro-apoptotic and survival signalling molecules may be transferred between the intracellular and extracellular environments via hemichannels (Kameritsch *et al.*, 2013).

As previously stated, there is mounting evidence suggesting that connexins can inhibit the development of cancer cells through mechanisms that are independent of channels (Sirnes *et al.*, 2011). For instance, in certain circumstances, the intracellular C terminus of CX43 can be expressed ectopically and can inhibit cell proliferation to a similar extent as full-length protein (Zhang *et al.*, 2001; Aasen *et al.*, 2019). Ovarian carcinoma cells exhibit a range of defects in cell communication, including GJC, which is one of the most ubiquitous forms of intercellular communication. The most predominant reduction observed in ovarian carcinoma or in serous cystadenocarcinomas is in the expression of CX43 (Fanning, Umhauer and Ruch, 2000). In summary, tumour cells appear to proliferate more effectively due to the absence of cell-to-cell junctional communication, which eliminates the growth inhibitory signals emanating from neighbouring cells. This suggests that connexins might be classified among the tumour suppressors, which makes them prime candidates for investigation and therapeutic targeting in the context of ovarian cancer in humans.

1.8.8 Connexins as Promoters of Invasion and Metastasis

Given the crucial role of cell contacts, research has predominantly focused on molecules regulating cell–matrix interactions (integrins) or cell-cell recognition molecules (cadherins) for an extended period. Concurrently, it has been demonstrated that gap junction proteins, or connexins, play a role in non-pathological migratory processes, such as the migration of neural crest cells and neuronal precursors to the cortex (Elias *et al.*, 2007). More recently, the function of connexins in migration has been expanded to include cancer. In recent years, there has been mounting evidence to suggest that connexins play a role in regulating the migration and invasion of cancer cells (Defamie, Chepied and Mesnil, 2014). Therefore, cell invasion and migration are frequently tightly regulated by connexins, especially CX43 (Sharma *et al.*, 2023). The precise mechanisms by which CX43 modulates cell migration remain unclear. However, in C6-glioma cells, increased cell motility was observed exclusively in cells expressing a full-length CX43, while cells expressing a C-terminal truncated CX43 did not demonstrate this phenomenon (Bates *et al.*, 2007). This suggests that the carboxyl tail of CX43 plays a crucial role in regulating glial cell migration (Bates *et al.*, 2007; Behrens *et al.*, 2010). In fact, the carboxyl-terminal tail of CX43 has been

demonstrated to mediate a more pronounced activation of p38 MAPK. This indicates that the carboxyl tail of CX43 plays a specific role in facilitating cell migration via p38 activation, which is independent of gap junctional communication (Bates *et al.*, 2007).

Additionally, it is crucial to consider the varying capacities of connexin isoforms, as well as the different tissue types and cancer stages, when evaluating the involvement of connexins in the pathophysiology of cancer. There is mounting evidence that, in certain circumstances, certain connexin isoforms may even cause tumours or prevent them (Defamie, Chepied and Mesnil, 2014; Kotini and Mayor, 2015). Additionally, it is postulated that connexins may contribute to resistance to cancer treatment and the establishment of metastases. This suggests that TNF-α plays a supportive role in this phenomenon (Chen *et al.*, 2016).

1.9 Cell Models of Ovarian Cancer

Tumour-derived cell lines are among the most widely used models in cancer research and their application has led to significant advancements in our understanding of cancer biology and greatly promoted the development of new biomarkers and targeted cancer therapies. Ovarian cancer cell lines have long been utilised as valuable in vitro models and experimental tools for basic research, owing to the limitations of in vivo animal models for studying ovarian cancer (McCabe *et al.*, 2023).

The necessity for high-quality cell line models of the various subtypes of ovarian cancer, particularly the most common HGSOC, has been emphasised in numerous publications (Hernandez *et al.*, 2016; McCabe *et al.*, 2023). There is no single solution for determining the most suitable cell line as a cancer model, as this depends on various criteria, including chemoresistance and the specific genetic alterations of interest, and more pragmatic considerations such as growth characteristics. However, maximal molecular similarity to tissue samples is preferred for certain investigations, such as drug sensitivity evaluation (Berns and Bowtell, 2012; Domcke *et al.*, 2013).

Scientists have re-examined the commonly used EOC cell lines to ensure accurate classification, in view of the established molecular characteristics of distinct EOCs, most notably the unique features of HGSOC, namely the universal TP53 mutation and extensive DNA copy number variation, including deletions and duplications (Table 2).

Table 2: The most common HGSOC cell lines with confirmed molecular and histological features of HGSC (Adapted from Domcke et al., 2013; Mei et al., 2021).

Cell name	Morphology	Original annotation	TP53	BRCA1	BRCA2
KURAMOCHI	E	AS	Mu	WT	Mu
SKOV6	E	Un	Mu	WT	WT
OVCAR3	E	AS	Mu	WT	WT
OVCAR4	Un	AC	Mu	WT	WT
OVCAR8	S	AC	Mu	WT	WT
SKOV6	E	Un	Mu	WT	WT
COV318	E/S	AS/SC	Mu	WT	WT
OVSAHO	E	SC	Mu	WT	WT
OV90	E	SC	Mu	WT	WT

Note: Morphology: E, epithelial; S, spindle. Original annotation: AC, adenocarcinoma; As, ascites; SC, serous cancer. Gene alternation: Mu, mutation; Un: unknown; WT, Wild type. OVCAR: ovarian carcinoma

When considering tumour cell lines for research, it is crucial to acknowledge that many existing lines have uncertain origins. This uncertainty arises from the limitations of identification techniques available at the time these cell lines were developed. The lack of precision in early fingerprinting methods has left researchers questioning about the true identity of numerous cell lines. Exacerbating this issue is the absence of original tumour samples, which prevents the application of cutting-edge technologies like next-generation sequencing for retrospective analysis. This gap in our understanding highlights the pressing need for developing new human tumour cultures that more accurately represent the heterogeneity of human tumours (Ince *et al.*, 2015).

Establishing such cultures would provide a more reliable and comprehensive foundation for drug discovery efforts. By better reflecting the complexity and variability found in actual human tumours, these improved cell lines could significantly enhance the effectiveness of pharmaceutical research and development processes (Ince *et al.*, 2015).

1.10 Animal Models of Ovarian Cancer

Due to the heterogeneous nature of EOC, the development of suitable preclinical animal models is essential to replicate the pathobiology of its various subtypes. Mouse models have been instrumental in elucidating the underlying pathobiology of EOC and are crucial for advancing therapeutic approaches that can be translated into clinical practice (House, Hernandez and Annunziata, 2014; Karakashev *et al.*, 2021). Recent advancements in preclinical in vivo EOC models have facilitated the development of several FDA-approved treatments. The efficacy of FDA-approved PARP inhibitors, including Olaparib, Niraparib, and Rucaparib, in the maintenance therapy of EOC has been extensively demonstrated in preclinical in vivo EOC models (AlHilli *et al.*, 2016).

Given the comparable nature of the human and mouse genomes, mice are frequently employed as in vivo models for human disease (Rämer *et al.*, 2011). A multitude of mouse strains have been utilised to elucidate the complexities of ovarian cancer and to identify and assess potential therapeutic agents. Nevertheless, only 5% of anticancer drugs studied in mice have demonstrated sufficient clinical efficacy in phase III trials to receive licensure. These limitations underscore the need for developing more sophisticated preclinical models (Ocana *et al.*, 2011).

To identify novel drugs for ovarian cancer, it is essential that effective mouse models replicate the tumour growth and metastasis patterns of actual patients, as well as their response to treatment. The source of the tumour cells (e.g., cancer cell line or PDX), the site of transplantation (e.g., orthotopic or heterotopic), and the status of the mouse immune system (e.g., mouse immune system, human immune system, or immunocompromised) are crucial factors to considered when developing mouse models (Magnotti and Marasco, 2018).

Historically, the earliest EOC animal models were developed using ovarian cancer cell lines engrafted into immunocompromised mice. Subsequently, several immunodeficient mouse strains were developed and rapidly gained recognition. Notable examples include NOD/SCID mice, which exhibit impaired cytokine signalling and B- and T-cell immunodeficiency (Shultz *et al.*, 2005). Mouse xenograft models, representing various EOC subtypes, allow the use of a wide range of human EOC cell lines for in vivo studies. These models are favoured in EOC research due to their rapid tumour development, high engraftment rates, cost-effectiveness, and reproducibility in tumour size. They are instrumental for studying tumour initiation, progression, metastasis, and therapeutic response. A key advantage of EOC xenografts is the ability to utilise genetically engineered cell lines, which facilitates detailed investigation of molecular mechanisms and therapeutic strategies in epithelial ovarian cancer (Karakashev *et al.*, 2021).

Subcutaneous xenograft models, in which ovarian cancer cells are injected subcutaneously, are widely used due to their technical simplicity and ease of tumour growth monitoring. However, these models have significant limitations: they do not recapitulate the physiological tumour microenvironment, fail to model metastasis or ovarian-specific tumour progression, and are unsuitable for studying angiogenesis. Consequently, their relevance to the clinical behaviour of ovarian cancer is limited (Karakashev *et al.*, 2021). Conversely, as ovarian cancer typically spreads within the peritoneal cavity, the intraperitoneal tumour introduction model is frequently used to study metastatic disease and evaluate intraperitoneal therapies. Following injection, cancer cells can adhere to various peritoneal surfaces, with their growth influenced by local microenvironmental factors. However, this model has notable limitations: it does not replicate primary tumour formation and is therefore unsuitable for investigating early-stage epithelial ovarian cancer or angiogenesis (Karakashev *et al.*, 2021).

As described, none of the previously discussed models can adequately represent the clinical disease course and therapeutic response of patients, given that ovarian malignancies originate in the ovary or fallopian tubes. In contrast, the orthotopic model involves transplantation of tumour cells or tissues into the ovaries (Guo *et al.*, 2017). This model closely mimics a number of key characteristics, including gene expression profiles, histopathological features and clinical disease development, as well as

interactions between cancer cells and the relevant microenvironment. This is achieved by modelling the microenvironment of human ovarian cancer. This model incorporates both spontaneous metastases and primary solid tumours, thereby enhancing its therapeutic relevance and applicability, particularly in predicting outcomes for patients with metastatic disease (Guo *et al.*, 2017; Falzone *et al.*, 2021).

It is therefore necessary to further investigate the impact of CASP8 on tumour metastatic and behavioural characteristics, and to study HGSOC cells in an experimental model for preclinical experiments. This will be accomplished using a bioluminescent orthotopic mouse model of ovarian cancer.

Bioluminescent imaging (BLI) demonstrates the light produced by luciferase in a living organism. Enzymes that produce light using luciferin as a substrate are termed luciferases. Firefly luciferase is the most commonly utilised luciferase in imaging applications (Tseng, Vasquez and Peterson, 2015). The enzyme catalyses the oxidation of luciferin in the presence of oxygen and adenosine triphosphate (ATP). The DNA coding sequence of firefly luciferase has been successfully identified and optimised for expression in mammals (Tseng, Vasquez and Peterson, 2015). Currently, the preferred method of providing substrate for BLI is intraperitoneal (IP) injection of D-luciferin. However, this method has a failure rate of 3–10% due to accidental intestinal injection (Khalil *et al.*, 2013).

2. Aims

This thesis investigates the roles of CASP8 and CX43 in HGSOC, focusing on their influence on tumour progression, metastasis, and cell communication. An orthotopic mouse model of ovarian cancer is used to reproduce the natural tumour environment and investigate the in vivo significance of CASP8.

Aim 1: CASP8's Role in Ovarian Cancer Progression and Metastasis

Research Question: Does the loss of CASP8 influence resistance to standard chemotherapy (paclitaxel and carboplatin), ovarian cancer growth and metastatic potential.

Hypothesis: CASP8 deficiency enhance resistance to paclitaxel- and carboplatin-based chemotherapy, promotes more aggressive tumour growth and increase metastatic spread in HGSOC.

Experimental Approach:

1. Generate stable CASP8 KO clones in OVCAR8 WT cells.
2. Evaluate cellular behaviour, Chemoresistance and tumour aggression between OVCAR8 WT and OVCAR8 KO:CASP8 cell lines.
3. Compare tumour size and growth rates between OVCAR8 WT and OVCAR8 KO:CASP8 cell lines in orthotopic mouse models.
4. Quantify and compare metastatic spread to organs such as the liver, kidney and colon between OVCAR8 WT and OVCAR8 KO:CASP8 tumours.
5. Perform Gene Ontology (GO) enrichment analysis in OVCAR8 WT and OVCAR8 KO:CASP8 cell lines.

Aim 2: Impact of CX43 on Ovarian Cancer Progression

Research Question: Do alterations in CX43 expression influence tumour invasion and migration?

Hypothesis: Dysregulation of CX43 expression promotes increased tumour invasion and migration.

Experimental Approach:

1. Evaluate the effects of CX43 KO on tumour invasion and migration in OVCAR3 cell line.

Aim 3: Interaction between CASP8 and CX43 in Ovarian Cancer

Research Questions:

1. Does CASP8 modulate CX43 expression in HGSOC?
2. Does combined loss of CASP8 and CX43 affect cellular behaviour and tumour aggression?

Hypotheses:

1. CASP8 deficiency alters CX43 expression in HGSOC cells.
2. The combined loss of CASP8 and CX43 synergistically enhances tumour cell migration and invasion.

Experimental Approach:

1. Compare CX43 expression levels in OVCAR3/8 WT and OVCAR3/8 KO:CASP8 cells.
2. Generate stable CX43 KO clones in OVCAR3 WT and OVCAR3 KO:CASP8 cells.
3. Assess migration and invasion capabilities of OVCAR3 WT, OVCAR3 KO:CASP8, OVCAR3 KO:CX43 and OVCAR3 KO:CASP8 KO:CX43 cell lines.

By addressing these specific research questions and testing the proposed hypotheses, this thesis aims to elucidate the molecular mechanisms underlying HGSOC progression and metastasis, potentially identifying novel therapeutic targets for this aggressive form of ovarian cancer.

3.Materials and Methods

3.1 Materials

3.1.1 Cell Lines

Cell line	Source	Passages used
OVCAR316-43 WT (OVCAR3 WT)	Donation from Prof. David Bowtell (3.2.1)	up to 35
OVCAR8 WT	Donation from National Institutes of Health (3.2.1)	up to 35
OVCAR3 KO:CASP8	Donation from Dr. Ranadip Mandal (3.2.1)	up to 35
OVCAR8 KO:CASP8	Generated from OVCAR8 WT(3.2.2)	up to 35
OVCAR3 KO:CX43	Generated from OVCAR3 WT (3.2.2)	up to 35
OVCAR3 KO:CASP8 KO:CX43	Generated from OVCAR3 KO:CASP8 (3.2.2)	up to 35

3.1.2 Culture Media

Cell line	Medium	Company	Cat. Number
All cell lines (3.1.1)	RPMI-1640	Sigma Aldrich	R8758
	10% FCS	GE Health Care	A15-101
	1% Penicillin-Streptomycin	Sigma Aldrich	P0781

3.1.3 Reagents and Drugs

Description	Company	Cat. Number
100 bp DNA ladder	NEB	N3231S
10x Fast Digest buffer	Thermo Scientific	B64
Ambion Nuclease-free water	ThermoFisher, Germany	AM9930

Description	Company	Cat. Number
BSA (Fraction V)	Biomol, Hamburg, Germany	01400
Butorphanol (Turbogesic Vet)	Zoetis, Germany	11283521
Carprofen (Rimadyl)	Zoetis, Germany	798392
cOmplete™ Proteasehemmer-Cocktail	Roche, Mannheim, Germany	11697498001
Cultrex UltiMatrix Reduced Growth Factor Basement Membrane Extract (BME)	R&D Systems	BME001-10
DAPI	ThermoFisher	D1306
ECL Blotting substrate	ThermoFisher	32106
FACSFlow	BD Biosciences	342003
Glycine	AppliChem, Darmstadt, Germany	56-40-6
Hematoxylin	Sigma Aldrich	GHS332-1L
Isofluran Piramal	Piramal	9714675
Lipofectamine RNAiMax Transfection Reagent	Invitrogen, Carlsbad, USA	13778-075
VivoGlo Luciferin	Promega, Walldorf, Germany	P1043
PageRuler Prestained Protein Ladder	Thermo Scientific, Lithuania	26616
PhosSTOP	Roche, Mannheim, Germany	04906837001
Rotiphorese Gel 30	Roth, Karlsruhe, Germany	3029.1
Roti-Quant (Bradford Reagent)	Roth, Karlsruhe, Germany	K015.1
SDS pellets	Roth, Karlsruhe, Germany	CN30.3

Description	Company	Cat. Number
TaqMan probe GJA1 (Hs06630780_s1)	Thermo Fisher	4351372
TaqMan probe GAPDH (Hs04194727_g1)	Thermo Fisher	4331182
TEMED	AppliChem, Darmstadt, Germany	A1148,0100
Trans-Blot Turbo 5x Transfer Buffer	Bio-Rad, USA	10026938
Tris	AppliChem, Darmstadt, Germany	77-86-1
Tween 20	AppliChem, Darmstadt, Germany	A1389.0500
Xylol	Thermo Scientific	140990010
H2O2	Roth, Karlsruhe	9681.1
bovine serum albumin	Roth, Karlsruhe,Germany	8076.2
Connexin-43 CRISPR/CAS9 KO Plasmid	Santa Cruz	Sc-400241

3.1.4 Antibodies

Description	Host	Dilution	Company	Cat. Number
Connexin-43	Rabbit	WB 1:10.000 IHC 1:100	Cell signaling	3512
Caspase-8 (12F5)	Mouse	WB 1:1.000 IHC 1:100	Enzo Life Sciences	ALX-804-242-C100

Description	Host	Dilution	Company	Cat. Number
GAPDH (6C5)	Mouse	WB 1:1.000	Santa Cruz	Sc-32233
p38 MAPK	Rabbit	WB 1:1.000 IF 1:100	Cell Signaling	9212
PARP 1	Rabbit	WB 1:1.000	Cell signaling	46D11
Paxillin	Rabbit	WB 1:1.000	Cell signaling	2542

3.1.5 Kits

Description	Company	Cat. Number
BioCoat Matrigel Invasion Chamber	Corning	354480
CellTiter-Blue Cell Viability Assay Kit	Promega	G8081
Culture-Insert (9mm x 9 mm x 5 mm)	ibidi	81171
ExtractME total RNA kit	blirt	EM09.1-250
Description	Company	Cat. Number
Go Script Reverse Transcription Mix	Promega	A2800
GoTaq Probe qPCR Master Mix	Promega	A6102
Caspase-Glo 3/7 Assay	Promega	G8091
Luciferase assay system	Promega	E105
QIAprep Spin Miniprep Kit	Qiagen	27104
The ApopTag Plus Peroxidase In Situ Apoptosis Detection Kit	Merck	S701

3.1.6 Equipment

Equipment	Model	Company
Bacterial Incubator	Certomat BS.1	B. Braun Biotech International, Germany
Cell culture incubator	BB6220	Thermo Scientific, Germany

Equipment	Model	Company
Developer	Optimax Typ TR	HS Laborgeräte, Germany
Plate Reader	Victor 1420 Multilable Counter	Wallac, USA
Flow Cytometer	FACSCalibur	Becton Dickinson, Germany
Immunofluorescence Microscope	Axio Observer Inverse Microscope	Zeiss, Germany
Microscope	DM750	Leica, Germany
In vivo imaging system (IVIS)	IVIS® Lumina II In Vivo Imaging System	PerkinElmer, UK
Laminar Air Flow Hood	Safe 2020	Thermo Scientific, Germany
pH Meter	Hydrus 400	Fischerbrand, USA
Power Packs	PowerPac 300/1000	Bio-rad, USA
RT-qPCR system	QuantStudio™ 3 Real-Time PCR System	Thermo Fisher
SDS-PAGE Electrophoresis Module	Mini Protean Tetra Cell	Bio-rad, China
Thermal Cycler	Flex Cycler^2	Biometra, Germany
UV/Visible Spectrophotometer	Ultrospec 3100 pro	Biochrom Ltd., UK
Western Blot Module	X Cell II Blot Module	Bio-Rad, USA
Western Blot Module	Transfer Blot Turbo Transfer System	Bio-Rad, USA
HistoBond®+ adhesive microscope slides	Paul Marienfeld GmbH & Co. KG	0810401

3.1.7 Software

Software	Company
Fiji (ImageJ)	-
Axio vision version 4.8	Zeiss
Microsoft Office	Microsoft
CellQuest Pro version 6.0	Becton Dickinson
Living Image	Perkin Elmer
QuantStudio Design and Analysis desktop software	ThermoFisher
Wallac 1420 Workstation	Perkin Elmer
GraphPad Prism 9	Graphpad

3.1.8 Solutions and Buffers

RIPA cell lysis buffer (without inhibitors)

Ingredients	Final concentration	Stock concentration	Volume
Tris pH 8.2	20 mM	1 M	4 ml
Ingredients	Final concentration	Stock concentration	Volume
NaCl	150 mM	1 M	30 ml
Triton X-100	1%	-	2 ml
Sodium-Deoxycholate	1%	10%	20 ml
SDS	0,1%	10%	2 ml
Distilled water	-	-	Adjusted to 200 ml
pH	-	-	Adjusted to 7.4

Running Buffer (western blot)

Ingredients	Final concentration	Quantity
Tris	50 mM	6 g
Glycine	190 mM	14 g
SDS	0,1%	1 g
Distilled water	-	1000 ml

2x Sample buffer (western blot)

Ingredients	Final concentration	Stock concentration	Volume
Tris pH 6.8	240 mM	1 M	48 ml
Glycerine	30 %	-	60 ml
SDS	6 %	-	12 g (Quantity)
Bromo-Phenol Blue (BPB)	0,06 %	-	120 mg (Quantity)
Distilled water	-	-	Adjusted to 200 ml
ß-Mercaptoethanol	5 %	-	50 µl/ 1ml

1 M Tris (pH 8.8 & 6.8)

Ingredients	1 M Tris pH 8.8	1 M Tris 6.8
Tris	60,57 g	60,57 g
Distilled water	500 ml	500 ml
pH	Adjusted to pH 8.8	Adjusted to pH 6.8

1x Transfer Buffer (western blot)

Ingredients	Volume
Trans-Blot Turbo 5x Transfer Buffer (Bio-Rad)	200 ml
Distilled water	600 ml
Ethanol	200 ml

Blocking & Antibody solution (western blot)

Ingredients	Blocking solution	Primary antibody	Secondary antibody
DPBS	10 ml	10 ml	10 ml
Tween 20	20 µl	20 µl	20 µl
BSA (Total 5%)	0.5 g per 10 mL	0.5 g per 10 mL	0.5 g per 10 mL
10% Sodium Azide	-	50 µl	-
Antibody	-	Primary antibody	Secondary antibody

Gels for SDS-PAGE (8,3 cm x 7,3 cm x 1,5 mm)

Ingredients	Separation gel10%	Separation gel 12%	Loading gel
Distilled water	4,7 ml	3,6 ml	3,6 ml
Rotiphorese gel 30	5,4 ml	6,6 ml	836 µl
1 M Tris pH 8,8	6,0 ml	6 ml	-
1 M Tris pH 6,8	-	-	626 µl
10 % SDS	162 µl	162 µl	50 µl
20 % APS	80 µl	80 µl	50 µl
TEMED	20 µl	20 µl	5 µl

TFBI buffer for generation of competent bacteria

Ingredients	Final concentration	Quantity
Potassium acetate	30 mM	2,94 g
Rubidium Chloride	100 mM	12,1 g
Calcium Chloride	10 mM	1,47 g
Magnesium Chloride	50 mM	10 g
Glycerol	15%	150 ml
Distilled water	-	Adjusted to 1000 ml
pH	-	Adjusted to pH 5.8

TFBII buffer for generation of competent bacteria

Ingredients	Final concentration	Quantity
MOPS	10 mM	2,1 g
Rubidium Chloride	10 mM	1,21 g
Calcium Chloride	75 mM	11 g
Glycerol	15%	150 ml
Distilled water	-	Adjusted to 1000 ml
pH	-	Adjusted to pH 6.5

Glycerol stock of transformed bacteria

Ingredients	Volume
Glycerol	50 µl
Bacterial culture	500 µl

DNA Transfection (for 1 well in a 6-well plate)

Components	Volume
Opti-MEM	Up to 507 µl
DNA	1-3 µg (Quantity)
Lipofectamine LTX	9 µl
Fugene HD	9 µl

Reverse Transcription

Components	Volume
Nuclease-free water	4 µl
GoScript Reaction buffer, random primers	4 µl
GoScript Enzyme Mix	2 µl
RNA	_µl (up to 5µg)
Nuclease-free water	Adjusted to 20 µl

RT-qPCR Mix

Components	Volume
GoTaq Probe qPCR Master Mix	5µl
TaqMan probe (GJA1)	0,5 µl
Ambion water	2,5µl
Sample cDNA (2,5 ng/µl)	2µl

Annexin binding buffer

Ingredients	Final concentration	Volume
HEPES pH 7,4	0,1 M	10 ml
Sodium Chloride	1,4 M	8,18 g (Quantity)
$CaCl_2x2H_2O$	25 mM	0,37 g (Quantity)
Distilled water	-	Adjusted to 100 ml

3.1.9 Mice

The orthotopic mouse model of ovarian cancer was developed using female NMRI nu/nu mice, purchased from Charles River Laboratories, Sulzfeld, Germany. Pre-experimental data indicated that the optimal age for the mice was 8 weeks, and the optimal body weight was approximately 30 g. The mice were housed and observed in the animal facility of the Georg-Speyer House, Frankfurt, in accordance with the FELASA guidelines (Tierversuchantrag FK/1128).

3.2. Methods

3.2.1 Cell culture

The HGSOC cell line OVCAR3, originally isolated from a patient's malignant ascites, was used to generate the murinised ovarian cancer cell line OVCAR316-43. In this study, OVCAR316-43 is referred to as OVCAR3 for simplicity. We thank to Prof. David Bowtell of the Australian Ovarian Cancer Study Group at the Peter Mac Callum Cancer Centre in Melbourne, Australia, for the development and donation of OVCAR316-43. The National Institutes of Health (NIH), USA, provided the OVCAR8 cell line for purchase. Acknowledgements are extended to Dr. Ranadip Mandal for the donation of the OVCAR3 KO:CASP8 cell line (Gasimli *et al.*, 2023). OVCAR8 WT, OVCAR8 KO:CASP8, OVCAR3 WT, OVCAR3 KO:CASP8, OVCAR3 KO:CX43 and OVCAR3 KO:CASP8 KO:CX43 cells were cultured in RPMI-1640 medium supplemented with 10% FCS and 1% Penicillin-Streptomycin at 37°C in a humidified atmosphere containing 5% CO2 with medium changes every 48-72 hours. Passaging was perfomed when cells reach 70-90% confluency. Given the fast-growth characteristics of these cells, mostly passage numbers of up to 35 were predominantly used in the experimental setup of this study.

3.2.2 Generation of Stable OVCAR8 KO:CASP8, OVCAR3 KO:CX43 and OVCAR3 KO:CASP8 KO:CX43 Cells Using CRISPR/Cas9 Genome Editing System by DNA Transfection

3.2.2.1 Generation of Stable OVCAR8 KO:CASP8 (Single and Mixed Clones)

For this study the sgCASP8 plasmid previously constructed by Dr. Ranadip Mandal (Johann Wolfgang Goethe University, Department of Gynaecology and Obstetrics, AG Strebhardt/Sanhaji) was used. This plasmid expresses two distinct single-guide RNAs (sgRNAs) targeting the sequences GCCTGGACTACATTCGCAAAGG and GCTCTTCCGAATTAATAGACTGG within exon 1 of the CASP8 gene. The initial selection of these cells (OVCAR8) was conducted using puromycin, followed by single-cell expansion. To ensure adherence to the protocol, all reagents were equilibrated to room temperature for at least 10 minutes prior to transfection.

For transfection using Fugene HD, approximately 2 µg of plasmid DNA (the optimal quantity of DNA) was diluted with 175 µl of Opti-MEM, followed by thorough vortexing. Subsequently, 12 µl of Fugene HD was added to the mixture, vortexed again, and the solution was incubated at room temperature for 15 minutes. For transfection with Lipofectamine LTX, 90 µl of Opti-MEM was combined with 9 µl of Lipofectamine LTX in one tube, while in a separate tube, 90 µl of Opti-MEM was mixed with 3 µg of plasmid DNA. After vortexing each tube, the contents were combined and incubated at room temperature for 20 minutes.

After counting and seeding approximately 150,000 OVCAR8 cells per well in a 6-well plate (50-60% confluence), the transfection mixture was added dropwise to 1.5 mL of fresh RPMI medium in each well. Following a 5-hour incubation period, the medium was replaced with fresh RPMI to ensure optimal cell viability and transfection efficiency. Subsequently, the cells were cultured in the appropriate growth medium supplemented with 2-3 µg/ml puromycin for a duration of 48-72 hours. Given that the plasmid vector harbourded the puromycin resistance gene, this selection process ensured the survival of only transfected cells. Parallel cultures of non-transfected cells were maintained under identical conditions to serve as negative controls. Following the selection period, the cells were allowed to recover in puromycin-free medium. To obtain single-cell clones of the OVCAR8 KO:CASP8, surviving cells were revived in their respective growth medium without antibiotic selection, Once the cultures had

recovered and reached sufficient confluence, cells were subjected to serial dilution and seeded into 96-well plates at an estimated density of one cell per well in up to 100 µL of medium. Cells were allowed to expand clonally until adequate confluence was achieved (approximately 3–5 weeks and with daily checking). Individual clones were then harvested and progressively expanded by sequential passaging into increasingly larger culture dishes. To generate a pooled population of OVCAR8 KO:CASP8 cells, individual single-cell clones were evaluated using proliferation assays to assess growth characteristics. Clones displaying similar proliferation trends were subsequently pooled and co-cultured in a single culture dishes, resulting in a mixed OVCAR8 KO:CASP8 cell population.

To optimise the transfection efficiency for generating CRISPR/Cas9-mediated gene knockout cells, two transfection reagents, Lipofectamine LTX and Fugene HD were tested independently under the same experimental conditions. Both reagents successfully mediated transfection. However, based on macroscopic observation of cell health and morphology following transfection, Fugene HD transfected cells exhibited better overall morphology compared to those transfected with Lipofectamine LTX. Consequently, Fugene HD was selected for all subsequent transfection experiments.

3.2.2.2 Generation of Stable OVCAR3 KO:CX43

To generate a stable OVCAR3 KO:CX43 cell line, the protocol previously established for OVCAR8 KO:CASP8 in section 3.2.2.1 was followed, using OVCAR3 cell line and Connexin-43 CRISPR/Cas9 knockout plasmids (catalog no. sc-400241). Three distinct sgRNA sequences were targeted: 5'-AAGCCTACTCCACGGCCGG-3', 5'-AAAGTGGCGCAGACCGACG-3', and 5'-CACCGGTTCAAGCCTACTCAACTGC-3' (Hua, Gu and Jiang, 2022). This approach facilitated the generation of a mixed stable knockout population of CX43. Following the insertion of GFP into the CX43 plasmid, successful transfection was confirmed by visualising GFP fluorescence under a microscope. This allowed for direct assessment of transfection efficiency through the detection of GFP signal in the transfected cells. The stability and efficacy of the knockout were consistently validated across all experimental replicates by western blot. The figure 4 illustrates the general mechanism of the CRISPR-Cas9 system employed to generate both CASP8 KO and CX43 KO cell lines (Figure 4).

3.2.2.3 Generation of Stable OVCAR3 KO:CASP8 KO:CX43

To generate the stable OVCAR3 KO:CASP8 KO:CX43 cell line, OVCAR3 KO:CASP8 cell line was used for processing the transfection. The transfection procedure was performed according to the protocol described in Section 3.2.2.2, using Connexin-43 CRISPR/Cas9 knockout plasmids (catalog no. sc-400241).

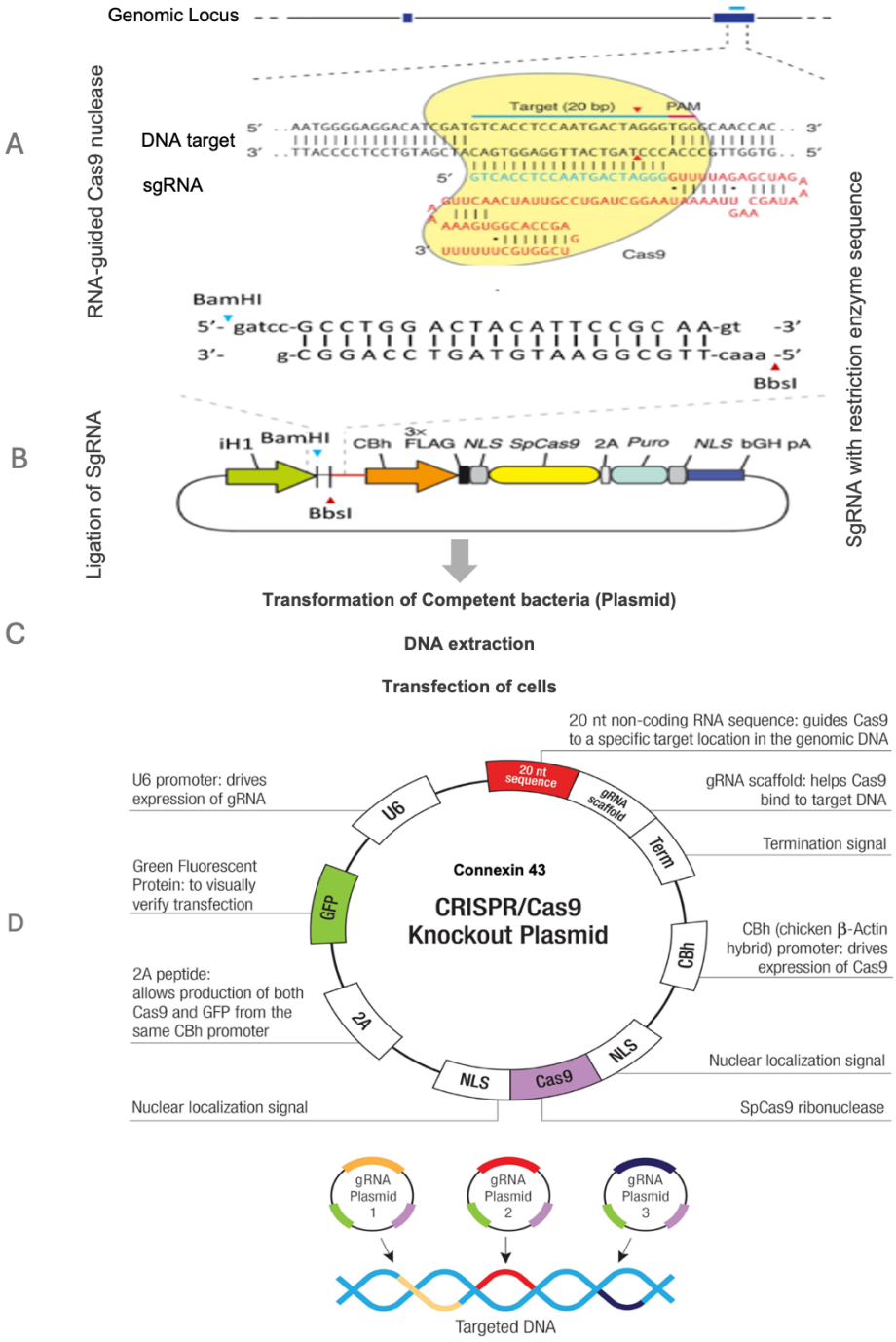

Figure 4: Schematic Representation of the CRISPR/Cas9 Genome Editing System (modified from Ran *et al.*, 2013). **(A)** The Cas9 endonuclease (depicted in yellow) is directed to specific genomic loci by a single-guide RNA (sgRNA), which consists of a scaffold region (red) and a gene-specific guide sequence (blue). **(B)** The sgRNA is engineered to include restriction enzyme recognition sites as overhangs, thereby facilitating its efficient cloning into the CRISPR plasmid vector. **(C)** For bacterial transformation, the complete CRISPR plasmid construct is introduced into competent E. coli cells. **(D)** Each CX43 CRISPR/Cas9 KO plasmid preparation consists of a mixture of three distinct plasmids, each designed to target and cleave the gene of interest, thus maximizing knockout efficiency. Each plasmid harbors a unique 20-nucleotide guide sequence sourced from the GeCKO (v2) library (modified from Santa Cruz Biotechnology).

3.2.3 Generation of Luciferase Expressing Cells

A previously constructed bacterial plasmid vector by Dr. Ranadip Mandal (Johann Wolfgang Goethe University, Department of Gynaecology and Obstetrics, AG Strebhardt/Sanhaji) was utilised to achieve stable expression of luciferase in OVCAR8 WT and OVCAR8 KO:CASP8 cells. The plasmid vector contained a 3Xflag tag, allowing assessment of transfection efficiency by detection of the flag signal via western blot analysis following overnight DNA transfection. Post-transfection, cells were cultured in medium supplemented with 4-6 mg/ml G418 for 48-72 hours to select for successfully transfected cells, as the plasmid encoded a G418 resistance gene. Non-transfected cells, maintained under identical conditions without G418, served as negative controls. After the selection period, surviving cells were allowed to recover in G418-free medium. Luciferase expression was subsequently evaluated using a luciferase assay system. For all further experiments, a heterogeneous population of luciferase-expressing cells was employed.

3.2.4 Luciferase Assay

The firefly luciferase expressed in transfected cells was quantified using the Promega Luciferase Assay System. In order to achieve approximately 90% confluency within a single day, cells were seeded in a standard 96-well plate on the first day of the experiment. With regard to the Luc-OVCAR8 KO:CASP8 and Luc-OVCAR8 WT, each well was seeded with 8,000 cells. On the following day, 30 µl of 1x cell lysis reagent was applied to each well, following the aspiration of the supernatant and the two subsequent washes with PBS. A total of 50 µl of the Luciferase assay reagent was

combined with 10 µl of the cell lysate in a white 96-well half-area microplate. The Luciferase signal was quantified using an instant plate reader (Victor 1420 Multilabel Counter) to facilitate the measurement. By maintaining the cells in culture for several weeks and monitoring the luciferase signal on a weekly basis, it was possible to verify that stable expression was maintained.

3.2.5 Generation of Competent Bacteria (DH5α -Max) and Transformation for Plasmid Construction and Amplification

For the amplification of the plasmid used to generate CASP8 KO, following the revival of non-competent DH5α-Max bacterial strains from glycerol stocks, 5 mL of Super Optimal Broth (SOB) medium was inoculated at 37°C for 24 hours with agitation. The resulting culture was subsequently expanded by transferring to 100 mL of SOB medium supplemented with 5 mL of 2 M $MgCl_2$, followed by incubation for an additional 1.5 hours under identical conditions. Bacterial growth was monitored by measuring absorbance at 550 nm using a spectrophotometer, with an optimal culture density established at an absorbance of 0.07. The bacterial suspension was then divided equally into two 50 mL falcon tubes and chilled on ice for five minutes. Cells were harvested by centrifugation at 12,160 × g for 10 minutes at 4°C. The resulting pellet was resuspended in 2 mL of ice-cold TFBII buffer (3.1.8), aliquoted into sterile 1.5 mL Eppendorf tubes, and stored at -80°C until further use.

For transformation, 50 µL of competent cells were mixed with 5 µL of plasmid DNA (Johann Wolfgang Goethe University, Department of Gynaecology and Obstetrics, AG Strebhardt/Sanhaji) and incubated on ice for 30 minutes. Heat shock was performed at 42°C for one minute to facilitate DNA uptake, after which the cells were immediately returned to ice for two minutes. Subsequently, 500 µL of antibiotic-free SOC medium was added, and the mixture was incubated at 37°C for one hour with shaking. Cells were pelleted by centrifugation at 3,000 rpm for three minutes at room temperature, and the supernatant was discarded. The bacterial pellet was plated onto 10 cm agar plates containing the appropriate antibiotic and incubated overnight at 37°C. Only successfully transformed bacteria formed colonies. Single colonies were selected the following day and cultured in 5 mL LB medium containing ampicillin (1:1,000) for further expansion.

3.2.6 DNA Extraction (Mini-Prep)

A 5 mL volume of LB medium supplemented with ampicillin (1:1,000) was inoculated with transformed bacterial cells, either sourced from the corresponding glycerol stock or from an LB agar plate. Cultures were grown in screw-capped, round-bottom tubes and incubated at 37°C for 24 hours in a shaking incubator. Plasmid DNA was subsequently extracted and purified using the QIAprep Spin Miniprep Kit, following the manufacturer's protocol. Bacterial cultures were centrifuged at 4°C and 4,000 rpm for 20 minutes to pellet the cells. The pellets were resuspended in 250 µL of resuspension buffer, followed by the addition of 250 µL of lysis buffer, with gentle inversion of the tubes six times to ensure thorough mixing. Subsequently, 350 µL of neutralisation buffer was added, and the tubes were gently mixed before centrifugation at 4,000 rpm for 10 minutes at 4°C. The resulting supernatant was transferred to the GeneJET spin column. The flow-through was discarded, and the column was washed twice with 500 µL of wash buffer. To remove residual wash buffer, the column was centrifuged at maximum speed for one minute at 4°C. DNA was eluted by adding 50 µL of elution buffer to the center of the column, incubating for five minutes, and centrifuging at full speed for one minute. The eluted DNA was collected in an Eppendorf tube, and DNA concentration was quantified using a spectrophotometer. DNA was stored at –20 °C for short-term use (e.g., within several weeks) and at –80 °C for long-term storage. Repeated freeze–thaw cycles were avoided by preparing aliquots of each DNA sample.

3.2.7 Cell Proliferation Assay (Cell Viability)

To measure the cell proliferation, 1200 cells (OVCAR8 and OVCAR3) per 100 µl medium were counted and seeded in three technical replicates in 96-well plates. 20 µl of the CellTiter-Blue reagent was added to each of the wells and incubated for 4 h at 37 °C, 5% CO2. For the 0 h time-point the reagent was added immediately after the cell seeding. Upon incubation the fluorescent signals from the wells were measured at 562/615 nm in a 96 well plate reader. During the analysis, the fluorescent read-out of the media blank from every time- point was subtracted from those of the cells. For the untreated (Control) experiments, cell proliferation was assessed over a total duration of 96 hours, with measurements taken at 24-hour intervals. In the

experimental groups, cells were treated with various concentrations of carboplatin (1, 10, 25, 50, and 100 μM) and paclitaxel (1, 2.5, 5, 7.5, and 15 nM) for IC50 determination. Proliferation was measured following a 96-hour treatment period.

3.2.8 Cell Cycle Analyses

For cell cycle analyses, OVCAR8 WT and OVCAR8 KO:CASP8 cells were harvested by trypsinisation, centrifuged, and washed with cold PBS. The resulting pellets were resuspended in 100 μl of PBS and fixed by adding 70% ethanol for at least 30 minutes on ice or at 4 °C, followed by a centrifugation and removal of the supernatant. Subsequently, 100 μl of RNase solution (1 mg/ml) and PI working solution (100 μg/ml) (stock solution 1 mg/ml) were added to the tube and incubated at 37°C for 30 minutes. The cells were analysed for their cell cycle profile using a FACSCalibur (BD) instrument. The instrument was set to count 10,000 events for each sample. The treatment scheme was as follows: In both the OVCAR8 WT and OVCAR8 KO:CASP8 groups, carboplatin was administered at concentrations of 25, 50, and 75 μM, and paclitaxel at concentrations of 2.5, 5, and 7.5 nM, followed by a 48-hour incubation period.

3.2.9 Annexin Assay

To assess overall apoptosis, following 48 hours of carboplatin and paclitaxel treatment, OVCAR8 WT and OVCAR8 KO:CASP8 cells were harvested by trypsinisation, centrifuged, washed with cold PBS for and the resulting cell pellets were resuspended in 100-200 μl of 1× Annexin Binding Buffer (3.1.8). Afterward, the cell suspension was transferred to a FACS tube. Then, 3 μl of PE-Annexin V and 1 μl of 7AAD were added to each tube. The samples were incubated at room temperature for 15 to 20 minutes. Following this, an additional volume of 200–300 μl of 1X Annexin Binding Buffer was added to each tube, after which the cells were analysed using FACSCalibur. It should be noted that the treatment scheme was the same as the cell-cycle protocol described: in both the OVCAR8 WT and OVCAR8 KO:CASP8 groups, treatment with carboplatin at concentrations of 25, 50 and 75 μM and paclitaxel at concentrations of 2.5, 5 and 7.5 nM was administered, followed by a 48-hour incubation period. In a PE-Annexin V and 7-AAD assay, early apoptotic cells are

identified by being positive for PE-Annexin V but negative for 7-AAD. In contrast, late apoptotic cells are positive for both PE-Annexin V and 7-AAD. Viable cells show no staining for either PE-Annexin V or 7-AAD.

3.2.10 Caspase-Glo 3/7 Assay

To this end, 1 µg of cell lysate (3.2.11) of OVCAR8 WT and OVCAR8 KO:CASP8 cell lines were added in triplicates (3 technical replicates) to the wells of a white 96 well plate and the volume was made up to 20 µl using Lysis Buffer without inhibitors (3.1.8). Twenty µl of Caspase-Glo 3/7 substrate were then added to each of the wells. The blank was measured by adding 1 µl RIPA buffer with inhibitors (3.1.8). The 96 well plate was incubated on a shaker under dark conditions for 30 min at RT. The treatment scheme was as follows: in both the OVCAR8 WT and OVCAR8 KO:CASP8 groups, treatment with carboplatin at concentrations of 75, 100, 150 and 200 µM were administered followed by a 72-hour incubation period. The fluorescent signals from the wells were then measured by using a 96 well plate reader (Victor Multiwell-Redader). For the final analysis the read-outs of the blank were subtracted from those of the samples.

3.2.11 Western Blot

3.2.11.1 Protein Extraction and Quantification

OVCAR8 and OVCAR3 cells were harvested via trypsinisation (0.25% trypsin-EDTA), neutralised with complete growth medium, and pelleted by centrifugation at 300 × g for 5 min at 4°C. The resulting cell pellets were washed twice with ice-cold PBS to remove residual media, then lysed on ice using RIPA buffer with protease inhibitors (3.1.8) for 30–120 min with intermittent vortexing to ensure complete disruption. Lysates were clarified by centrifugation at 12,000 × g for 10 min at 4°C, and supernatants were collected for downstream analysis. Protein concentrations were determined using the Bradford assay (Bio-Rad). Absorbance was measured at 595 nm using a microplate reader, and sample concentrations were interpolated from the standard curve. All samples were normalised to equal concentrations with RIPA buffer. Throughout the procedure, samples were maintained on ice, and centrifugations were performed at 4°C. Aliquots of quantified proteins were stored at −80°C until further use.

3.2.11.2 Western Blot

For western blot firstly 10% or 12% SDS-PAGE gels were prepared (3.1.8). Once the gels have been prepared, between 20 and 30 µg of protein lysate (3.2.8.1) were combined with 10 µl of 2× sample buffer (3.1.8). The final volume of each sample was adjusted to a maximum of 30 µl using distilled water. Prior to electrophoresis, samples were incubated at 95 °C for 5 min and subsequently centrifuged at maximum speed for 10 seconds at room temperature before loading into each lane.

Proteins were separated by SDS-PAGE under a constant voltage of 160 V for 60 min using approximately 500 ml of 1× running buffer (3.1.8). Following electrophoresis, gels were processed for semi-dry transfer (blotting). A 0.2 µm PVDF membrane was first activated in 100% methanol for 1 min. The membrane, two sponges, two sheets of Whatman filter paper, and the gel were then equilibrated in transfer buffer (3.1.8). The transfer sandwich was assembled carefully to avoid air bubbles by layering a sponge and filter paper, followed by the membrane, the gel, a second filter paper, and the final sponge. The assembled sandwich was placed into a semi-dry transfer apparatus and blotted at a constant 2.5/1.3A and voltage limit of 25V for 10–20 min, depending on the molecular weight of the target proteins. Once the blotting process was complete, the membranes were incubated in 10ml of blocking solution (5% BSA in PBST) for at least 20-30 minutes. Subsequently, the blocking solution was removed and replaced with the requisite primary antibody solution (3.1.8) and left to incubate overnight at 4 °C. Following the incubation of the membrane in the primary antibody, it was rinsed three times with PBST. Thereafter, the appropriate secondary antibody was added and the membrane was incubated for 30–60 minutes at room temprature. Prior to development, the membranes were rinsed three times for ten minutes with PBST, followed by a one-minute incubation in Enhanced Chemiluminescence (ECL) solution at room temprature. The membrane was subsequently placed in a cassette, covered with a transparent plastic sheet to prevent drying, and exposed to X-ray film in a dark room. The exposure time was optimised depending on the signal intensity. The films were developed and fixed using an automated film processor, and when required, the resulting bands were scanned for analysis by Fiji (ImageJ). Protein expression levels were normalised to the appropriate loading control and expressed relative to the corresponding experimental control condition.

3.2.12 3D Invasion Assay

Cellular invasiveness was evaluated utilising Corning Biocoat Matrigel Invasion Chambers with an 8.0 µm PET membrane in a 12-well plate format. Initially, chambers were rehydrated with a serum-free and antibiotic-free medium, incubated at 37°C with 5% CO2 for two hours. Subsequently, a cell suspension containing 125,000 of each cell (OVCAR3 WT, OVCAR3 KO:CASP8, OVCAR3 KO:CX43 and OVCAR3 KO:CASP8 KO:CX43) in 750 µl of the same medium was introduced into the each chamber, and cells were allowed to settle overnight in a cell culture incubator to induce starvation. The following day, the medium in the wells was replaced with a serum-supplemented medium containing antibiotics, while the chambers remained undisturbed. Cells were then incubated for an additional 24 hours. Following incubation, the medium was carefully aspirated from both the wells and the chambers. The chambers were then transferred to wells containing 750 µl of ice-cold methanol for 10 minutes to fix the invaded cells to the membrane, followed by a 10-minute wash with PBS. Next, the chambers were placed in wells with 750 µl of DAPI (1:30,000 in PBS) and incubated for two minutes at 37°C with 5% CO2, followed by two 10-minute washes with PBS in the dark. The membranes were then excised from the chambers using a scalpel, inverted to position the invaded cells at the top, and transferred to a glass slide. Coverslips were applied and sealed with mounting medium and glue. Slides were stored in a refrigerator for at least three hours to ensure complete drying before examination under an immunofluorescence microscope. The quantification of invaded cells was conducted by counting in about four to five microscopic fields on the membrane by ImageJ, and the average number of cells per field was calculated and graphically represented.

3.2.13 2D Migration Assay

To evaluate the migratory capacity of cancer cells, ibidi 2-well culture inserts were utilised, enabling the assessment of cell migration within a controlled microenvironment. These inserts adhere securely to the culture plate, creating a defined, cell-free gap between the two wells. To ensure complete confluency within 24 hours, cells were counted and seeded at a density of 150,000 cells per well (using 70 µl of medium per well, with two inserts per well per cell line in a 12-well plate, by using

OVCAR3 WT, OVCAR3 KO:CASP8, OVCAR3 KO:CX43 and OVCAR3 KO:CASP8 KO:CX43 cells). Following seeding, the cells were incubated overnight at 37°C in a humidified incubator with 5% CO_2 to facilitate cell attachment and monolayer formation. After incubation, the inserts were carefully removed, and the wells were washed twice with PBS to eliminate non-adherent cells. The width of the cell-free gap was subsequently monitored and measured by microscopy at intervals of 8 hours. The endpoint was reached when the cells from both sites migrated enough to close the gap. The measured areas which quantified by ImageJ, were finally plotted on a graph.

3.2.14 RT-qPCR

The initial step involved the extraction of RNA from the OVCAR3 WT, OVCAR3 KO:CASP8, OVCAR3 KO:CX43 and OVCAR3 KO:CASP8 KO:CX43 cells using the ExtractME total RNA kit. The quantity of RNA was determined using a spectrophotometer, and 500 ng of RNA were employed for reverse transcription with Go Script Reverse Transcription Mix. In this process, the RNA served as a template for the synthesis of cDNA. The reverse transcription mixture was incubated in a programmed thermal cycler as follows: 25 °C for 5 minutes (1 cycle, annealing), followed by 42 °C for 60 minutes (1 cycle, extension). The reverse transcriptase was then inactivated at 70 °C for 15 minutes (1 cycle). After the inactivation step, the reaction was cooled to room temperature and subsequently held at 4 °C until further use.

For the qPCR reaction, 5 µl of GoTaq Probe qPCR Master Mix was combined with 2.5 µl of nuclease-free water and 0.5 µl of TaqMan sample, resulting in a total volume of 8 µl for one well on a 96-well TaqMan plate. Subsequently, the cDNA was diluted with Ambion water to a concentration of 2.5 ng/µl, with 2 µl being pipetted for each well. The final step in the process was to perform the reaction in the QuantStudio™ 3 Real-Time PCR System. The results were subsequently analysed using the QuantStudio Design and Analysis desktop software.

To clarify the method of analysis, the following terms are defined:

- **Ct value**: The cycle threshold (Ct) value is generated by the qPCR device and indicates the cycle number at which the fluorescence signal exceeds the background level.
- **Delta Ct (ΔCt)**: Calculated as the difference between the Ct value of the gene of interest and the Ct value of a housekeeping gene (ΔCt = Ct [Gene of interest] – Ct [Housekeeping gene]).
- **Delta Delta Ct (ΔΔCt)**: Represents the difference between the ΔCt of the target groups and the ΔCt of the control groups (ΔΔCt = ΔCt [KO] – ΔCt [Control]).
- **Fold change**: Determined using the formula Fold change = 2^(-ΔΔCt), this value reflects the relative expression level of the target gene compared to the control.
- **Relative expression**: Calculated by dividing the fold change of each sample by the fold change of the corresponding control.

In this analysis, Ct values generated by the qPCR device were used to calculate ΔCt, ΔΔCt, fold change, and relative expression for both control groups based on the comparison (OVCAR3 WT, OVCAR3 KO:CASP8) and targeted groups (OVCAR3 KO:CX43, OVCAR3 KO:CASP8 KO:CX43). These calculations enabled data analysis and graphical representation of gene expression differences among the groups.

3.2.15 Immunofluorescence (IF)

A total of approximately 300,000 for OVCAR8 WT and 350,000 for OVCAR3 WT cells were enumerated and plated in six-well plates on the coverslips. Prior to utilisation, the IF coverslips were incubated in ethanol for a minimum of 30 minutes, followed by two PBS washes, a 20-minute incubation in poly L-lysine solution, and another two PBS washes. Once the cells had settled, the medium was removed from each well and the samples were cleaned with PBS. Then the cells fixed by 4% paraformaldehyd for at least 15 minutes following 3 times washing with PBS for 10 minutes. Subsequently, the cells were incubated for a period of 30 minutes in a solution of blocking buffer (comprising 3% BSA and 0.1% Triton X-100). The coverslips were taken from the six-well plate and placed on slides. A volume of 100 µl of the primary antibody solution was pipetted on the cells and incubated at 4°C over night in a

humidified chamber. The IF coverslips were reinserted into the six-well plate and underwent two PBS washes the following day. Then, the IF coverslips were repositioned on slides and incubated for 30 minutes at 4°C with the secondary antibody. The coverslips were returned to the wells and washed once with PBS, followed by a 5-minute incubation with DAPI (1:30,000). Thereafter, the coverslips were transferred to new slides. To maintain the fluorescence of each sample, a Vectashield mountain medium was employed. Subsequently, the IF coverslips were examined using a fluorescence microscope, after being adhered to the slides with a fixogum. For each slide, four to five fields of view were imaged per slide, and the signal intensity of individual cells was quantified using ImageJ software. The mean signal intensity was then calculated and used for graphical representation.

3.2.16 Mouse Experiments

Surgery (Tierversuchantrag FK/1128)

Prior to the surgical procedure, mice (N=2) were administered butorphanol (3 mg/kg, subcutaneously) and carprofen (2 mg/kg, subcutaneously) as analgesic agents, 20 minutes before the operation. Anaesthesia was induced using isoflurane delivered in an induction chamber. To prevent perioperative hypothermia, animals were placed in a ventral recumbent position on a heating pad situated beneath a dissecting microscope and maintained under anaesthesia for the duration of the procedure. Adequacy of anaesthesia was confirmed by the absence of a pedal withdrawal reflex following toe pinch with forceps. The procedure was initiated only after a complete lack of response was observed. To prevent corneal desiccation, ophthalmic ointment was applied to the eyes. The optimal site for incision to access the ovary was identified as the dorsal midline, directly beneath the ribs.

The procedure commenced with the application of 70% ethanol for antiseptic preparation of the surgical site (Figure 5A). Following disinfection, the cutaneous layer was carefully elevated using sterile forceps, and a precise incision was created utilising sharp-tipped surgical scissors (Figure 5B). The abdominal musculature was subsequently dissected employing blunt scissors (Figure 5C), followed by complete incision of the peritoneum to access the abdominal cavity (Figure 5D). Upon adequate exposure, the ovarian adipose tissue became readily identifiable under microscopic

visualisation, characterised by its distinctive lustrous white appearance (Figure 5E). This substantial anatomical structure is located in immediate proximity to the oviduct and ovarian tissue. The adipose pad was meticulously extracted from the peritoneal cavity utilising forceps and transferred to sterile gauze. The specimen was then immersed in physiological saline solution and secured with forceps to ensure positional stability throughout subsequent manipulations (Figure 5F). It is noteworthy that the bursa, a delicate membranous structure encompassing the ovaries and oviduct, creates a confined anatomical space that significantly limits the potential volume for fluid injection between the ovarian tissue and bursal membrane.

A total of 1 x 10^6 Luc-OVCAR8 WT or Luc-OVCAR8 KO:CASP8 cells were enumerated and then resuspended in 5 µl of PBS containing 2% matrigel. Subsequently, the cell suspension was injected into the ovary bursa (space between the ovary and bursa) using a Hamilton 10 µl syringe and a 30 G needle (Figure 5G). Once the needle had been inserted into the bursa, the second individual applied pressure to the plunger while the surgeon maintained the needle in the correct position under the microscope.

Injection of the cell suspension resulted in a noticeable enlargement of the bursa, suggesting that the tumour cells remained localised within the space between the bursa and the ovary. Following this, the ovarian fat pad was repositioned into the abdominal cavity (Figure 5H). The incision was then closed using wound clips (Figure 5I), and the two sites of the abdominal wall were carefully approximated (Figure 5J, Izabela Kostova, 2023). Postoperative analgesia was provided on days one and two after surgery, consisting of subcutaneous administration of carprofen (2 mg/kg) and butorphanol (3 mg/kg). Wound clips were removed seven days post-surgery.

The surgical procedure is associated with minimal discomfort, stress, and harm for the animals. All mice survived the surgical procedure and exhibited no abnormalities in their behaviour post-operatively. The aforementioned behaviours are indicative of normal grooming, eating and drinking behaviours. Furthermore, the absence of pain-specific signs and social behaviours serves to reinforce this conclusion.

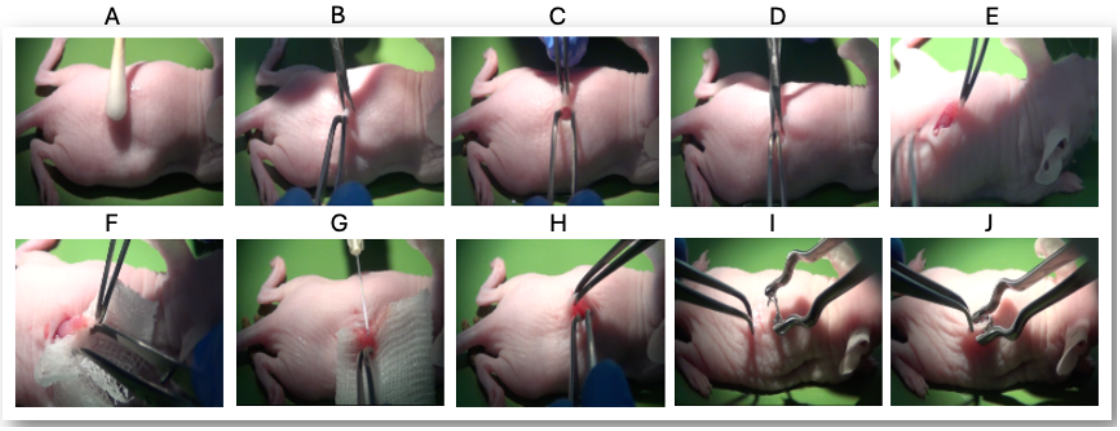

Figure 5: The figures illustrate the various steps involved in the surgical implantation of high-grade serous ovarian carcinoma (HGSOC) cells into the mouse ovary. These steps include the preparation of the surgical site, the injection of HGSOC cells into the ovarian tissue, and the closure of the incision. Each figure highlights a critical phase of the procedure to ensure reproducibility and provide a clear visual guide for the surgical technique employed in this model (Photos generated by Izabela Kostova, 2023).

In-vivo imaging system (IVIS)

Bioluminescence imaging (BLI), utilising the in-vivo imaging system (IVIS), is a non-invasive technique employed to monitor tumour progression and metastasis in live animal models. In this procedure, mice were first anesthetised using isoflurane. Subsequently, 100 µl of luciferin was administered subcutaneously, and following a 15-minute incubation period, bioluminescence was measured. Bioluminescence, a form of chemiluminescence, occurs when the substrate luciferin is oxidised in the presence of oxygen within living organisms. Tumour cells genetically engineered to express the luciferase enzyme catalyse this reaction, resulting in the emission of light. The emitted bioluminescent signal was detected and quantified using the IVIS Lumina II Multispectral Imaging System (Tseng, Vasquez and Peterson, 2015). The first

measurement was obtained seven days post-surgery, after which the animals were monitored and measured weekly. Animal project was conducted collaboratively in the AG Strebhardt with Izabela Kostova. however, I independently performed the data analysis, interpretation, and presentation of results.

3.2.17 Immunohistochemical (IHC) Assay

After harvesting the organs from the animal model, the tissues (ovaries) were placed fresh in 10% neutral buffered formalin (3.7-4% formaldehyde) at room temperature for 12-24 hours (depending on the thickness of the tissue). The formalin was removed and the tissues were rinsed 1-2 times with PBS for paraffin embedding.

Formalin's-fixed paraffin embedded (FFPE) tissues were sectioned at a thickness of 3–5 µm. Subsequently, two portions of each section were placed on slides coated with 3-aminopropyltriethoxysilane (APTES). Following a two-day drying period at 37°C, immunohistochemistry (IHC) was conducted on the slides in accordance with standard laboratory procedures. In summary, 5-µm tissue sections were placed on slides in a glass staining tray. The sections were deparaffinised for two minutes in xylene and subsequently rehydrated through a graded ethanol series (100%, 96%, 80%, and 70%), with each step lasting five minutes, and then rinsed twice in double distilled water (ddH2O). Afterwards, heat-mediated antigen retrieval was conducted in Tris-EDTA buffer (pH 9, 3.1.7) for 20 minutes (the first five minutes at 770 W and then 15 minutes at 460 W) in a microwave oven. Thereafter, the slides were returned to room temperature for 15 minutes to allow cooling. Subsequently, the slides were washed once with a wash buffer solution (Tris-buffer solution (TBS, pH 7.4) + 0.1% Triton-X-100) for a period of three minutes. Thereafter, the slides were incubated in a solution of 3% hydrogen peroxide in wash buffer for 15 minutes at room temperature on a shaker plate, in order to inhibit the endogenous peroxidase activity. Subsequently, the sections were washed in wash buffer for three time with 3-minute intervals and then incubated with 1.5% bovine serum albumin in wash buffer at room temperature for 30 minutes in order to block unspecific binding sites. The primary antibodies were diluted in 1.5% bovine serum albumin (BSA) and applied to the tissue sections. In the negative controls, the 1.5% BSA solution was used instead of the primary antibodies. The sections were incubated overnight at 4 °C in a humidified chamber, then washed and

incubated with secondary antibody for 60 minutes at room temperature. Following the incubation period with the secondary antibody, the section is washed three times for a total of 15 minutes. The slide is then stained with NovaRED for a few seconds, immediately washed with PBS and carefully mounted. Due to the very high intensity and saturation of the IHC signal, as well as the marked heterogeneity of the tissue sections, quantitative analysis in ImageJ was not reliable. Therefore, I performed a blinded qualitative assessment to comparatively score the slides.

3.2.18 TUNEL Assay

The TUNEL assay was performed on FFPE tissue sections using the ApopTag® Plus Peroxidase In Situ Apoptosis Detection Kit (MilliporeSigma, S7101) according to the manufacturer's protocol with modifications.

Following standard IHC pretreatment procedures (3.2.17), tissue sections were equilibrated in ApopTag® equilibration buffer for 10 minutes at room temperature. After the excess liquid has been tapped off and carefully blotted or aspirated around the sections, immediately working strength TdT enzyme is pipetted onto the section and incubated for 1 hour in a humidified chamber at 37°C. For the negative control, the step involving the application of the TdT enzyme to the tissue section was omitted. The slide is then agitated for 15 seconds and incubated in the Stop/Wash Buffer for 10 minutes. Slides were washed four times in PBS and then the anti-digoxigenin conjugate was applied to the sections. The slides were incubated in a humidity chamber for 30 minutes at room temperature. After four times (each time 2 minutes) wahsing in PBS, The slide was then stained with NovaRED for a few seconds and immediately washed with PBS. For counterstaining, the slides were inverted in 0.5% methyl green for approximately 10 minutes at room temperature, then immediately rinsed three times in dH2O and then three times in 100% n-Butanol. Finally, the slides were dehydrated by passing the slide through three jars of xylene, incubating for 2 minutes in each jar before mounting. Under the microscope, nuclei showing light to medium brown staining and displaying apoptotic features such as chromatin condensation, were manually counted as apoptotic cells.

3.2.19 Transcriptome

The following experimental groups have been prepared for transcriptome analysis: 1) OVCAR8 WT; 2) OVCAR8 KO:CASP8 by using CRISPR/Cas9, and each group consisted of three independent biological replicates, meaning that three separate culture wells of each cell line were grown, harvested, and processed independently throughout the entire RNA extraction workflow. The ExtractME total RNA kit was employed to extract the RNA from each group. Each sample had a minimum volume of 10 µl and a minimum concentration of 50 ng. Subsequent to this, the samples were dispatched to Novogene in Cambridge, UK, where samples were sequenced and analysed using bioinformatics to examine gene expression patterns (transcriptome) in the different experimental groups, which included internal quality control. Consequently, a bioinformatic analysis was conducted, and the results were received.

Sequencing projects at Novogene are conducted according to the following workflow (Figure 6):

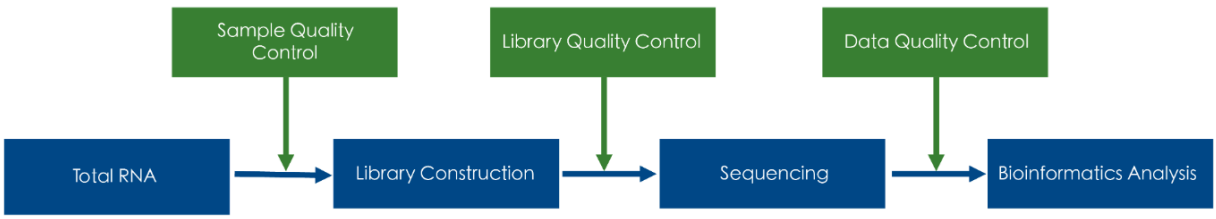

Figure 6: Workflow for RNA sequencing projects (Generated by Novogene)

The mRNA sequencing data were processed using a standard bioinformatics workflow based on a well-annotated reference genome. All analyses were carried out by Novogene following their established best-practice pipeline, summarised as follows (Figure 7):

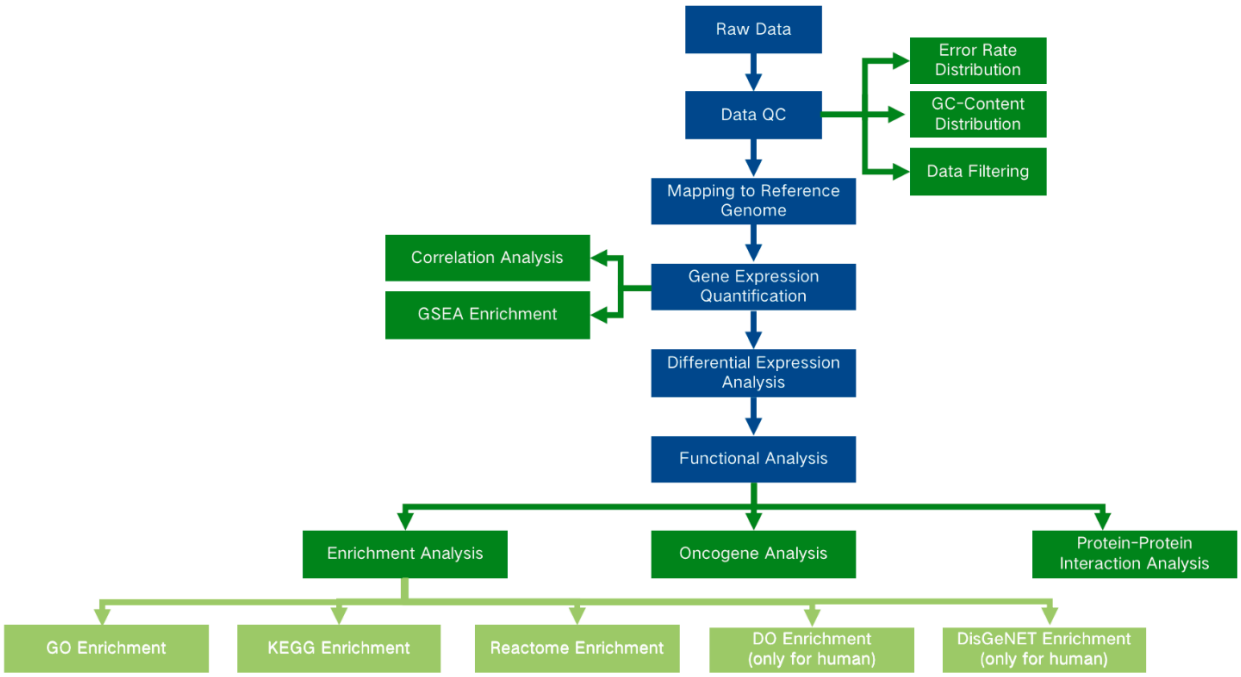

Figure 7: Workflow of RNA sequencing data analysis (Generated by Novogene)

By using a comparative approach based on p-value and fold change cut-offs, the PhD candidate was able to reduce the number of genes considered significant when comparing expression levels between the experimental OVCAR8 WT and OVCAR8 KO:CASP8 groups. A p-value of less than 0.05 and a cut off of +/- 0.58 log2 fold change, or 1.5 times the change in gene expression, were additional requirements. A DAVID gene ontology study was performed on the final list of 753 genes in order to get biological process.

3.2.20 Statistical Analysis

All statistical analyses were performed using GraphPad Prism version 9. Experimental data were obtained from both biological and technical replicates, where applicable. Different cell passages were considered independent biological replicates. Data are presented as the mean ± standard error of the mean (SEM), as indicated in the figure legends.

statistical analyses were conducted exclusively for datasets with an adequate number of biological and technical replicates, and where comparisons between experimental groups were necessary to determine statistical significance. For datasets lacking adequate replication, statistical analysis was not performed, and additional experiments are required to enable robust statistical evaluation. The specific statistical tests applied for each experiment are indicated in the corresponding figure legends. Statistical significance was defined using the following thresholds: $p < 0.05$ (*), $p < 0.01$ (**), $p < 0.001$ (***), and $p < 0.0001$ (****).

3.2.21 Diagram of the experimental structure and contributions

3.2.21.1 In vivo experiments

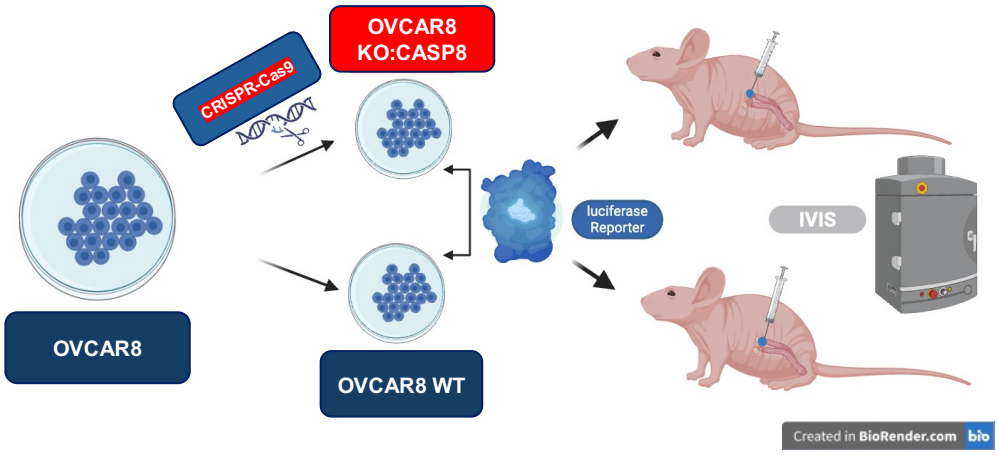

Figure 8: The figure illustrates in vivo experimental structure.

3.2.21.2 In vitro experiments

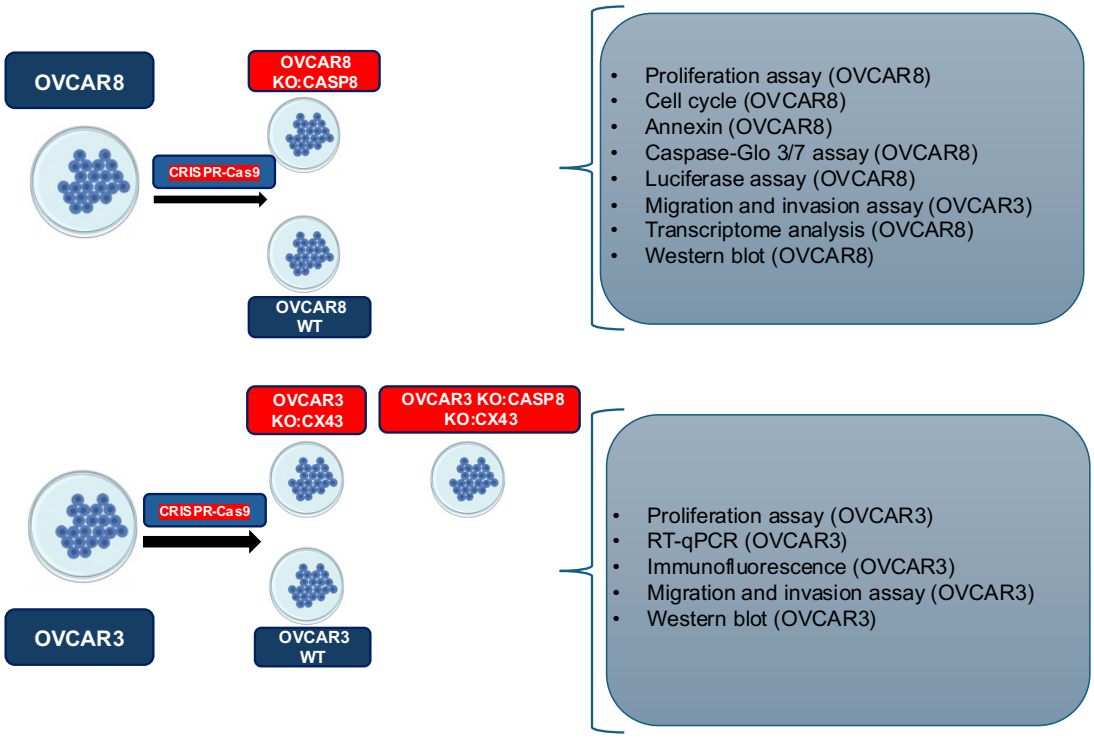

Figure 9: The figure illustrates in vitro experimental structure.

3.2.21.3 Experimental Contributions in this Thesis

Experiments	Contribution
Mouse Experiment	Due to the collaborative nature of this experiment as a joint project, PhD candidate was responsible for conducting the in vivo imaging system (IVIS) process. The surgical procedures and organ harvesting were performed by Prof. Daniela Fietz, with assistance from Ms.Izabela Kostova.
Generation of OVCAR8 KO:CASP8 (Single and Mixed Clones) and Lucifease Expressing Cells	The sgCASP8 and luciferase plasmids were originally constructed by Dr. Ranadip Mandal. PhD candidate performed all subsequent experiments, including transfection and generation of single knockout clones.
Generation of OVCAR3 KO:CASP8	Due to time constraints and cell contamination issues, PhD candidate utilised OVCAR3 KO:CASP8 cells previously generated by Dr. Ranadip Mandal for this experiments.
IC50 of carboplatin and paclitaxel	PhD candidate performed these experiments independently, with technical assistance from Ms. Andrea Krämer.
Transcriptome data analysis	Transcriptome data were acquired and processed by Novogene (Cambridge, UK).
Generation of OVCAR3 KO:CX43 and OVCAR3 KO:CASP8 KO:CX43 Transfection Immunofluorescence Cell Cycle Western Blot Annexin Caspase-Glo 3/7 Assay TUNEL Assay Immunohistochemical Assay Enrichment analysis on the transcriptome data by DAVID enrichment tool RT-qPCR 2D Migration Assay 3D Invasion Assay Cell Proliferation Assay Luciferase Assay	All listed experiments were performed solely by PhD candidate.

4. Results

4.1 In Vitro Study of Caspase-8

4.1.1 Establishment of OVCAR8 KO:CASP8 Single Clones, Mixed Clone and Growth Behaviour of OVCAR8 KO: CASP8 Single Clones

Stable OVCAR8 KO:CASP8 clones were generated using the CRISPR-Cas9 system to investigate the impact of long-term loss of CASP8 expression on cancer cell behaviour. Following the expansion of individual cells, four distinct clones, K5, K7, K8, and K9, were obtained, and all clones were then combined in equal proportions (mixed clone) to capture the clonal heterogeneity observed in patient tumours (Figure 10).

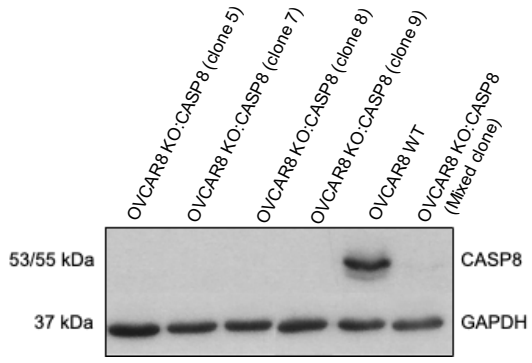

Figure 10: Immunodetection of CASP8 protein in OVCAR8 WT and OVCAR8 KO:CASP8 clones.

Next, using a cellular growth assay, it was confirmed that OVCAR8 KO:CASP8 single clones exhibited proliferation capacities similar to their WT counterpart after 96 hours (Figure 11).

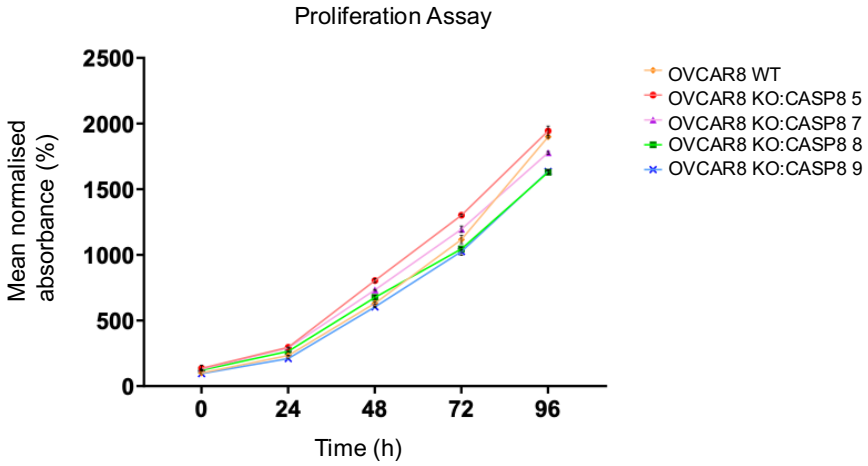

Figure 11: Assessment of cell proliferation in OVCAR8 WT and OVCAR8 KO:CASP8 single clones. Growth kinetics were comparable across all groups, with most comparisons showing no statistically significant differences over a 96-hour period (Mixed-effects model (Geisser–Greenhouse), Tukey test; mean ± SEM, n = 3 technical replicates; $P < 0.05$).

4.1.2 CASP8 KO Cells Demonstrate Resistance to Carboplatin and Paclitaxel

The CellTiter-Blue reagent was employed to assess cell proliferation. After a 96-hour incubation with the substances, loss of CASP8 expression significantly decreased OVCAR8 cell sensitivity to carboplatin and paclitaxel at all concentrations, except at 1 µM for carboplatin and 1 nM for paclitaxel. The calculated IC50 values were 14.56 µM versus 54.75 µM for carboplatin (Figure 12A) and 1.84 nM versus 6.05 nM for paclitaxel (Figure 12B) in OVCAR8 WT and OVCAR8 KO:CASP8 cells, respectively (Figure 12).

A

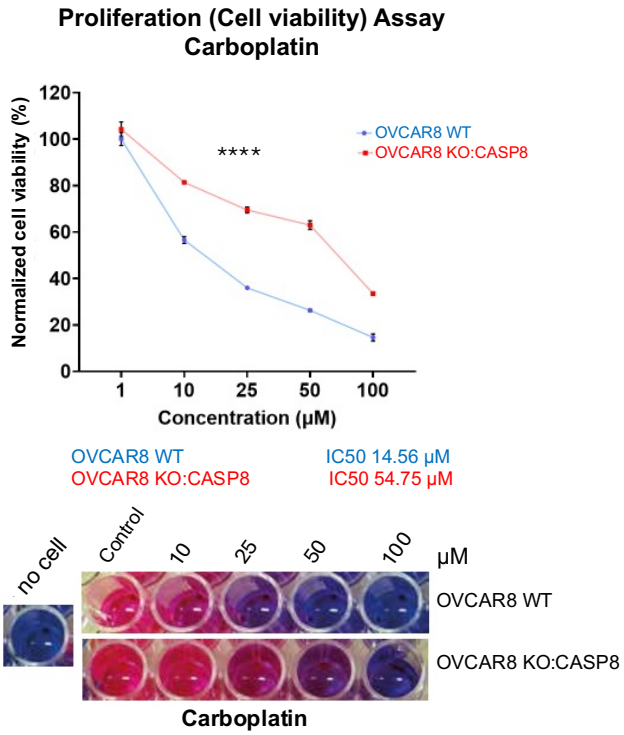

B

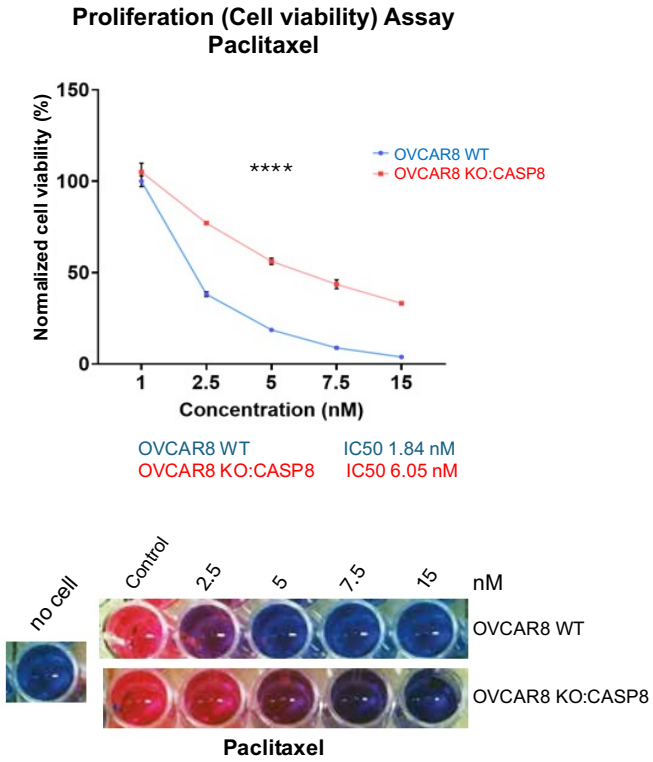

Figure 12: See next page for caption.

Figure 12: Chemosensitivity and IC50 of OVCAR8 WT and OVCAR8 KO:CASP8 cells to carboplatin and paclitaxel. Upper panel: dose response curves for **(A)** carboplatin and **(B)** paclitaxel after 96 h. Lower panels: pink wells indicate viable/proliferating cells; blue wells indicate proliferation arrest (Two way ANOVA, Bonferroni correction; mean ± SEM, n = 3 technical replicates; p- **** < 0.0001 at all concentrations, except at 1 µM for carboplatin and 1 nM for paclitaxel).

4.1.3 Cell Cycle Regulation by CASP8

Transcriptome analysis of the OVCAR8 WT and OVCAR8 KO:CASP8 cell lines revealed a downregulation of genes involved in cell cycle regulation, including S-phase kinase-associated protein 2 (SKP2), MAP3K12 binding inhibitory protein 1 (MBIP), and Forkhead Box M1 (FOXM1). Consequently, the impact of CASP8 deletion on cell cycle regulation and the response to DNA damage induced by carboplatin treatment was investigated. The initial results demonstrated a reduction in the G2/M phase in the OVCAR8 KO:CASP8 group relative to the OVCAR8 WT group following carboplatin treatment (Figure 13). This experiment was conducted with a limited number of replicates; therefore, additional investigations with increased replication are required for definitive confirmation.

A

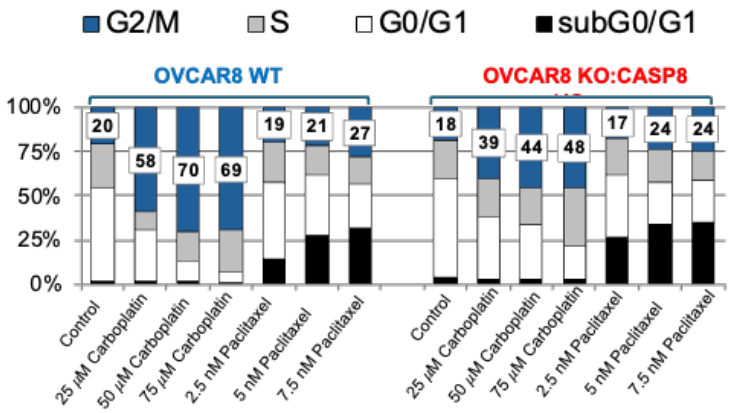

Figure 13: See next page for caption.

B

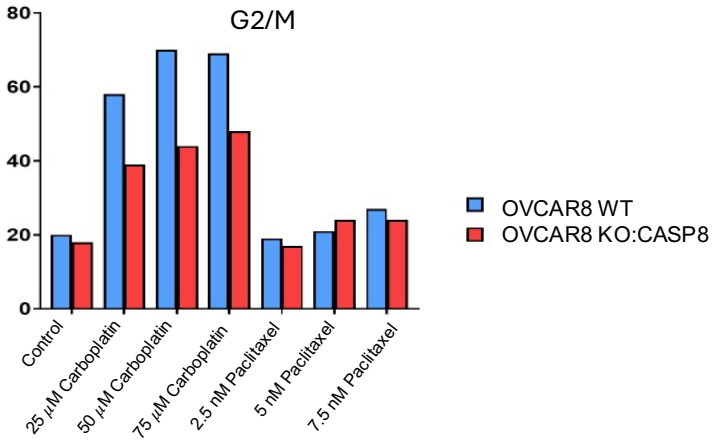

Figure 13: Cell cycle distribution of OVCAR8 WT and OVCAR8 KO:CASP8 cells following chemotherapy treatment. (A) Cell-cycle profiles of OVCAR8 WT and OVCAR8 KO:CASP8 cells were quantified after treatment with carboplatin or paclitaxel followed by a 48-hour incubation period . The distribution across G0/G1, S, and G2/M phases is shown for each condition. **(B)** Quantification of the G2/M phase population in the OVCAR8 KO:CASP8 cells compared with their WT counterparts across all treatment conditions (Given n=1, further replicated experiments are necessary to validate these results).

4.1.4 Impact of CASP8 on Apoptosis Pathways and DNA Repair

Annexin V/7-AAD results showed a reduction in early and late apoptosis of 7%, 6%, 11%, and 8% in the untreated, 25, 50, and 75 μM carboplatin groups, respectively, in the OVCAR8 KO:CASP8 group compared with the OVCAR8 WT group (Figure 14). These experiments were conducted with a limited number of replicates; therefore, additional investigations with increased replication are required to obtain definitive confirmation.

A

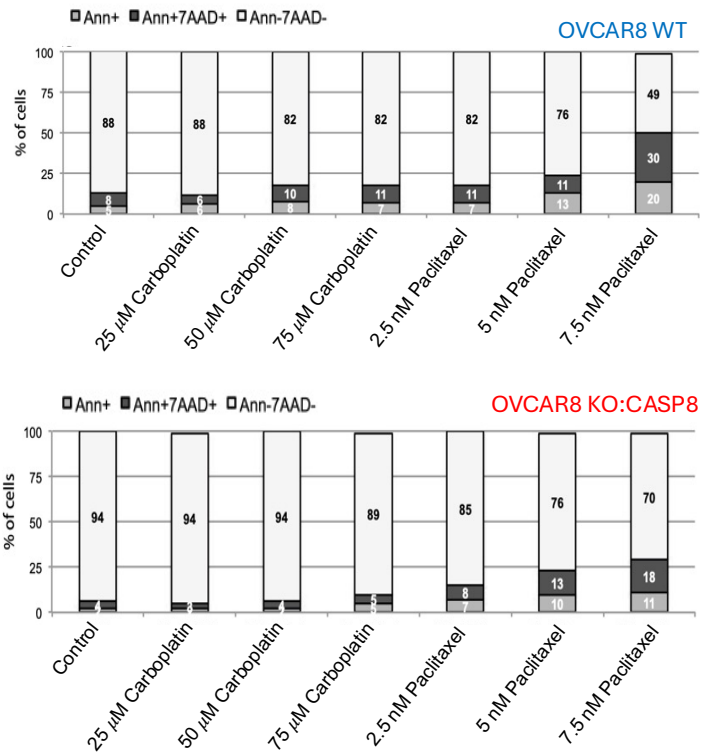

B

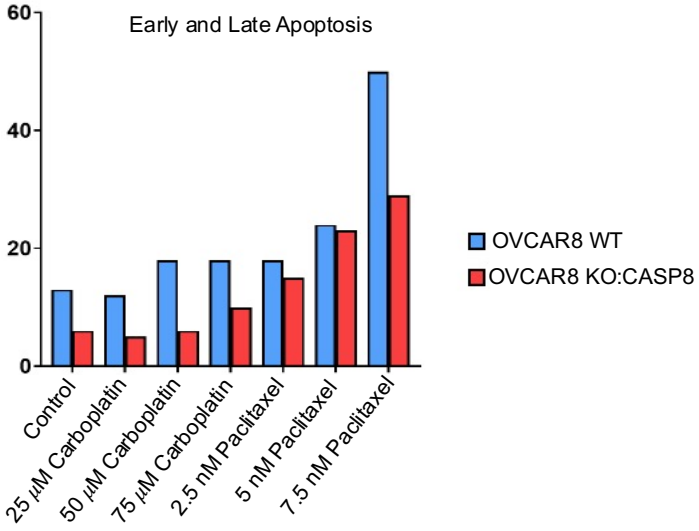

Figure 14: Apoptotic response in OVCAR8 WT and OVCAR8 KO:CASP8 cells following chemotherapy treatment. (A) Distribution of viable, early apoptotic, late apoptotic, and necrotic cell population in OVCAR8 WT (upper panel) and OVCAR8 KO:CASP8 (lower panel) after treatment with carboplatin or paclitaxel followed by a 48-hour incubation period **(B)** Quantification of early and late apoptosis in the OVCAR8 KO:CASP8 cells compared with their WT counterparts across all treatment conditions (Given n=1, further replicated experiments are necessary to validate these results).

Caspase 3/7 activity, measured in bioluminescence units per 1,000 cells (RLU/1,000), generally increased in OVCAR8 WT cells with increasing carboplatin concentrations. In contrast, OVCAR8 KO:CASP8 cells showed lower caspase 3/7 activity across all carboplatin concentrations compared with OVCAR8 WT cells (Figure15).

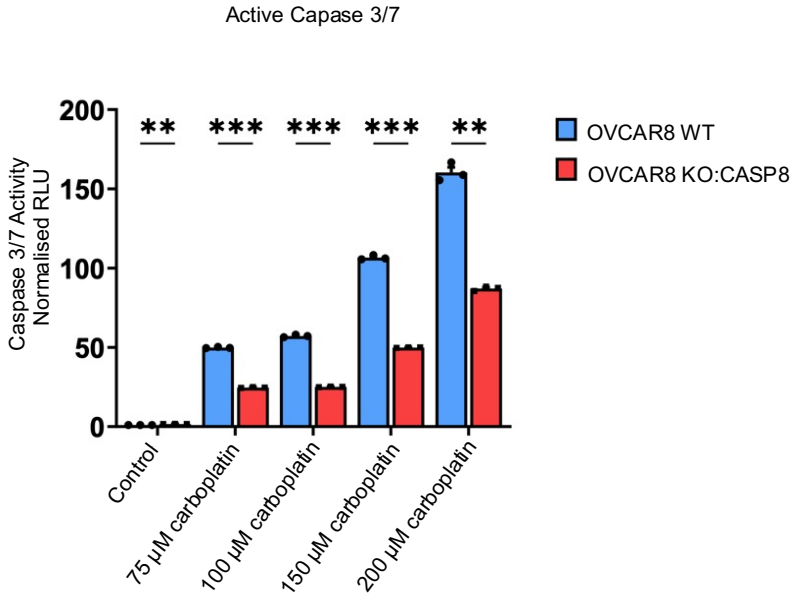

Figure 15: Caspase-3/7 activity in OVCAR8 WT and OVCAR8 KO:CASP8 cells following chemotherapy treatment. Caspase-3/7 activity was quantified using the Caspase-Glo 3/7 assay as relative luminescence units per 1000 cells (RLU/1000) after carboplatin treatment followed by a 72-hour incubation period (Paired T-test; mean ± SEM, n = 3 technical replicates; p- ** < 0.01, *** < 0.001).

In addition, initial western blot results revealed that the expression of PARP1, which plays a role in DNA repair, was elevated in the OVCAR8 KO:CASP8 group relative to the OVCAR8 WT group (Figure 16).

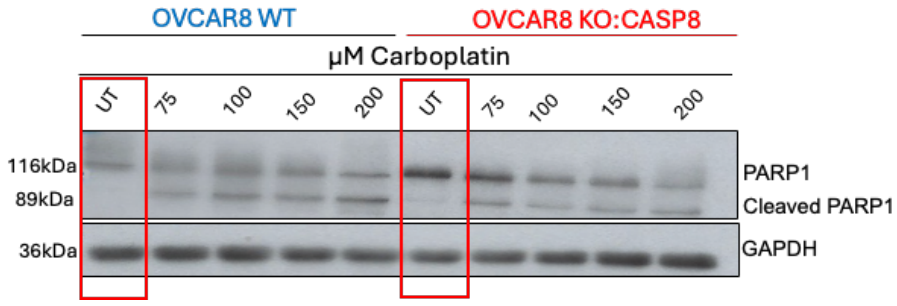

Figure 16: Immunodetection of PARP1 in OVCAR8 WT and OVCAR8 KO:CASP8 cells following carboplatin treatment followed by a 72-hour incubation period.

4.1.5 CASP8 in Cell Migration and Invasion

Initial analysis of the transcriptome data from the OVCAR8 cell line revealed the upregulation of genes associated with cell migration, including NCKAP1L (which regulates the actin cytoskeleton), ADGRG1 (which acts downstream of the Rac1 pathway, known to regulate cell migration, Castro *et al.*, 2020; Ghaffari *et al.*, 2021), and CDH15 (regulating T cell migration, Chimen *et al.*, 2015). In addition, downregulation of genes such as CDH4, ITGB8 (which mediates cell-cell and cell-extracellular matrix interactions), S1PR1 (which couples to Gαi proteins and activates Rac, inducing migration towards S1P gradients, Baeyens *et al.*, 2015) was observed (Table 3). These findings led to the use of 3D invasion assays to investigate whether the absence of CASP8 affects the aggressiveness of OVCAR3 cancer cell lines. To this end, the number of cells invading through the membrane separating the two incubation chambers was quantified. Compared with their respective WT counterparts, a greater number of cells were observed to penetrate the Matrigel membrane in the 3D invasion assay in the OVCAR3 KO:CASP8 groups (Figure 17).

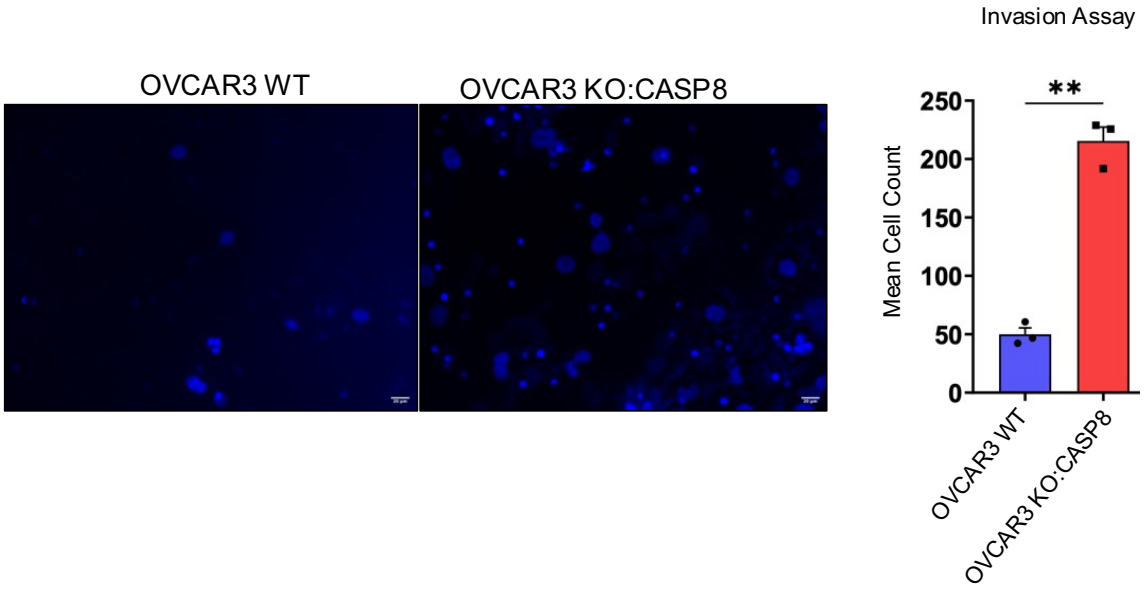

Figure 17: 3D invasion assay comparing OVCAR3 WT and OVCAR3 KO:CASP8 cells. Left panel: Representative microscopic images of cells that invaded through Matrigel-coated transwell membranes after 24 h. Nuclei were stained with DAPI (blue). Magnification: 20×; scale bar: 20 µm. Right panel: Quantitative analysis of cell invasion after 24 hours (Paired t-test; mean ± SEM, n = 3 biological replicates; p- ** < 0.01).

A migration assay was performed to analyse the metastatic potential of tumour cells in both the OVCAR3 WT and OVCAR3 KO:CASP8 groups. OVCAR3 WT cells demonstrated a more rapid migration rate, with significant differences observed at the 24-hour and 40-hour time points, outperforming the OVCAR3 KO:CASP8 cells (Figure 18).

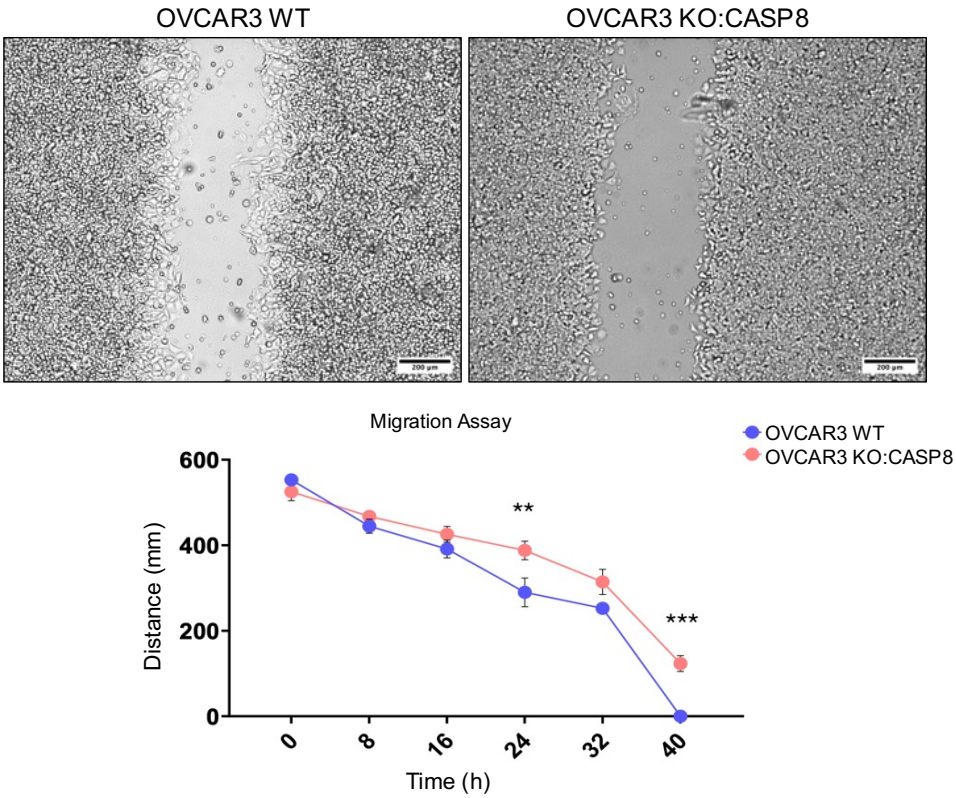

Figure 18: 2D migration assay comparing OVCAR3 WT and OVCAR3 KO:CASP8 cells. Upper panel: Representative microscopic images of the migration assay over a 40-hour period. Magnification: 5×; scale bar: 200 µm. Lower panel: Quantitative analysis of the gap over the indicated time course. WT cells demonstrated a faster migration rate and more efficient gap closure than CASP8 KO cells at the 24h and 40h time points (Unpaired t-test; mean ± SEM, n = 3 biological replicates; p- ** < 0.01, *** < 0.001).

4.1.6 Establishment of Orthotopic Mouse Model of Ovarian Cancer

Luciferase assays were conducted to assess and confirm stable luciferase expression following transfection and cell expansion, which demonstrated successful transfection. In contrast to Luc-OVCAR8 WT cells, luciferase signal intensity was reduced in Luc-OVCAR8 KO:CASP8 cells (Figure 19). As anticipated, non-transfected cells exhibited no detectable signal.

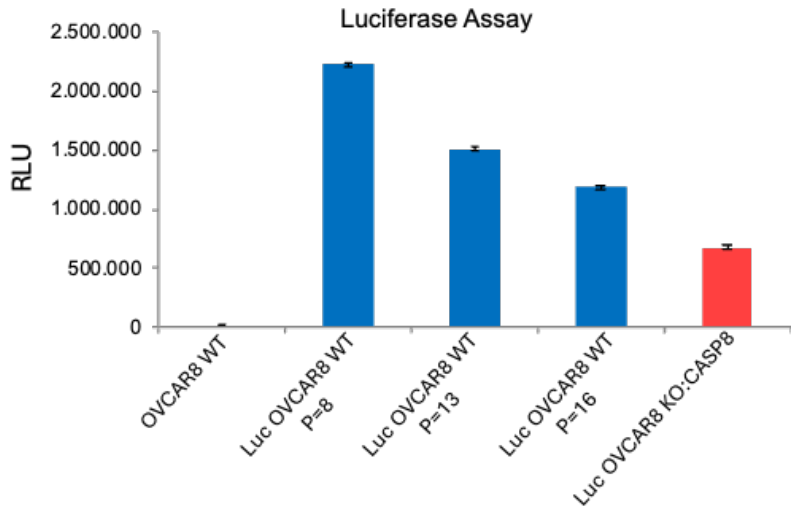

Figure 19: Luciferase assay assessing bioluminescence in OVCAR8 WT and OVCAR8 KO:CASP8 cells. Luciferase signal was quantified to confirm stable luciferase expression (P denotes the passage number of the cells; Luc = luciferase; n = 2 technical replicates).

Results from the orthotopic mouse model showed that OVCAR8 KO:CASP8 tumours grew faster than their WT counterparts. These experiments also demonstrated that the results were more robust when cells were injected exclusively into the bursa of the right ovary, followed by evaluation of potential migration to distant organs. All mice demonstrated a reduction in tumour growth during the initial two- to three-week period following inoculation (Figure 20).

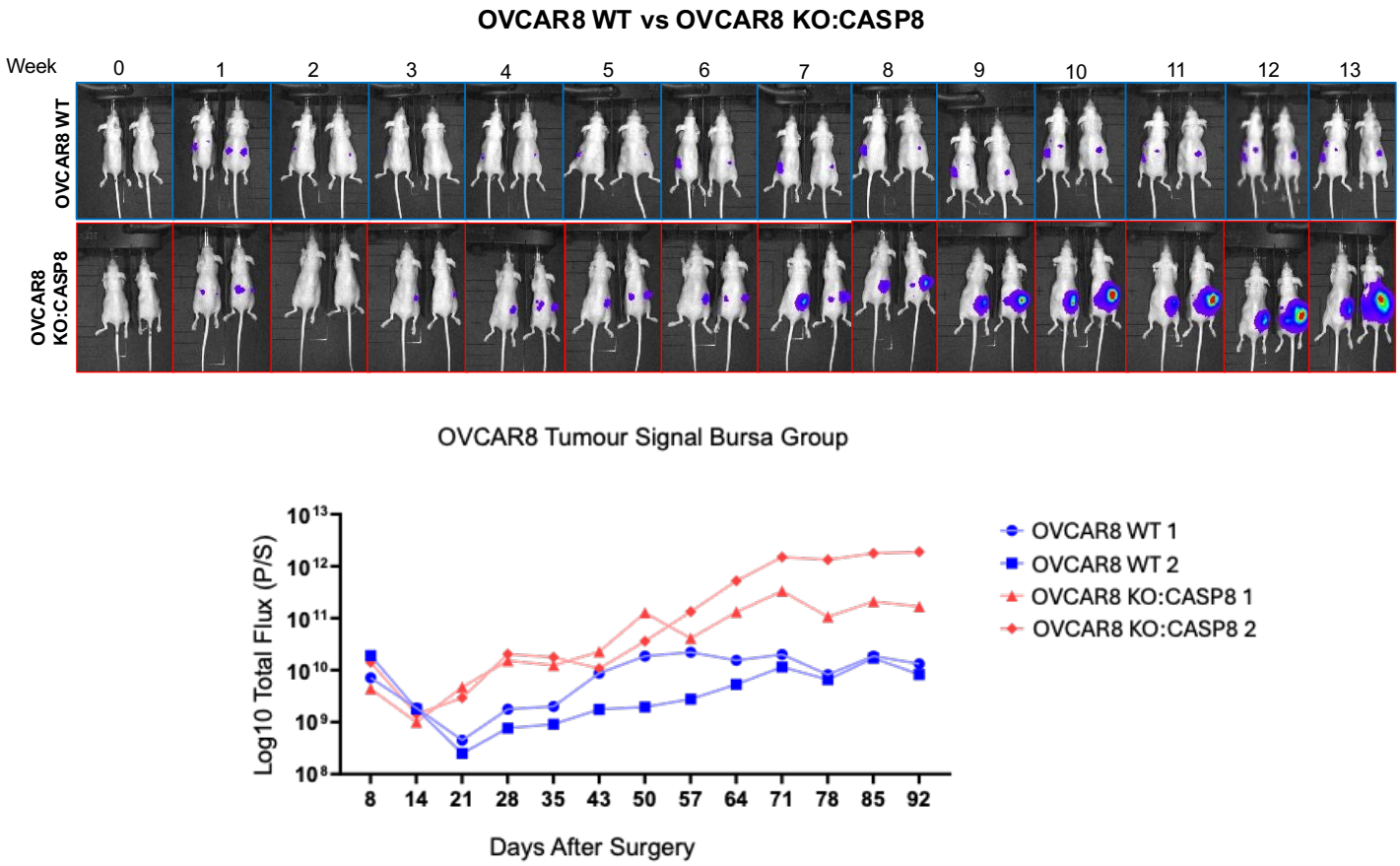

Figure 20: OVCAR8 ovarian cancer orthotopic mouse models. Upper panel: Representative IVIS bioluminescence images acquired weekly over a 13-week period. Lower panel: Quantification of bioluminescent tumour signal in OVCAR8 WT and OVCAR8 KO:CASP8 mice across the duration of the study (n = 2 biological replicates).

Furthermore, CASP8 KO tumours demonstrated metastatic potential to multiple organs, including the kidney, colon, lung, liver, stomach, and omentum. No metastases were identified in these organs in the WT group (Figure 21).

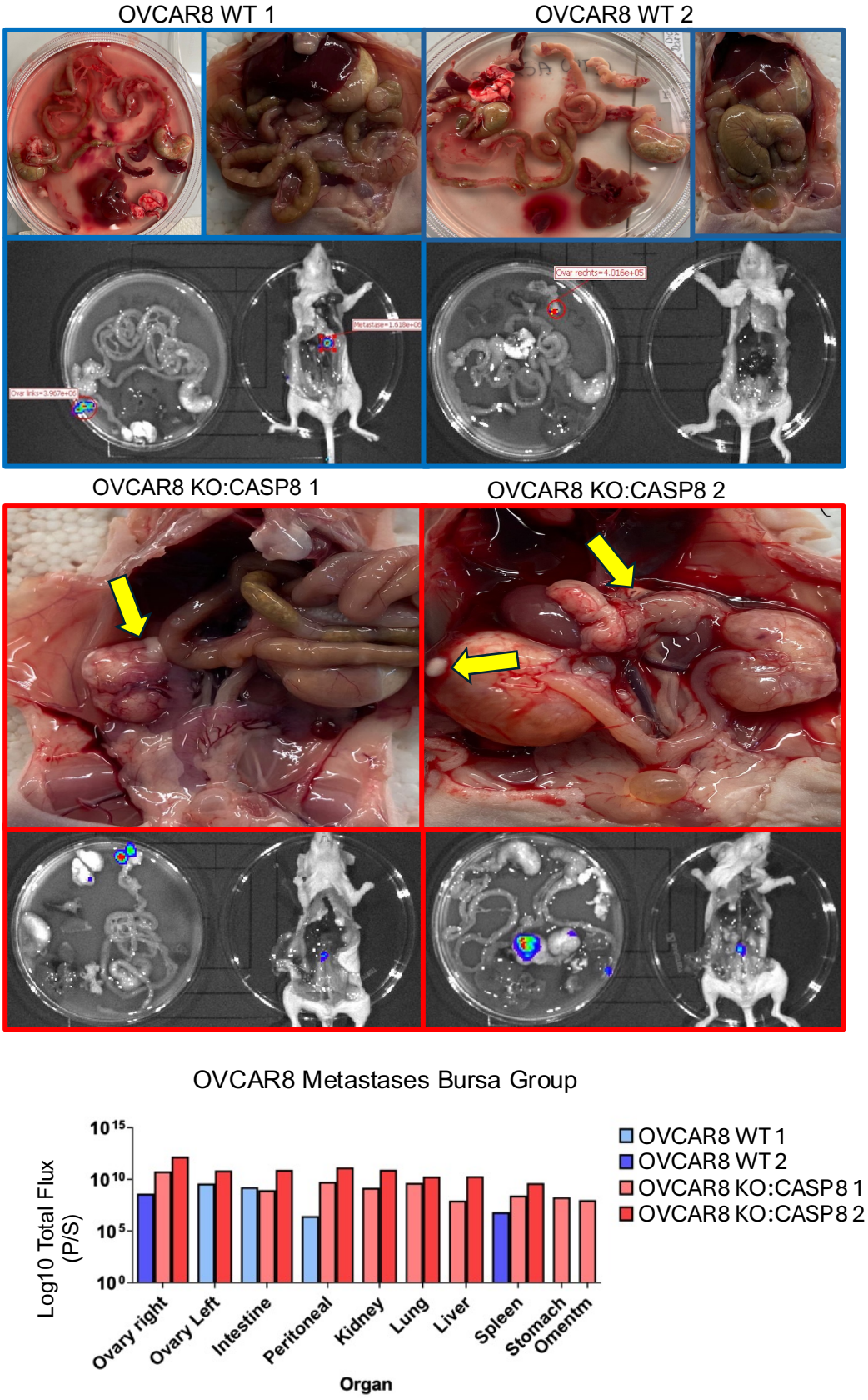

Figure 21: OVCAR8 ovarian cancer orthotopic mouse models. Upper and middle panels: Representative IVIS bioluminescence images of harvested organs (the arrows indicate the visible tumour tissue). Lower panel: Quantification of bioluminescent tumour signals in harvested organs from OVCAR8 WT and OVCAR8 KO:CASP8 mice (n = 2 biological replicates).

Tissue analysis following the TUNEL assay demonstrated that the number of apoptotic cells was comparable between the OVCAR8 WT and OVCAR8 KO:CASP8 groups. No differences were observed between the two groups (Figure 22).

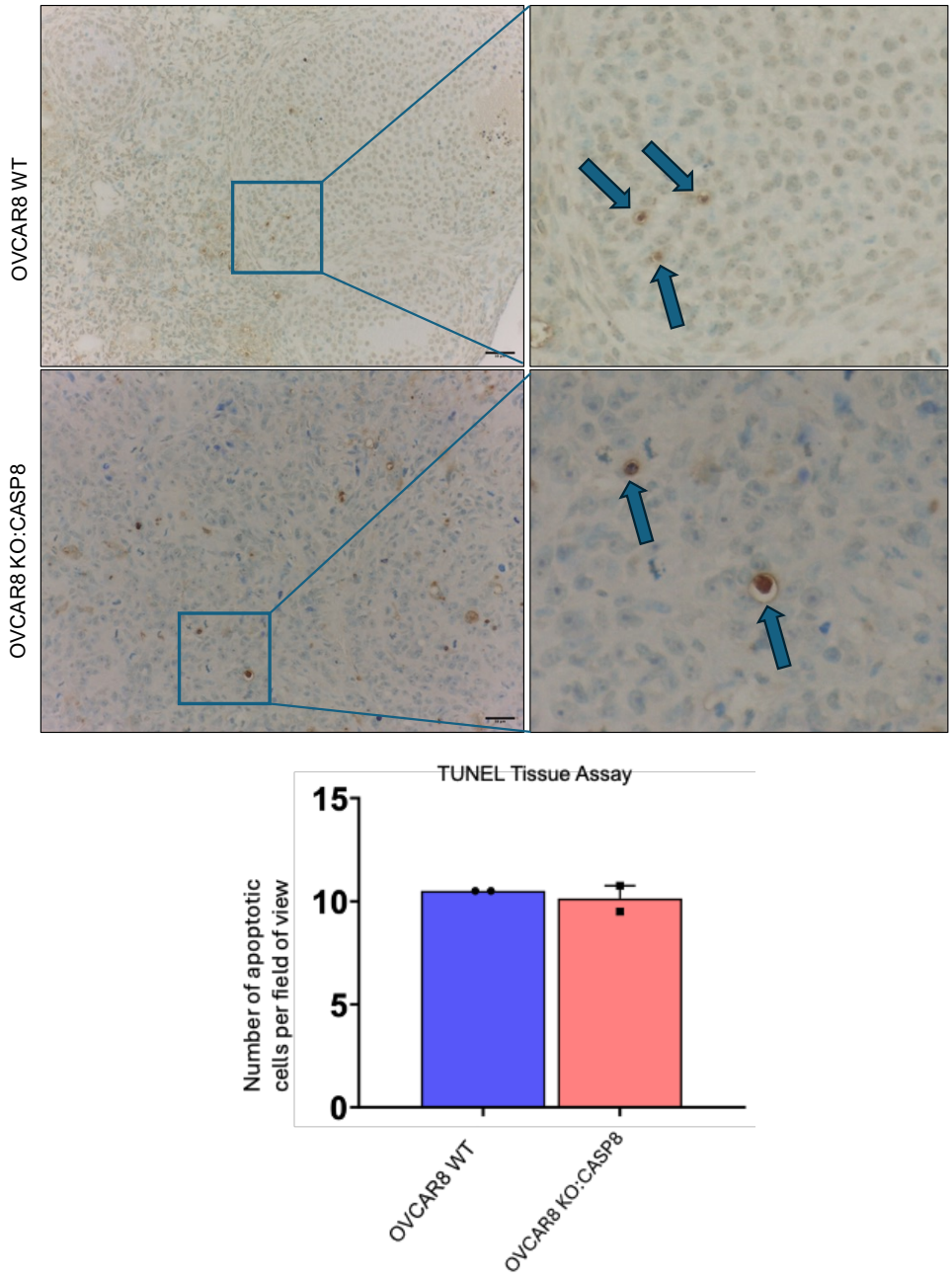

Figure 22: Detection of apoptosis in ovarian tissue of the OVCAR8 orthotopic mouse models. Upper panel: Representative images of apoptotic cells (light brown) in ovarian tissue from OVCAR8 WT and OVCAR8 KO:CASP8 mice using TUNEL assay Counterstaining was performed with methyl green. Magnification = 40×, scale bar = 10 µm. Lower panel: Manual quantification of apoptotic cells in both groups (the arrows indicate the apoptotic cells, n = 2 biological replicates).

4.1.7 Transcriptome Analysis of OVCAR8 Ovarian Cancer Cell Line

First, the effects of CASP8 KO on gene expression in the HGSOC cell line OVCAR8 were investigated. Accordingly, gene expression levels were examined in the following two experimental groups: (1) OVCAR8 WT and (2) OVCAR8 KO:CASP8. Transcriptome analysis revealed 463 up-regulated and 290 down-regulated genes in the CASP8 KO group compared with WT cells (Figure 23).

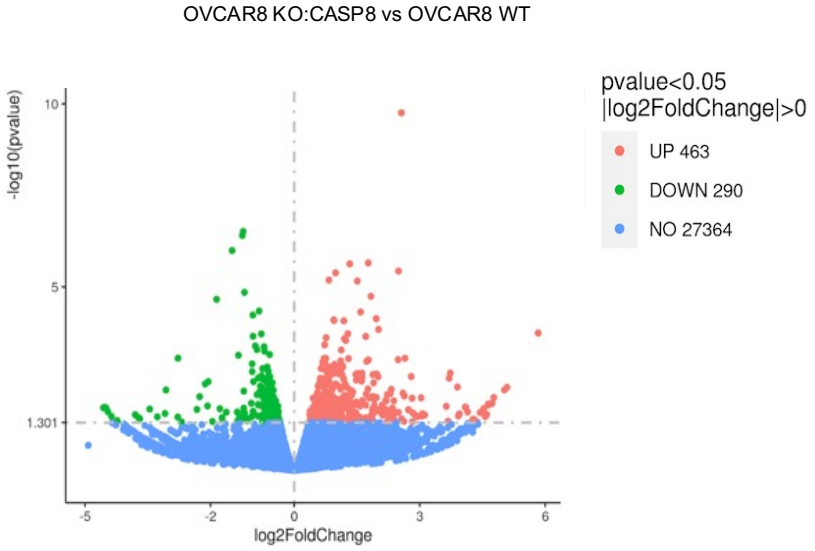

Figure 23: Differential expression analysis of OVCAR8 KO:CASP8 versus OVCAR8 WT cells visualised by volcano plot.
Genes are plotted according to log2fold change (x-axis) and -log10 (p-value, y-axis). Using a significance cutoff of -log10 (p-value) ≥ 1.3, 463 genes were identified as up-regulated (red) and 290 as down-regulated (green) in OVCAR8 KO:CASP8 cells. Genes not meeting the significance threshold are shown in blue.

By applying a comparative approach based on p-value and fold-change cut-offs, the number of genes deemed to be of interest was reduced when comparing expression levels between the experimental OVCAR8 WT and OVCAR8 KO:CASP8 groups.

To ensure that the transcriptomic differences observed between OVCAR8 WT and OVCAR8 KO:CASP8 samples reflect true biological variation rather than technical artifacts, several layers of quality-control validation were performed on the sequencing dataset generated by Novogene. Raw reads showed high quality (Phred Q30 >92%, error rate ~0.03%). After adapter trimming and low-quality read filtering, >95% of reads were retained per sample. Guanine and cytosine (GC) content was uniform across

replicates with no bias. Hierarchical indexing for spliced alignment of transcripts (HISAT2) yielded 95–96% mapped reads, ~93% uniquely mapped, indicating successful library preparation and minimal contamination. Overall, sequencing depth, read quality, GC distribution, and mapping efficiency were sufficient for reliable differential expression analysis.

Functional enrichment analysis of the differentially expressed genes (DEGs) was carried out using DAVID (Database for Annotation, Visualisation, and Integrated Discovery) on the final list of 753 genes. Enriched Gene Ontology (GO) terms revealed that specific biological processes, such as immune response, angiogenesis, cell adhesion, and migration, were upregulated as a result of CASP8 deletion (Figure 24).

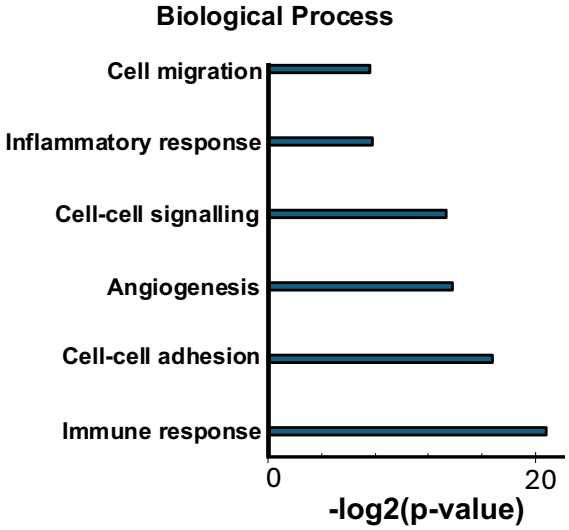

Figure 24: Enrichment analysis of mRNAs up-regulated in the OVCAR8 KO: CASP8 cell line in comparison to OVCAR8 WT: Bar chart representing the six top enriched GO terms within the biological processes category among up-regulated genes associated with CASP8 KO in OVCAR8 cells using DAVID (p-value <0.05 and cutoff +/- 0.58 log2 fold change).

Concurrently, downregulation of genes involved in the regulation of the cell cycle, cell morphology, protein phosphorylation, and miRNA transcription was observed (Figure 25).

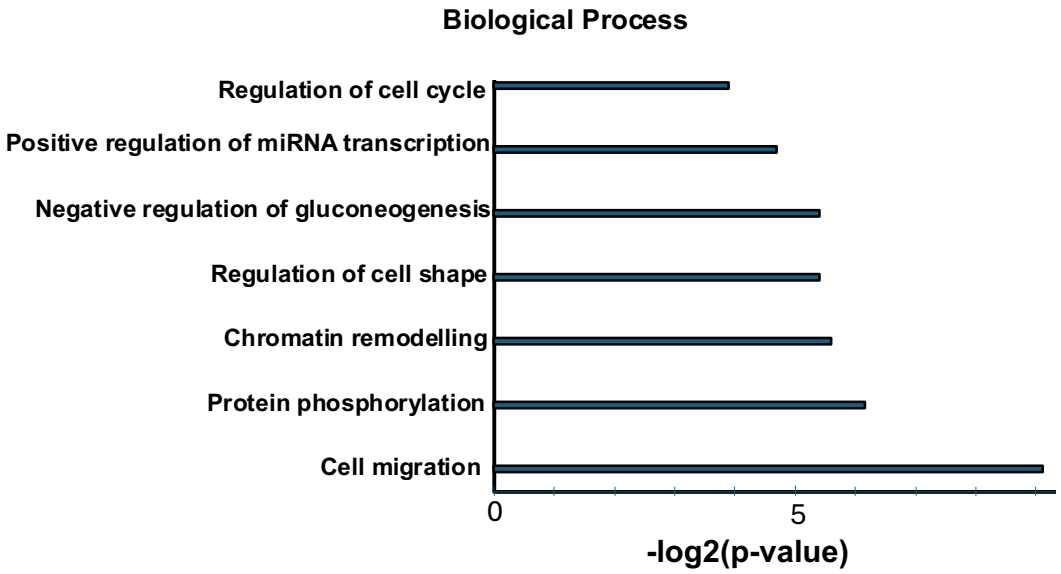

Figure 25: Enrichment analysis of mRNAs down-regulated in the OVCAR8 KO: CASP8 cell line in comparison to OVCAR8 WT: Bar chart representing the seven top enriched GO terms within the biological processes category among down-regulated genes associated with CASP8 KO in OVCAR8 cells using DAVID (p-value <0.05 and cutoff +/- 0.58 log2 fold change).

Finally, genes involved in migration that were either up-regulated or down-regulated were selected (Table 3).

Table 3: Gene Ontology analysis of cell migration associated genes in OVCAR8 KO:CASP8 cells compared with OVCAR8 WT.

Cell Migration	
Up-regulated	**Down-regulated**
NCK associated protein 1 like (NCKAP1L)	cadherin 4 (CDH4)
cadherin 15 (CDH15)	CDC42 binding protein kinase alpha (CDC42BPA)
adhesion G protein-coupled receptor G1 (ADGRG1)	integrin subunit beta 8 (ITGB8)
laminin subunit beta 3 (LAMB3)	sphingosine-1-phosphate receptor 1 (S1PR1)
matrix metallopeptidase 9 (MMP9)	GDNF family receptor alpha 1 (GFRA1)

4.2 In vitro Study of Connexin-43

4.2.1 Establishment of CX43 KO Cell Lines and Analysis of CX43 Expression in OVCAR3 WT and OVCAR3 KO:CASP8 Cells

Following the CRISPR-Cas9 procedure, OVCAR3 cells were harvested for western blot analysis to confirm CX43 KO in both OVCAR3 WT and OVCAR KO:CASP8 cells (Figure 26).

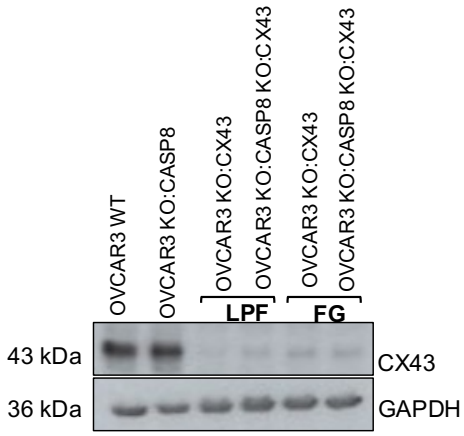

Figure 26: Immunodetection of CX43 protein in OVCAR3 cells (FG= Fugene HD, LPF= Lipofectamin LTX).

The effect of CX43 KO on cell proliferation in OVCAR3 WT and OVCAR3 KO:CASP8 cells was characterised. This analysis revealed that cell lines lacking CX43 exhibited markedly increased proliferation compared with both OVCAR3 WT and OVCAR3 KO:CASP8 cells at the 72- and 96-hour time points (Figure 27).

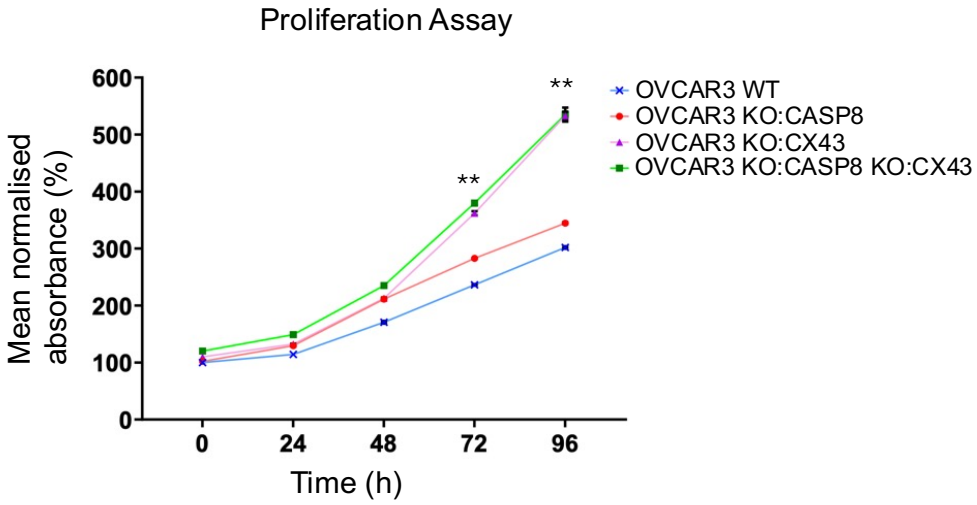

Figure 27: Assessment of cell proliferation in OVCAR3 WT, OVCAR3 KO:CASP8, OVCAR3 KO:CX43, OVCAR3 KO:CASP8 KO:CX43 over a 96-hour period (Mixed-effects model (Geisser–Greenhouse), Tukey test; mean ± SEM, n = 3 technical replicates; p- ** < 0.01 all groups vs. OVCAR3 WT at the 72- and 96-hour time points).

Furthemore, RT-qPCR confirmed that expression of GJA1, the gene encoding CX43, was notabl reduced in the CX43 KO groups compared with their WT counterparts (Figure 28).

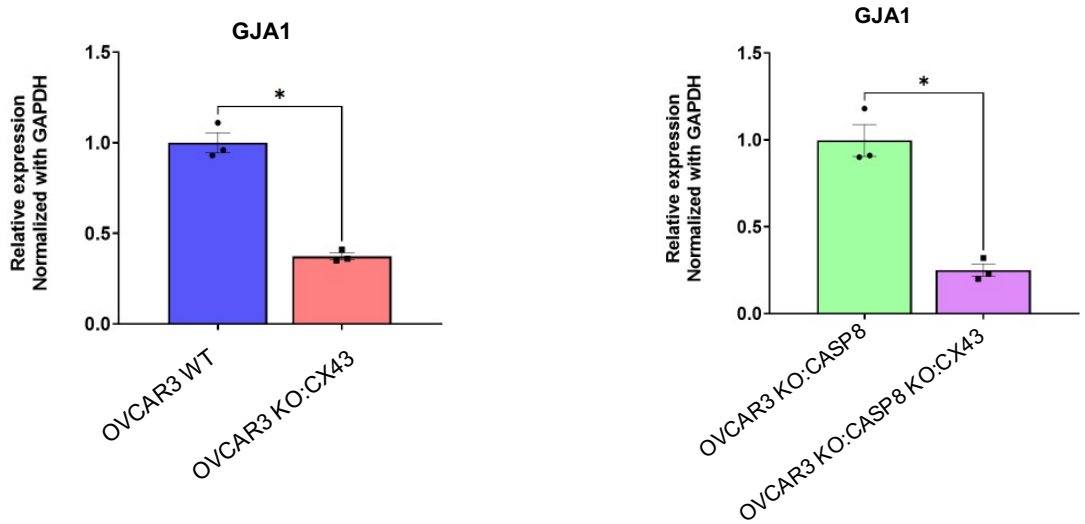

Figure 28: Relative expression of GJA1 mRNA in OVCAR3 WT, OVCAR3 KO:CASP8, OVCAR3 KO:CX43, OVCAR3 KO:CASP8 KO:CX43 cells measured by RT-qPCR (Paired T-test; mean ± SEM, n = 3 technical replicates; p- * < 0.05).

4.2.2 Loss of Caspase-8 in HGSOC Leads to Increased CX43 Expression In Vitro and In Vivo

Transcriptomic analysis of OVCAR8 cells indicated that loss of CASP8 led to increased expression of genes involved in cell-cell adhesion (Figure 24). Consequently, we investigated whether CASP8 KO in HGSOC cell lines, OVCAR3 and OVCAR8, affects CX43 expression. Immunofluorescence analysis revealed that loss of CASP8 in both OVCAR3 and OVCAR8 cell lines resulted in an increase in CX43 protein expression compared with their respective WT cells, as evidenced by the more intense CX43 staining (Figure 29).

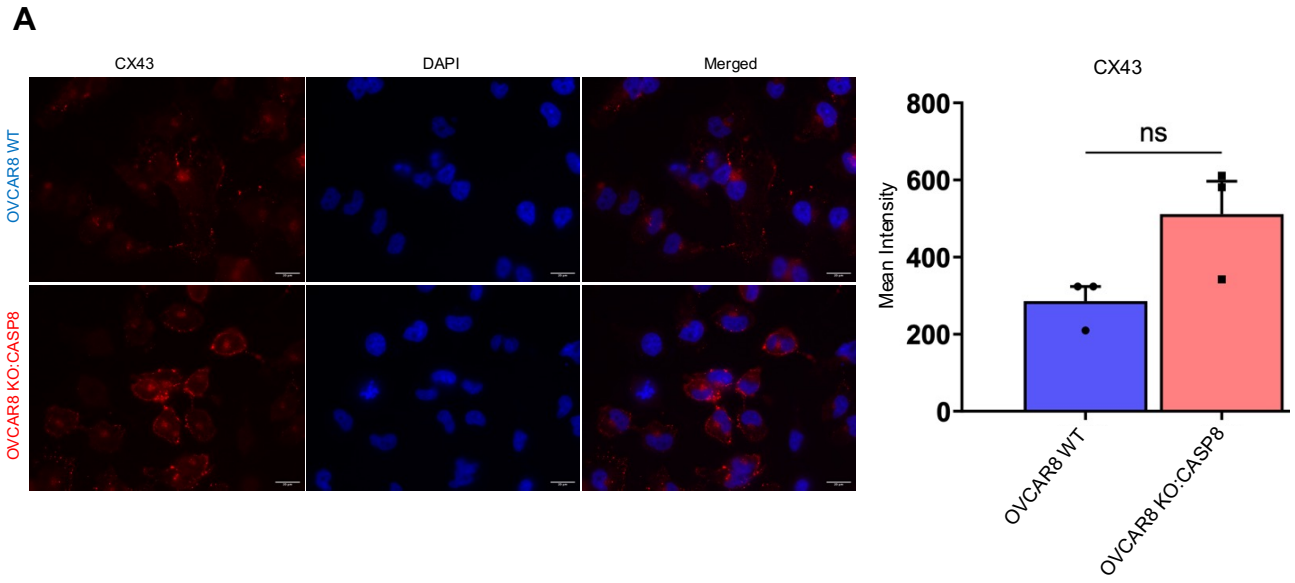

Figure 29: See next page for caption.

B

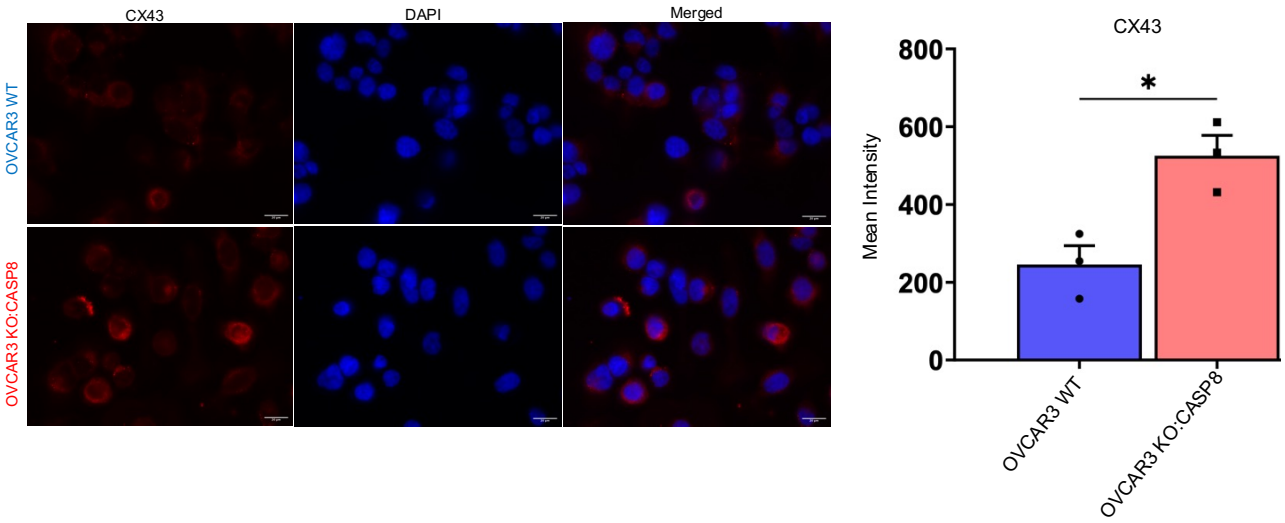

Figure 29: Immunofluorescence staining of CX43 in OVCAR8 and OVCAR3 cells. **(A)** OVCAR8 WT, OVCAR8 KO:CASP8 and **(B)** OVCAR3 WT, OVCAR3 KO:CASP8. Left panels: Representative microscopic images of cells demonstrating CX43 protein expression. Magnification: 40×; scale bar: 20 µm. Right panels: Quantitative analysis of CX43 expression; CX43 is shown in red, nuclei are counterstained with DAPI (blue), and merged images are provided (Paired T-test, mean ± SEM, n = 3 biological replicates; p- *< 0.05) .

This was further confirmed by western blot analysis of cell lysates prepared from OVCAR8 WT, OVCAR8 KO:CASP8, OVCAR3 WT, OVCAR3 KO:CASP8 cells. Consistent with the immunofluorescence results, CX43 expression was elevated in cells lacking CASP8 (Figure 30).

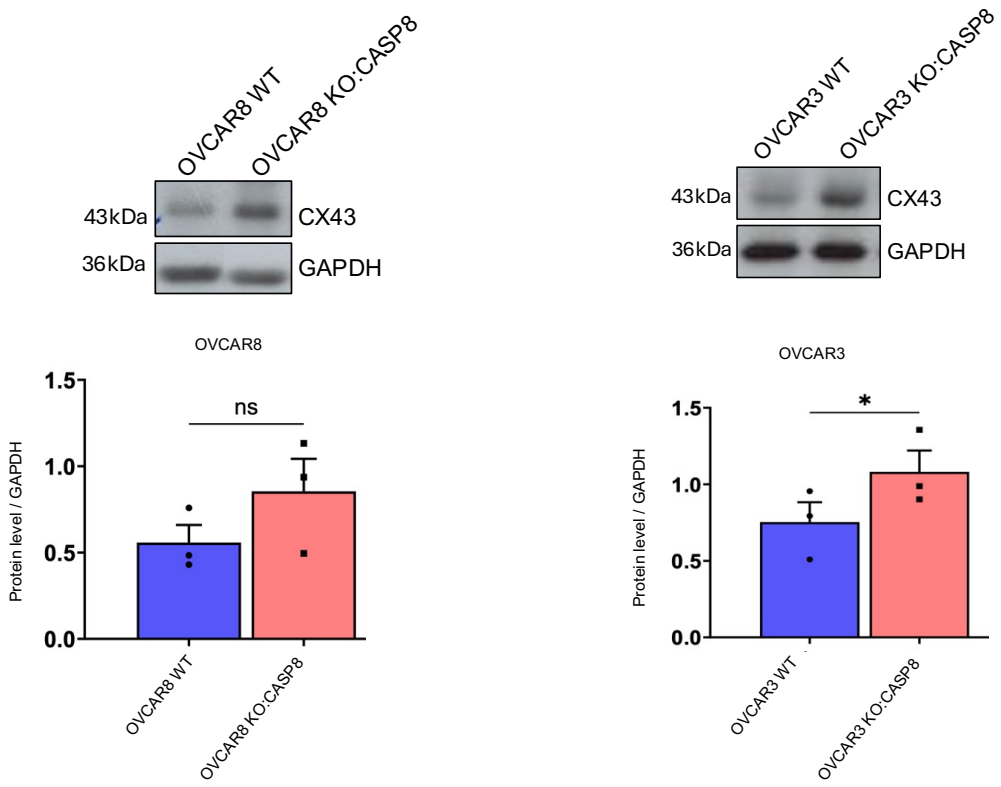

Figure 30: Immunodetection of CX43 protein in OVCAR3/8 WT and OVCAR3/8 KO:CASP8 cells (Paired T-test, mean ± SEM, n = 3 biological replicates; p- *< 0.05).

Subsequently, GJA1 gene expression was analysed by RT-qPCR across all groups, revealing a reduction in GJA1 expression in the OVCAR3 KO:CX43 and OVCAR3 KO:CASP8 KO:CX43 groups (Figure 31).

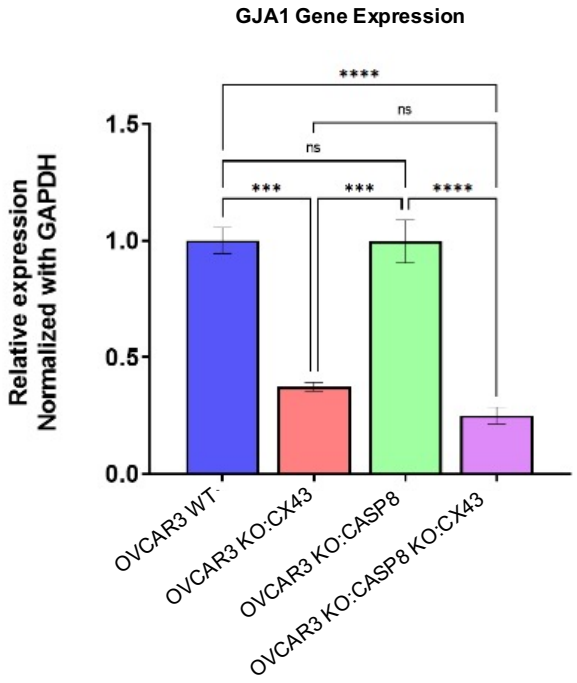

Figure 31: Relative expression of GJA1 mRNA in OVCAR3 WT, OVCAR3 KO:CASP8, OVCAR3 KO:CX43 and OVCAR3 KO:CASP8 KO:CX43 cells measured by RT-qPCR (One way ANAOVA, multiple comparison test using tukey; mean ± SEM, n = 3 technical replicates; p- ***< 0.001, ****<0.0001).

Furthermore, the elevated expression of CX43 in ovarian tissue was observed in an in vivo orthotopic mouse model. CX43 protein levels were higher in the OVCAR8 KO:CASP8 group compared with the WT group (Figure 32). However, due to the high heterogeneity and variability of CX43 staining intensity in the immunohistochemical tissue sections, it was not possible to quantitatively compare signal intensity with the Wt counterpart; therefore, qualitative assessment was employed. In summary, loss of CASP8 in HGSOC results in an upregulation of CX43 expression in both in vitro and in vivo models.

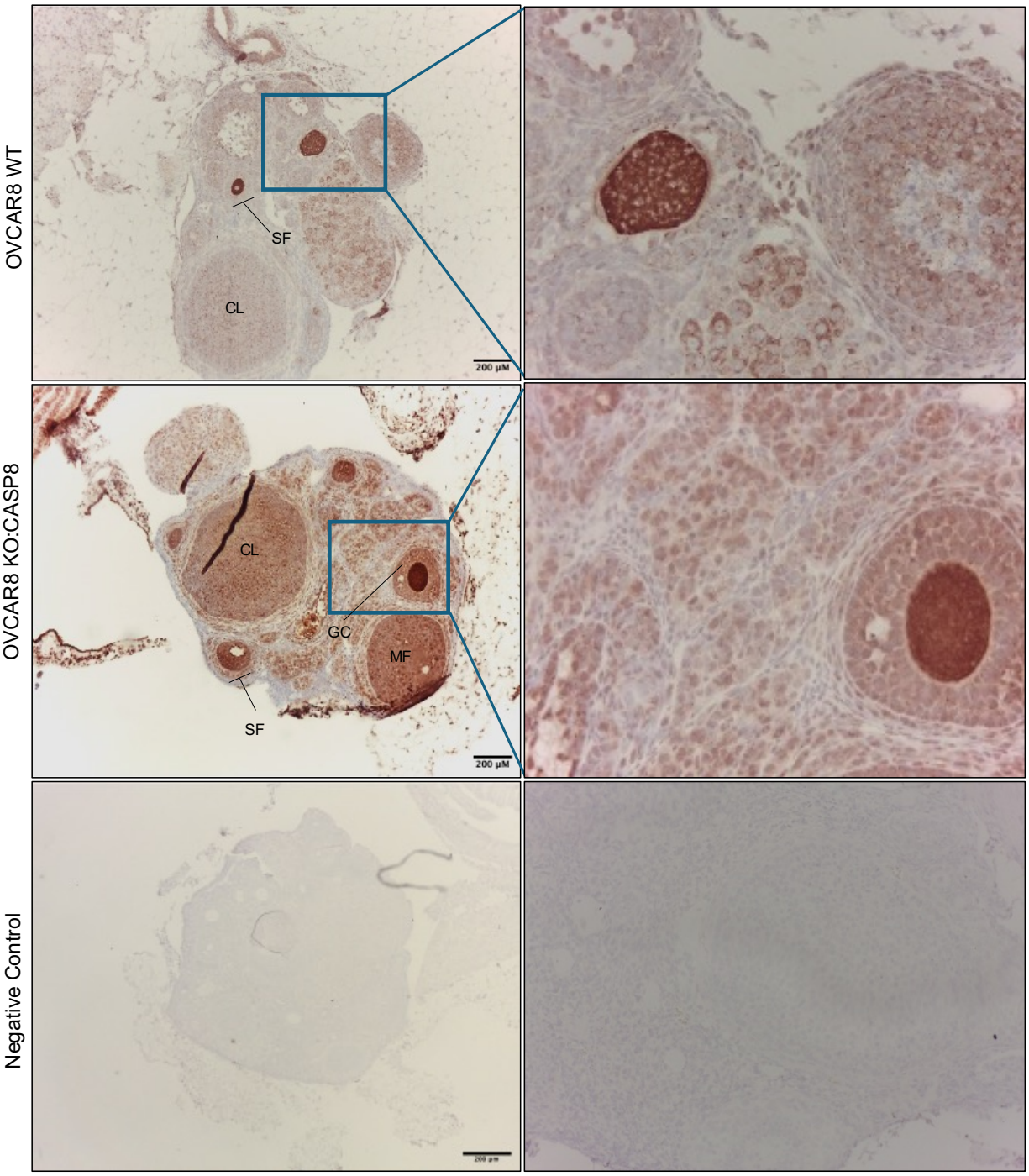

Note: Functional bodies: CL, Corpus luteum; MF, Mature follicle; SF, Secondary follicle; GC, Granulosa cells.

Figure 32: Immunohistochemical detection of CX43 of ovarian tissue in OVCAR8 orthotopic mouse models. Representative immunohistochemical staining for CX43 in ovarian tissue from OVCAR8 WT, OVCAR8 KO:CASP8, and negative control groups. Magnification = 10×, scale bar = 200 µm (n = 2 biological replicates)

4.2.3 Migration and Invasion (CX43)

In view of the aforementioned evidence demonstrating increased CX43 expression in HGSOC cell lines and ovarian tumours lacking CASP8, the aim of this study was to investigate the potential role of CX43 in the invasive capacity of ovarian cancer and its association with CASP8. To this end, 3D invasion assays was performed on OVCAR3 WT, OVCAR3 KO:CASP8, OVCAR3 KO:CX43 and OVCAR3 KO:CASP8 KO:CX43 cells.

The OVCAR3 KO:CASP8 KO:CX43 cells exhibited a significant reduced invasive capacity, as evidenced by the limited number of cells penetrating the Matrigel membrane in the 3D invasion assay, compared with OVCAR3 KO:CASP8 cells. However, no significant difference in invasive potential was observed between the OVCAR3 WT and OVCAR3 KO:CX43 cells (Figure 33).

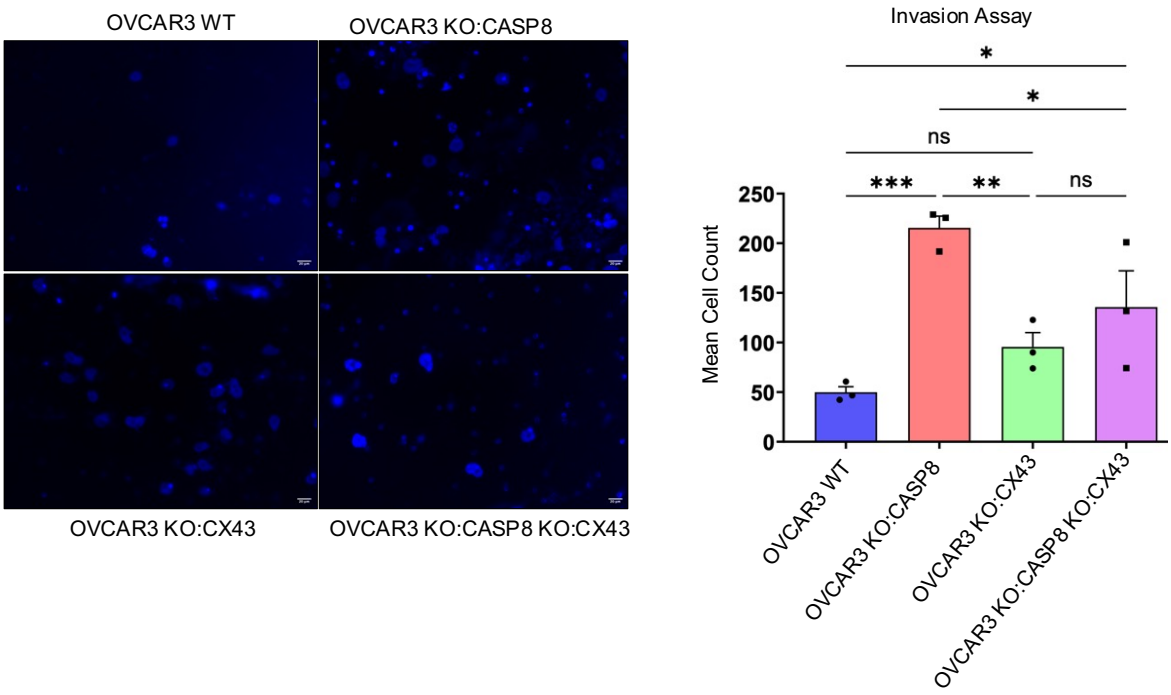

Figure 33: See next page for caption.

Figure 33: 3D invasion assay comparing OVCAR3 WT, OVCAR3 KO:CASP8 OVCAR3 KO:CX43 and OVCAR3 KO:CASP8 KO:CX43 cells. Left panel: Representative microscopic images of cells that invaded through Matrigel-coated transwell membranes. Nuclei were stained with DAPI (blue). Magnification: 20×; scale bar: 20 µm. Right panel: Quantitative analysis of invaded cells after 24 hour (Ordinary one way ANOVA, mean ± SEM, n = 3 biological replicates; p- *< 0.05, ** < 0.01,***< 0.001).

A transwell chamber-based migration assay was performed to determine whether altered CX43 expression also modulates the migratory capacity of ovarian cancer cells. Overall, cells in the OVCAR3 KO:CASP8 KO:CX43 group closed the gap more rapidly than the other experimental groups. Consistent with this observation, at the 24-hour time point, OVCAR3 KO:CASP8 KO:CX43 cells exhibited increased significantly migratory capacity relative to the other groups (Figure 34A). This enhanced migration may be attributable to the elongated cellular morphology observed in OVCAR3 KO:CASP8 KO:CX43 cells (Figure 34B).

The migration assay presented technical limitations. Deletion of CX43, a key component of gap junctions, impaired cell-cell and cell-substrate adhesion. As a result, CX43 KO cells exhibited poor attachment and substantial cell loss during the washing steps prior to measurement. Consequently, the OVCAR3 KO:CX43 group was excluded from subsequent migration analyses.

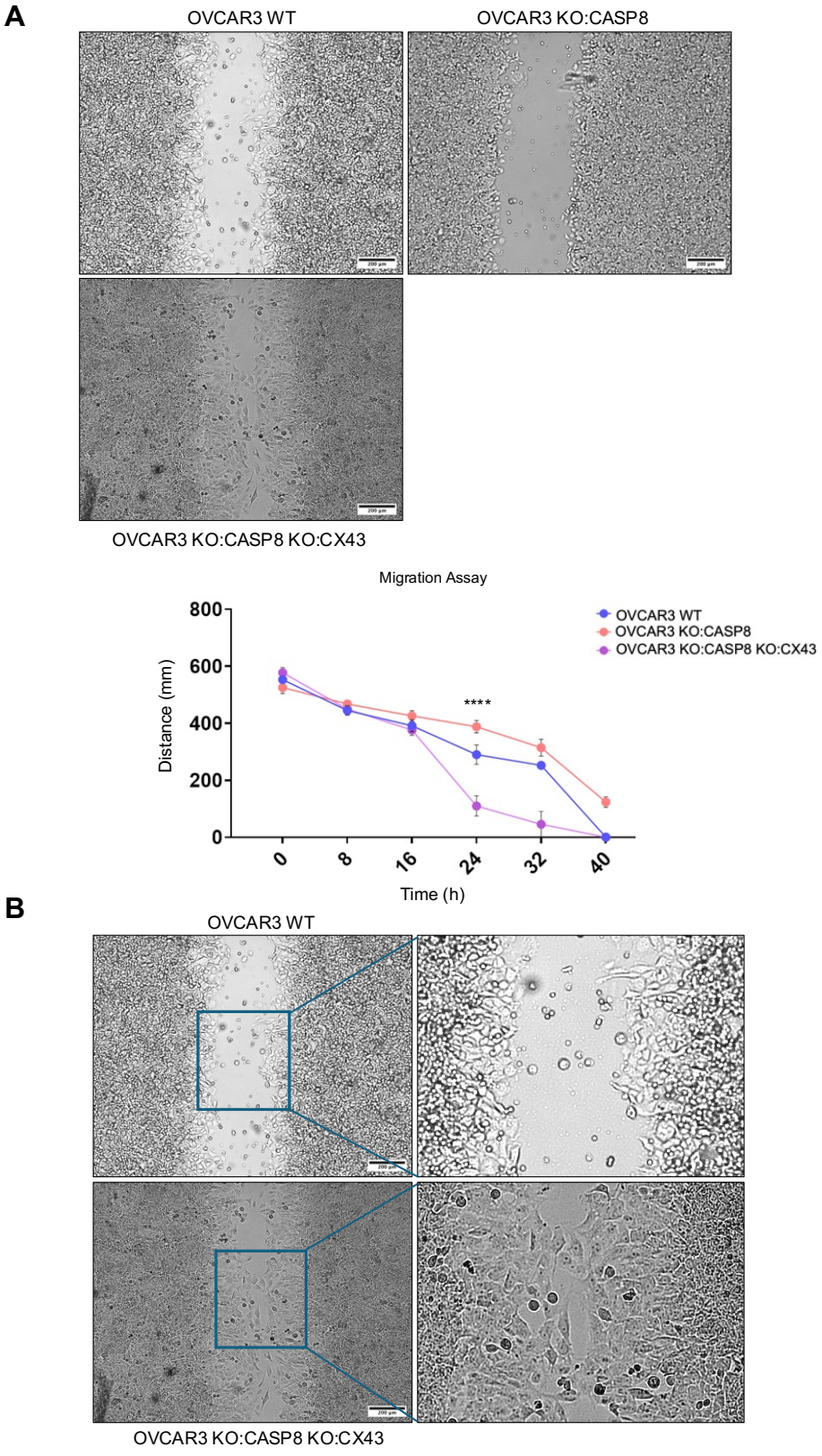

Figure 34: See next page for caption.

Figure 34: 2D migration assay comparing OVCAR3 WT, OVCAR3 KO:CASP8 and OVCAR3 KO:CASP8 KO:CX43. (A) Upper panel: Representative microscopic images of the migration assay over a 40-hour period. Magnification: 5×; scale bar: 200 µm. Lower panel: Quantitative analysis of the gap over the indicated time course (2-way ANOVA, multiple comparison test using tukey, mean ± SEM, n = 3 biological replicates; p ****< 0.0001 OVCAR3 KO:CASP8 KO:CX43 vs. other groups). **(B)** Representative microscopic images of elongated cells morphology in the OVCAR3 KO:CASP8 KO:CX43 cells compared with the OVCAR3 WT cells.

Moreover, the data indicated that loss of CX43 was associated with increased paxillin protein expression; however, further experiments are required to confirm this observation (Figure 35).

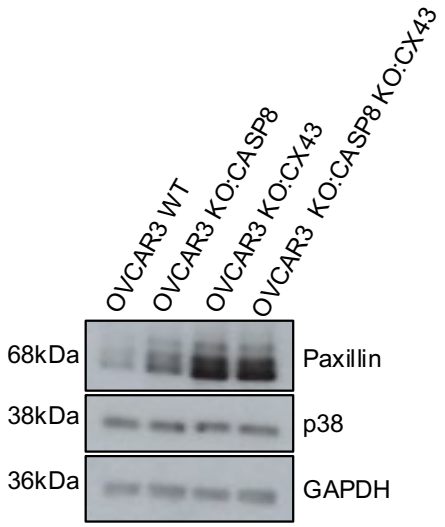

Figure 35: Immunodetection of Paxillin and p38 proteins in OVCAR3 cells.

5. Discussion and Outlook

5.1 Discussion Part I: Study Caspase-8 in High Grade Serous Ovarian Cancer

The standard treatment for ovarian cancer involves a combination of surgical, chemotherapeutic and, in some cases, radiotherapeutic modalities. The typical chemotherapy regimen comprises a platinum-based compound, most commonly carboplatin, in combination with a taxane, usually paclitaxel (Garrido *et al.*, 2021). However, the carboplatin-paclitaxel combination remains the preferred first-line chemotherapy regimen for the treatment of ovarian cancer, with 95% of women diagnosed with ovarian cancer receiving this treatment (Pokhriyal *et al.*, 2019).

Among the most challenging clinical scenarios in ovarian cancer treatment are cases of platinum resistance. These typically recur within six months of completing the initial course of chemotherapy and exhibit a low response rate to subsequent treatments. The PFS is approximately two to four months, and the median survival is greater than one year (Gasimli *et al.*, 2023). In conclusion, the current range of therapeutic options available for the treatment of advanced ovarian cancer is by far insufficient.

According to current estimates, approximately 80% of patients will experience tumour recurrence, while nearly 90% will develop significant toxicity or chemoresistance (Oronsky *et al.*, 2017). It is therefore imperative to develop novel therapeutic strategies to improve overall survival rates (Oronsky *et al.*, 2017). Despite extensive research into the genetic and biochemical pathways associated with platinum resistance in ovarian cancer, the precise mechanisms underlying this phenomenon remain unclear (Li *et al.*, 2020). Among the plethora of potential regulatory mechanisms, the most pivotal ones can be enumerated as follows: (1) DNA repair can be triggered and augmented to rectify DNA damage, (2) Alterations in signalling pathways enabling the cells to circumvent the programmed death or apoptosis (Wang and Lippard, 2005). The available evidence indicates that the most significant genes involved in these mechanisms are, for example, TP53, PARP1, CASP3 and BCL2 (Li *et al.*, 2020).

The findings of this study indicate that low CASP8 expression in ovarian cancer patients is associated with a significantly poorer prognosis compared with patients exhibiting high CASP8 expression.

Clinical evidence obtained from the Kaplan–Meier Plotter database indicates that low CASP8 expression is significantly associated with reduced overall survival in ovarian cancer patients across all tumour grades and stages (https://kmplot.com/analysis/).

Based on the clinical relevance of CASP8 in ovarian cancer, a more comprehensive investigation into the impact of CASP8 deficiency on disease progression and drug response was undertaken in this thesis. Firstly, a transcriptome analysis of the OVCAR8 cell line was performed confirming the aggressive phenotype of ovarian cancers expressing low CASP8.
The absence of CASP8 resulted in the altered expression of numerous genes, including NCKAP1L, ADGRG1, BDKRB1, CDH15, EFNA1 CDH4, ITGB8, S1PR1, SDC2, and GFRA1. These genes are implicated in cell migration, cell adhesion and inflammatory responses, highlighting the non-apoptotic roles of CASP8. In particular, in modulating the cellular transcription through the regulation of RNA polymerase II, as previously demonstrated (Mandal *et al.*, 2022a; Gasimli *et al.*, 2023).

According to the results of the mentioned study, OVCAR3 cell line lacking CASP8 expression showed an increase in the number of invasive cells in the KO group compared to their WT counterparts. This observation contradicts the findings presented in this thesis, in which the migration assay results were reversed. This might be ascribed to the high number of passages of the OVCAR3 used in experiment described in this thesis compared to those in the published study (Gasimli *et al.*, 2023). It is known that the significant difference in cell passage numbers is a critical factor to be considered regarding experimental assays. Notably, cells lacking CASP8 may exhibit an altered and unstable gene expression profile, particularly in the genes identified by the gene enrichment analysis. However, it also confirmed that depletion of CASP8 resulted in both OVCAR8 and OVCAR3 cell lines becoming more aggressive and metastatic, characterised by increased invasion and rapid filling of the migration gap (Gasimli *et al.*, 2023).

Moreover, it has previously been proposed that in MDA-MB-231 cells, CASP8 knockdown markedly diminished cell proliferation in comparison to control cells, while having no impact on cell viability. The elevated levels of the cell cycle regulators p21 and p27 and the delayed G0/G1 → S phase transition were observed to coincide with this reduction in cell growth (De Blasio *et al.*, 2016).

The results of this thesis further suggest that OVCAR8 cells lacking CASP8 expression exhibit increased resistance to carboplatin and paclitaxel; however, additional experiments are required to validate this observation. The observed resistance can be attributed either to a low sensitivity of these cells to DNA damaging agents or to the fact that the loss of CASP8 increases the baseline levels rendering these cells more resilient to DNA damage agents. This hypothesis could be experimentally validated by assessing markers of double-strand breaks, such as γ-H2AX and 53BP1, using immunofluorescence. An increase in these markers would be expected in untreated OVCAR3/8 KO:CASP8 cells compared to their WT counterparts. Unfortunately, due to time constraints, these experiments could not be conducted during this thesis; however, they are planned as part of future investigations.

Furthermore, it was determined that loss of CASP8 in HGSOC cells interferes with the response to DNA damage by significantly lowering the G2/M arrest upon treatment with carboplatin compared with the WT counterparts. This finding confirms the previous hypothesis and suggests that the loss of CASP8 desensitises HGSOC cells to platin-based standard therapy and increases their tolerance to DNA damage.

The results are corroborated by the study of Ranadip Mandal, who has previously demonstrated that cervical tumours with dysregulated expression of CASP8 display heightened aggressiveness, invasiveness and chemoresistance. This is achieved through the regulation of the cell cycle and the modulation of the G2/M phase arrest upon DNA damage treatment (Mandal *et al.*, 2022a).

Taken together, these findings indicate that CASP8 possesses a broader functional repertoire beyond its well-established role in apoptosis initiation. The differential activation, expression and regulation of CASP8 in different cancer types illustrates the extensive context-dependent roles it plays in ovarian cancers. CASP8 appears to play key roles in controlling the pathways involved in metastasis in cervical an ovarian cancer. It is noteworthy that CASP8's anti-metastatic action in this context appears to

be regulated at the transcriptional level and, more significantly, is independent of its involvement in apoptosis induced by death receptors.

5.2 Discussion Part II : Orthotopic Mouse Model

The development of appropriate animal models of ovarian cancer is essential for drug screening and the conduct of preclinical studies. Positive findings observed in early-stage (preclinical) research are frequently reported as being highly promising. This is evidenced by the fact that highly encouraging preclinical results obtained in mouse models often fail to demonstrate efficacy in phase III clinical trials involving patients with metastatic tumours (Guo *et al.*, 2017). It is likely that this discrepancy between preclinical success and clinical outcomes is largely attributable to the limited use of mouse models that recapitulate spontaneous metastatic or advanced disease (Guo *et al.*, 2017).

In orthotopic models, tumour cells or tissues are grafted directly into the ovaries. This model closely mimics several key characteristics of human ovarian cancer, including gene expression profiles, histopathological features, clinical disease progression and interactions between cancer cells and the surrounding microenvironment (Céspedes et al. 2017). The establishment of a bioluminescent orthotopic mouse model for HGSOC required the testing of multiple cell lines and optimisation of the procedure, with due consideration of ethical and regulatory requirements. In addition to the technical complexities associated with orthotopic tumour inoculation, two factors require particular attention: 1) the accurate implantation of cells into the ovary, and 2) the monitoring of tumour growth. With respect to the first factor, previous studies have reported variable outcomes following intraperitoneal and subcutaneous implantation approaches. However, implantation of tumours within the ovarian bursa remains a relatively rare occurrence (Hernandez *et al.*, 2016).

The capacity of injected cancer cells to proliferate differs depending on the type of mouse tissue. Prior to this project, colleagues in our laboratory attempted to orthotopically inoculate the OVCAR3 cell line into the mouse ovary. Despite undergoing several passages in mouse models, the OVCAR3 cells failed to form intra-bursal tumours. Consequently, the choice of animal model (intraperitoneal, subcutaneous or intrabursal) and the tissue microenvironment are critical factors

determining the suitability of one cell line over another. Secondly, long-term surveillance of mouse models is essential to monitor tumour growth, progression, metastasis and therapeutic response. The BLI system as a non-invasive method monitors the luminescence produced by luciferase in a living organism (Khalil *et al.*, 2013). The OVCAR8 tumour cell line, stably transfected with a luciferase-expressing vector, successfully demonstrated the potential of this technique as a valuable, non-invasive tool for monitoring tumour growth in vivo.

In comparison to conventional xenograft models (such as subcutaneous or intraperitoneal injections of tumour cells), an orthotopic animal model offers the following advantages: 1) it accurately replicates the primary site of tumour formation, 2) it accurately represents the common site of metastases and 3) it allows tumour cells to interact with the appropriate microenvironment (Cordero *et al.*, 2010). In rodents, the ovary is enclosed within a unique structure known as the bursal membrane (ovarian bursa), which is connected to the oviduct. The distinctive anatomy of rodents allows for the orthotopic injection of ovarian tumour cells. Intrabursal implantation of ovarian tumour cells results in disease progression that closely mirrors the behaviour observed in human ovarian cancer. As the tumour grows, it expands within the intrabursal membrane and subsequently disseminates into the peritoneal cavity.

The objective of this study was to develop an HGSOC mouse model, despite the existence of a previously described method for generating an ovarian orthotopic murine model (Cordero *et al.*, 2010). In this study, the addition of 2% Matrigel to the cell suspension for intrabursal injection at body temperature helped to minimise cell leakage from the ovarian bursa.
The results of the 3D invasion assays, which demonstrate the aggressiveness of OVCAR3 KO:CASP8 cells in an invasion chamber, were extended to a small group of mice in the bioluminescence orthotopic mouse model of ovarian cancer. The HGSOC model revealed that ovarian cancer cells lacking CASP8 were more aggressive in vivo than their WT counterparts. Tumours lacking CASP8 exhibited increased invasiveness and the capacity to metastasise from the ovary to multiple distant organs.

In summary, the use of orthotopic models of OVCAR8 WT and OVCAR8 KO:CASP8 KO ovarian cancers will facilitate the acquisition of important insights into three key

areas: 1) the growth and metastasis of ovarian cancer, 2) the impact of CASP8 loss on tumour growth, metastasis and potential therapy response, and 3) the development of innovative therapeutic strategies to enhance standard treatment modalities which could be considered in near future.

5.3 Discussion Part III : Study Connexin-43 in High Grade Serous Ovarian Cancer

CX43 channels represent a promising target for direct drug delivery into the cytoplasm of cancer cells due to their permeability to both small and large molecules. Given that CX43 hemichannels increase the permeability of cancer cells to chemotherapeutic agents, they may enhance therapeutic efficacy. A substantial body of experimental evidence indicates that connexins, due to their pro- and anti-tumourigenic properties, may play a causal role in cancer aetiology (Bonacquisti and Nguyen, 2019). In this study, the first to address this topic, the role of CX43 in HGSOC, its relation to CASP8, and its potential as a target for therapy in the context of HGSOC were investigated. Clinical correlation analysis using the Kaplan-Meier Plotter database revealed that, irrespective of tumour stage or grade, high CX43 expression is significantly associated with poor overall survival in ovarian cancer patients (https://kmplot.com/analysis/).

To ascertain the relationship between CASP8 and CX43, experiments were conducted to analyse CX43 expression in the absence of CASP8. Immunofluorescence analysis indicated that CX43 expression was significantly higher in OVCAR3/8 CASP8 knockout cells than in their WT counterparts. In light of the immunofluorescence results, it can be inferred that the absence of CASP8 prompts tumour cells to overexpress both membranous and cytosolic CX43, thereby promoting tumour growth and invasion of HGSOC.

Previous studies investigating the interplay between CX43 and apoptosis have suggested that the CX43-Bax interaction may contribute to the initiation of the mitochondrial apoptotic pathway (Sun *et al.*, 2012). Bax is a key effector protein involved in mitochondrial membrane permeabilisation, which initiates the intrinsic apoptotic pathway (Peña-Blanco and García-Sáez, 2018). This suggests recruitment

of CX43 to the mitochondria, where it may form hemichannels that transduce apoptotic signals, including calcium signalling and cytochrome c release, highlighting the significance of CX43 in cellular apoptosis (Sun *et al.*, 2012).

Interestingly, the results of this study also demonstrated that reduced CX43 expression in HGSOC cells decreased invasive capacity. This finding highlights the pro-tumourigenic effects of CX43 in the cell models used in this study. This finding also corroborates the clinical evidence indicating that CX43 is associated with a reduction in the overall survival of ovarian cancer patients.

Gap junctions are of significant importance in the processes of tumour cell invasion and migration, occurring through both EMT-dependent and independent pathways (Zhou *et al.*, 2023). EMT is a process that transforms epithelial cells into mesenchymal cells, enhancing cell invasion and migration. This process is typically associated with a reduction in E-cadherin levels and an increase in mesenchymal markers, such as N-cadherin (Odero-Marah *et al.*, 2018). CX43, which is co-localised with E-cadherin or N-cadherin, has been detected in numerous types of cancer cells (Yang *et al.*, 2021). It has the capacity to regulate EMT, either as monomers or in a GJIC-dependent manner. Overexpression of CX43 can increase E-cadherin expression and decrease cellular invasive and migratory abilities (Yu *et al.*, 2014). This phenomenon may be regulated by aberrant paxillin expression, which in turn regulates a number of different biological functions, including tumour migration, heterotypic adhesion and invasion (Liu *et al.*, 2023).

The migration assay yielded technically challenging results. To perform the migration assay, a OVCAR3 KO:CX43 and OVCAR3 KO:CASP8 KO:CX43 cell lines were generated. Given the crucial role of CX43 in forming gap junctions, the deletion of CX43 appears to disrupt cellular contact, resulting in CX43 KO cells exhibiting weaker attachment to the surface of cell culture dishes and to each other compared to OVCAR3 WT counterparts. Consequently, the OVCAR3 KO:CX43 group was excluded from migration assay analyses due to substantial cell loss during the washing steps preceding measurement.

It was detected that the OVCAR3 KO:CASP8 KO:CX43 cells displayed a significantly higher migration compared with OVCAR3 WT or OVCAR3 KO:CASP8 cells. Moreover, the loss of CX43 results in an increase in the protein expression of Paxillin,

a multifunctional multidomain focal adhesion adaptor protein that can positively and negatively regulate cell migration (Nishiya *et al.*, 2005; Nayal *et al.*, 2006; Liu *et al.*, 2023). These preliminary findings suggest a complex role for CX43 in ovarian cancer progression that warrants further investigation, particularly with respect to the activated form of p38 (p-p38). p38 activation can increase tumour cell invasion and migratory activity in various cancer types (Hong *et al.*, 2015). Furthermore, the transcriptomic and proteomic data of the OVCAR8 and OVCAR3 cell lines will be subjected to an in-depth analysis to identify key genes or proteins, with altered expression, that are pivotal for the biological process of migration. Subsequently, the aim will be to re-assess cell migration and metastatic behaviour in HGSOC cells deficient in CX43 following the sequential deletion of this target within our experimental framework.

In conclusion, CX43 might represent a significant target for HGSOC treatment, given its role in the pro-tumourigenic processes. However, further investigations are necessary to elucidate the underlying mechanism and its relationship with CASP8. Furthermore, comprehensive analysis of transcriptomic and proteomic datasets, together with the generation of orthotopic mouse models of CX43 Ko alone and in combination with CASP8 KO, would be invaluable for in vivo studies.

References

1) Loewenstein WR, Kanno Y. Intercellular communication and the control of tissue growth: lack of communication between cancer cells. Nature. 1966;209:1248–9.

2) Aasen, T. *et al.* (2016) 'Gap junctions and cancer: communicating for 50 years', *Nature Reviews Cancer*, 16(12), pp. 775–788. Available at: https://doi.org/10.1038/nrc.2016.105.

3) Aasen, T. *et al.* (2019) 'Connexins in cancer: bridging the gap to the clinic', *Oncogene*, 38(23), pp. 4429–4451. Available at: https://doi.org/10.1038/s41388-019-0741-6.

4) Ackert, C.L. *et al.* (2001) 'Intercellular Communication via Connexin43 Gap Junctions Is Required for Ovarian Folliculogenesis in the Mouse', *Developmental Biology*, 233(2), pp. 258–270. Available at: https://doi.org/10.1006/dbio.2001.0216.

5) AlHilli, M.M. *et al.* (2016) 'In vivo anti-tumor activity of the PARP inhibitor niraparib in homologous recombination deficient and proficient ovarian carcinoma', *Gynecologic Oncology*, 143(2), pp. 379–388. Available at: https://doi.org/10.1016/j.ygyno.2016.08.328.

6) Alsop, K. *et al.* (2012) '*BRCA* Mutation Frequency and Patterns of Treatment Response in *BRCA* Mutation–Positive Women With Ovarian Cancer: A Report From the Australian Ovarian Cancer Study Group', *Journal of Clinical Oncology*, 30(21), pp. 2654–2663. Available at: https://doi.org/10.1200/JCO.2011.39.8545.

7) Oronsky, Bryan et al. "A brief review of the management of platinum-resistant-platinum-refractory ovarian cancer." *Medical oncology (Northwood, London, England)* vol. 34,6 (2017): 103. doi:10.1007/s12032-017-0960-z'.

8) Baeyens, A. *et al.* (2015) 'Exit Strategies: S1P Signalling and T Cell Migration', *Trends in Immunology*, 36(12), pp. 778–787. Available at: https://doi.org/10.1016/j.it.2015.10.005.

9) Bandiera, E. *et al.* (2013) 'Cancer antigen 125, human epididymis 4, kallikrein 6, osteopontin and soluble mesothelin-related peptide immunocomplexed with immunoglobulin M in epithelial ovarian cancer diagnosis', *Clinical Chemistry and Laboratory Medicine*, 51(9), pp. 1815–1824. Available at: https://doi.org/doi:10.1515/cclm-2013-0151.

10) Bast, R.C., Hennessy, B. and Mills, G.B. (2009) 'The biology of ovarian cancer: new opportunities for translation', *Nature Reviews Cancer*, 9(6), pp. 415–428. Available at: https://doi.org/10.1038/nrc2644.

11) Bates, D.C. *et al.* (2007) 'Connexin43 enhances glioma invasion by a mechanism involving the carboxy terminus', *Glia*, 55(15), pp. 1554–1564. Available at: https://doi.org/10.1002/glia.20569.

12) Behrens, J. *et al.* (2010) 'The carboxyl tail of Cx43 augments p38 mediated cell migration in a gap junction-independent manner', *European Journal of Cell Biology*, 89(11), pp. 828–838. Available at: https://doi.org/10.1016/j.ejcb.2010.06.003.

13) Bejarano, I., Rodríguez, A.B. and Pariente, J.A. (2018) 'Apoptosis Is a Demanding Selective Tool During the Development of Fetal Male Germ Cells', *Frontiers in Cell and Developmental Biology*, 6, p. 65. Available at: https://doi.org/10.3389/fcell.2018.00065.

14) Berek, J.S. *et al.* (2021) 'Cancer of the ovary, fallopian tube, and peritoneum: 2021 update', *International Journal of Gynecology & Obstetrics*, 155(S1), pp. 61–85. Available at: https://doi.org/10.1002/ijgo.13878.

15) Berns, E.M.J.J. and Bowtell, D.D. (2012) 'The Changing View of High-Grade Serous Ovarian Cancer', *Cancer Research*, 72(11), pp. 2701–2704. Available at: https://doi.org/10.1158/0008-5472.CAN-11-3911.

16) Bonacquisti, E.E. and Nguyen, J. (2019) 'Connexin 43 (Cx43) in cancer: Implications for therapeutic approaches via gap junctions', *Cancer Letters*, 442, pp. 439–444. Available at: https://doi.org/10.1016/j.canlet.2018.10.043.

17) Borella, F. *et al.* (2023) 'Hormone Receptors and Epithelial Ovarian Cancer: Recent Advances in Biology and Treatment Options', *Biomedicines*, 11(8), p. 2157. Available at: https://doi.org/10.3390/biomedicines11082157.

18) Castro, C.N. *et al.* (2020) '*NCKAP1L* defects lead to a novel syndrome combining immunodeficiency, lymphoproliferation, and hyperinflammation', *Journal of Experimental Medicine*, 217(12), p. e20192275. Available at: https://doi.org/10.1084/jem.20192275.

19) Chambers, L.M. *et al.* (2019) 'Evaluation of non-completion of intraperitoneal chemotherapy in patients with advanced epithelial ovarian cancer', *Journal of Gynecologic Oncology*, 30(6), p. e93. Available at: https://doi.org/10.3802/jgo.2019.30.e93.

20) Chandra, A. *et al.* (2019) 'Ovarian cancer: Current status and strategies for improving therapeutic outcomes', *Cancer Medicine*, 8(16), pp. 7018–7031. Available at: https://doi.org/10.1002/cam4.2560.

21) Chang, A.S., Dale, A.N. and Moley, K.H. (2005) 'Maternal Diabetes Adversely Affects Preovulatory Oocyte Maturation, Development, and Granulosa Cell Apoptosis', *Endocrinology*, 146(5), pp. 2445–2453. Available at: https://doi.org/10.1210/en.2004-1472.

22) Chen, Q. *et al.* (2016) ‘Carcinoma–astrocyte gap junctions promote brain metastasis by cGAMP transfer’, *Nature*, 533(7604), pp. 493–498. Available at: https://doi.org/10.1038/nature18268.

23) Chimen, M. *et al.* (2015) ‘Homeostatic regulation of T cell trafficking by a B cell–derived peptide is impaired in autoimmune and chronic inflammatory disease’, *Nature Medicine*, 21(5), pp. 467–475. Available at: https://doi.org/10.1038/nm.3842.

24) Conklin, C.M.J. *et al.* (2007) ‘Genistein and quercetin increase connexin43 and suppress growth of breast cancer cells’, *Carcinogenesis*, 28(1), pp. 93–100. Available at: https://doi.org/10.1093/carcin/bgl106.

25) Cordero, A.B. *et al.* (2010) ‘In vivo Imaging and Therapeutic Treatments in an Orthotopic Mouse Model of Ovarian Cancer’, *Journal of Visualized Experiments*, (42), p. 2125. Available at: https://doi.org/10.3791/2125.

26) Dai, P. *et al.* (2007) ‘Cx43 Mediates TGF-␣ Signalling through Competitive Smads Binding to Microtubules□D □V’, *Molecular Biology of the Cell*, 18.

27) De Blasio, A. *et al.* (2016) ‘Unusual roles of caspase-8 in triple-negative breast cancer cell line MDA-MB-231’, *International Journal of Oncology*, 48(6), pp. 2339–2348. Available at: https://doi.org/10.3892/ijo.2016.3474.

28) Defamie, N., Chepied, A. and Mesnil, M. (2014) ‘Connexins, gap junctions and tissue invasion’, *FEBS Letters*, 588(8), pp. 1331–1338. Available at: https://doi.org/10.1016/j.febslet.2014.01.012.

29) DeSantis, C.E. *et al.* (2019) ‘Cancer statistics for adults aged 85 years and older, 2019’, *CA: A Cancer Journal for Clinicians*, 69(6), pp. 452–467. Available at: https://doi.org/10.3322/caac.21577.

30) Domcke, S. *et al.* (2013) ‘Evaluating cell lines as tumour models by comparison of genomic profiles’, *Nature Communications*, 4(1), p. 2126. Available at: https://doi.org/10.1038/ncomms3126.

31) Elmore, S. (2007) ‘Apoptosis: A Review of Programmed Cell Death’, *Toxicologic Pathology*, 35(4), pp. 495–516. Available at: https://doi.org/10.1080/01926230701320337.

32) Elzarrad, M.K. *et al.* (2008) ‘Connexin-43 upregulation in micrometastases and tumor vasculature and its role in tumor cell attachment to pulmonary endothelium’, *BMC Medicine*, 6(1), p. 20. Available at: https://doi.org/10.1186/1741-7015-6-20.

33) Falzone, L. *et al.* (2021) ‘A multidisciplinary approach remains the best strategy to improve and strengthen the management of ovarian cancer (Review)’, *International Journal of Oncology*, 59(1), p. 53. Available at: https://doi.org/10.3892/ijo.2021.5233.

34) Fong, P.C. *et al.* (2009) 'Inhibition of Poly(ADP-Ribose) Polymerase in Tumors from *BRCA* Mutation Carriers', *New England Journal of Medicine*, 361(2), pp. 123–134. Available at: https://doi.org/10.1056/NEJMoa0900212.

35) Fukushima, M. *et al.* (2007) 'Combination of non-viral connexin 43 gene therapy and docetaxel inhibits the growth of human prostate cancer in mice', *International Journal of Oncology* [Preprint]. Available at: https://doi.org/10.3892/ijo.30.1.225.

36) Fulda, S. (2009) 'Caspase-8 in cancer biology and therapy', *Cancer Letters*, 281(2), pp. 128–133. Available at: https://doi.org/10.1016/j.canlet.2008.11.023.

37) Garrido, M.P. *et al.* (2021) 'Current Treatments and New Possible Complementary Therapies for Epithelial Ovarian Cancer', *Biomedicines*, 10(1), p. 77. Available at: https://doi.org/10.3390/biomedicines10010077.

38) Gasimli, K. *et al.* (2023) 'Synergistic Sensitization of High-Grade Serous Ovarian Cancer Cells Lacking Caspase-8 Expression to Chemotherapeutics Using Combinations of Small-Molecule BRD4 and CDK9 Inhibitors', *Cancers*, 16(1), p. 107. Available at: https://doi.org/10.3390/cancers16010107.

39) Gershon, E., Plaks, V. and Dekel, N. (2008) 'Gap junctions in the ovary: Expression, localization and function', *Molecular and Cellular Endocrinology*, 282(1–2), pp. 18–25. Available at: https://doi.org/10.1016/j.mce.2007.11.001.

40) Ghaffari, K. *et al.* (2021) 'NCK-associated protein 1 like (nckap1l) minor splice variant regulates intrahepatic biliary network morphogenesis', *PLOS Genetics*. Edited by M.C. Mullins, 17(3), p. e1009402. Available at: https://doi.org/10.1371/journal.pgen.1009402.

41) Goldar, S. *et al.* (2015) 'Molecular Mechanisms of Apoptosis and Roles in Cancer Development and Treatment', *Asian Pacific Journal of Cancer Prevention*, 16(6), pp. 2129–2144. Available at: https://doi.org/10.7314/APJCP.2015.16.6.2129.

42) González-Sánchez, A. *et al.* (2016) 'Connexin43 recruits PTEN and Csk to inhibit c-Src activity in glioma cells and astrocytes', *Oncotarget*, 7(31), pp. 49819–49833. Available at: https://doi.org/10.18632/oncotarget.10454.

43) Guo, J. *et al.* (2017) 'Establishment of two ovarian cancer orthotopic xenograft mouse models for in vivo imaging: A comparative study', *International Journal of Oncology*, 51(4), pp. 1199–1208. Available at: https://doi.org/10.3892/ijo.2017.4115.

44) Guo, S. *et al.* (2010) 'Vascular endothelial growth factor receptor-2 in breast cancer', *Biochimica et Biophysica Acta (BBA) - Reviews on Cancer*, 1806(1), pp. 108–121. Available at: https://doi.org/10.1016/j.bbcan.2010.04.004.

45) Häcker, G. (2000) 'The morphology of apoptosis', *Cell and Tissue Research*, 301(1), pp. 5–17. Available at: https://doi.org/10.1007/s004410000193.

46) Hagemann, T. *et al.* (2006) 'Ovarian Cancer Cells Polarize Macrophages Toward A Tumor-Associated Phenotype', *The Journal of Immunology*, 176(8), pp. 5023–5032. Available at: https://doi.org/10.4049/jimmunol.176.8.5023.

47) Halperin, R. *et al.* (2003) 'Luteinizing hormone in peritoneal and ovarian cyst fluids: a predictor of ovarian carcinoma', *European Journal of Obstetrics & Gynecology and Reproductive Biology*, 110(2), pp. 207–210. Available at: https://doi.org/10.1016/S0301-2115(03)00122-2.

48) Hernandez, L. *et al.* (2015) 'A dual role for Caspase8 and NF-κB interactions in regulating apoptosis and necroptosis of ovarian cancer, with correlation to patient survival', *Cell Death Discovery*, 1(1), p. 15053. Available at: https://doi.org/10.1038/cddiscovery.2015.53.

49) Hernandez, L. *et al.* (2016) 'Characterization of ovarian cancer cell lines as in vivo models for preclinical studies', *Gynecologic Oncology*, 142(2), pp. 332–340. Available at: https://doi.org/10.1016/j.ygyno.2016.05.028.

50) Hervé, J.-C. *et al.* (2007) 'Gap junctional complexes: From partners to functions', *Progress in Biophysics and Molecular Biology*, 94(1–2), pp. 29–65. Available at: https://doi.org/10.1016/j.pbiomolbio.2007.03.010.

51) Hicklin, D.J. and Ellis, L.M. (2005) 'Role of the Vascular Endothelial Growth Factor Pathway in Tumor Growth and Angiogenesis', *Journal of Clinical Oncology*, 23(5), pp. 1011–1027. Available at: https://doi.org/10.1200/JCO.2005.06.081.

52) Hong, B. *et al.* (2015) 'p38 MAPK inhibits breast cancer metastasis through regulation of stromal expansion: p38 signalling in breast cancer metastasis', *International Journal of Cancer*, 136(1), pp. 34–43. Available at: https://doi.org/10.1002/ijc.28958.

53) House, C.D., Hernandez, L. and Annunziata, C.M. (2014) 'Recent Technological Advances in Using Mouse Models to Study Ovarian Cancer', *Frontiers in Oncology*, 4. Available at: https://doi.org/10.3389/fonc.2014.00026.

54) Hua, R., Gu, S. and Jiang, J.X. (2022) 'Connexin 43 Hemichannels Regulate Osteoblast to Osteocyte Differentiation', *Frontiers in Cell and Developmental Biology*, 10, p. 892229. Available at: https://doi.org/10.3389/fcell.2022.892229.

55) Ince, T.A. *et al.* (2015) 'Characterization of twenty-five ovarian tumour cell lines that phenocopy primary tumours', *Nature Communications*, 6(1), p. 7419. Available at: https://doi.org/10.1038/ncomms8419.

56) Itamochi, H. (2010) 'Targeted therapies in epithelial ovarian cancer: Molecular mechanisms of action', *World Journal of Biological Chemistry*, 1(7), p. 209. Available at: https://doi.org/10.4331/wjbc.v1.i7.209.

57) Jaunky, D.B. *et al.* (2021) 'Characterization of a recently synthesized microtubule-targeting compound that disrupts mitotic spindle poles in human

cells', *Scientific Reports*, 11(1), p. 23665. Available at: https://doi.org/10.1038/s41598-021-03076-3.

58) Jeong, S.-Y. and Seol, D.-W. (no date) 'The role of mitochondria in apoptosis'.

59) Jin, Z. *et al.* (2013) 'miR-125b Inhibits Connexin43 and Promotes Glioma Growth', *Cellular and Molecular Neurobiology*, 33(8), pp. 1143–1148. Available at: https://doi.org/10.1007/s10571-013-9980-1.

60) Johnstone, S.R. *et al.* (2010) 'Enhanced connexin 43 expression delays intra-mitoitc duration and cell cycle traverse independently of gap junction channel function', *Journal of Cellular Biochemistry*, 110(3), pp. 772–782. Available at: https://doi.org/10.1002/jcb.22590.

61) Kameritsch, P. *et al.* (2013) 'Gap junctional communication promotes apoptosis in a connexin-type-dependent manner', *Cell Death & Disease*, 4(4), pp. e584–e584. Available at: https://doi.org/10.1038/cddis.2013.105.

62) Kampan, N.C. *et al.* (2015) 'Paclitaxel and Its Evolving Role in the Management of Ovarian Cancer', *BioMed Research International*, 2015, pp. 1–21. Available at: https://doi.org/10.1155/2015/413076.

63) Karakashev, S. *et al.* (2021) 'Mouse models of epithelial ovarian cancer for preclinical studies', *Zoological Research*, 42(2), pp. 153–160. Available at: https://doi.org/10.24272/j.issn.2095-8137.2020.382.

64) Kerbel, R.S. (2008) 'Tumor Angiogenesis', *New England Journal of Medicine*, 358(19), pp. 2039–2049. Available at: https://doi.org/10.1056/NEJMra0706596.

65) Khalil, A.A. *et al.* (2013) 'Subcutaneous Administration of D-Luciferin is an Effective Alternative to Intraperitoneal Injection in Bioluminescence Imaging of Xenograft Tumors in Nude Mice', *ISRN Molecular Imaging*, 2013, pp. 1–7. Available at: https://doi.org/10.1155/2013/689279.

66) Kim, A. *et al.* (2012) 'Therapeutic strategies in epithelial ovarian cancer', *Journal of Experimental & Clinical Cancer Research*, 31(1), p. 14. Available at: https://doi.org/10.1186/1756-9966-31-14.

67) Kordowitzki, P. *et al.* (2021) 'Pannexins and Connexins: Their Relevance for Oocyte Developmental Competence', *International Journal of Molecular Sciences*, 22(11), p. 5918. Available at: https://doi.org/10.3390/ijms22115918.

68) Kostova, I. *et al.* (2021a) 'The role of caspase-8 in the tumor microenvironment of ovarian cancer', *Cancer and Metastasis Reviews*, 40(1), pp. 303–318. Available at: https://doi.org/10.1007/s10555-020-09935-1.

69) Kostova, I. *et al.* (2021b) 'The role of caspase-8 in the tumor microenvironment of ovarian cancer', *Cancer and Metastasis Reviews*, 40(1), pp. 303–318. Available at: https://doi.org/10.1007/s10555-020-09935-1.

70) Kotini, M. and Mayor, R. (2015) ‘Connexins in migration during development and cancer’, *Developmental Biology*, 401(1), pp. 143–151. Available at: https://doi.org/10.1016/j.ydbio.2014.12.023.

71) Kurokawa, M. and Kornbluth, S. (2009) ‘Caspases and Kinases in a Death Grip’, *Cell*, 138(5), pp. 838–854. Available at: https://doi.org/10.1016/j.cell.2009.08.021.

72) Kutova, O.M., Pospelov, A.D. and Balalaeva, I.V. (2023) ‘The Multifaceted Role of Connexins in Tumor Microenvironment Initiation and Maintenance’, *Biology*, 12(2), p. 204. Available at: https://doi.org/10.3390/biology12020204.

73) Ledermann, J.A. (2018) ‘First-line treatment of ovarian cancer: questions and controversies to address’, *Therapeutic Advances in Medical Oncology*, 10, p. 175883591876823. Available at: https://doi.org/10.1177/1758835918768232.

74) Li, H. *et al.* (2020) ‘Systematic analysis of ovarian cancer platinum-resistance mechanisms via text mining’, *Journal of Ovarian Research*, 13(1), p. 27. Available at: https://doi.org/10.1186/s13048-020-00627-6.

75) Li, H. *et al.* (2021) ‘Hormone therapy for ovarian cancer: Emphasis on mechanisms and applications (Review)’, *Oncology Reports*, 46(4), p. 223. Available at: https://doi.org/10.3892/or.2021.8174.

76) Li, Z., Zhou, Z. and Donahue, H.J. (2008) ‘Alterations in Cx43 and OB-cadherin affect breast cancer cell metastatic potential’, *Clinical & Experimental Metastasis*, 25(3), pp. 265–272. Available at: https://doi.org/10.1007/s10585-007-9140-4.

77) Lin, J.H.-C. *et al.* (2003) ‘Connexin Mediates Gap Junction-Independent Resistance to Cellular Injury’, *The Journal of Neuroscience*, 23(2), pp. 430–441. Available at: https://doi.org/10.1523/JNEUROSCI.23-02-00430.2003.

78) Liu, W. *et al.* (2023) ‘The Role of Paxillin Aberrant Expression in Cancer and Its Potential as a Target for Cancer Therapy’, *International Journal of Molecular Sciences*, 24(9), p. 8245. Available at: https://doi.org/10.3390/ijms24098245.

79) Longoria, T.C. and Eskander, R.N. (2015) ‘Immunotherapy in endometrial cancer - an evolving therapeutic paradigm’, *Gynecologic Oncology Research and Practice*, 2(1), p. 11. Available at: https://doi.org/10.1186/s40661-015-0020-3.

80) Magnotti, E. and Marasco, W.A. (2018) ‘The latest animal models of ovarian cancer for novel drug discovery’, *Expert Opinion on Drug Discovery*, 13(3), pp. 249–257. Available at: https://doi.org/10.1080/17460441.2018.1426567.

81) Mandal, R. *et al.* (2020) ‘Caspase-8: The double-edged sword’, *Biochimica et Biophysica Acta (BBA) - Reviews on Cancer*, 1873(2), p. 188357. Available at: https://doi.org/10.1016/j.bbcan.2020.188357.

82) Mandal, R. *et al.* (2022a) ‘The non-apoptotic function of Caspase-8 in negatively regulating the CDK9-mediated Ser2 phosphorylation of RNA polymerase II in cervical cancer’, *Cellular and Molecular Life Sciences*, 79(12), p. 597. Available at: https://doi.org/10.1007/s00018-022-04598-3.

83) Mandal, R. *et al.* (2022b) ‘The non-apoptotic function of Caspase-8 in negatively regulating the CDK9-mediated Ser2 phosphorylation of RNA polymerase II in cervical cancer’, *Cellular and Molecular Life Sciences*, 79(12), p. 597. Available at: https://doi.org/10.1007/s00018-022-04598-3.

84) McCabe, A. *et al.* (2023) ‘Investigating the suitability of in vitro cell lines as models for the major subtypes of epithelial ovarian cancer’, *Frontiers in Cell and Developmental Biology*, 11, p. 1104514. Available at: https://doi.org/10.3389/fcell.2023.1104514.

85) McLachlan, E. *et al.* (2006) ‘Connexins Act as Tumor Suppressors in Three-dimensional Mammary Cell Organoids by Regulating Differentiation and Angiogenesis’, *Cancer Research*, 66(20), pp. 9886–9894. Available at: https://doi.org/10.1158/0008-5472.CAN-05-4302.

86) Mizdrak, M. *et al.* (2024) ‘The Role of the Gap Junction Protein Connexin in Adrenal Gland Tumorigenesis’, *International Journal of Molecular Sciences*, 25(10), p. 5399. Available at: https://doi.org/10.3390/ijms25105399.

87) Murphy, S.F. *et al.* (2016) ‘Connexin 43 Inhibition Sensitizes Chemoresistant Glioblastoma Cells to Temozolomide’, *Cancer Research*, 76(1), pp. 139–149. Available at: https://doi.org/10.1158/0008-5472.CAN-15-1286.

88) Muzio, M. *et al.* (1998) ‘An Induced Proximity Model for Caspase-8 Activation’, *Journal of Biological Chemistry*, 273(5), pp. 2926–2930. Available at: https://doi.org/10.1074/jbc.273.5.2926.

89) Naus, C.C. and Laird, D.W. (2010) ‘Implications and challenges of connexin connections to cancer’, *Nature Reviews Cancer*, 10(6), pp. 435–441. Available at: https://doi.org/10.1038/nrc2841.

90) Nayal, A. *et al.* (2006) ‘Paxillin phosphorylation at Ser273 localizes a GIT1–PIX–PAK complex and regulates adhesion and protrusion dynamics’, *The Journal of Cell Biology*, 173(4), pp. 587–589. Available at: https://doi.org/10.1083/jcb.200509075.

91) Nishiya, N. *et al.* (2005) ‘An α4 integrin–paxillin–Arf-GAP complex restricts Rac activation to the leading edge of migrating cells’, *Nature Cell Biology*, 7(4), pp. 343–352. Available at: https://doi.org/10.1038/ncb1234.

92) Ocana, A. *et al.* (2011) ‘Preclinical development of molecular-targeted agents for cancer’, *Nature Reviews Clinical Oncology*, 8(4), pp. 200–209. Available at: https://doi.org/10.1038/nrclinonc.2010.194.

93) Odero-Marah, V. *et al.* (2018) ‘Epithelial-Mesenchymal Transition (EMT) and Prostate Cancer’, in H. Schatten (ed.) *Cell & Molecular Biology of Prostate*

Cancer. Cham: Springer International Publishing (Advances in Experimental Medicine and Biology), pp. 101–110. Available at: https://doi.org/10.1007/978-3-319-95693-0_6.

94) Oronsky, B. *et al.* (2017) 'A brief review of the management of platinum-resistant–platinum-refractory ovarian cancer', *Medical Oncology*, 34(6), p. 103. Available at: https://doi.org/10.1007/s12032-017-0960-z.

95) Palaia, I. *et al.* (2020) 'Immunotherapy For Ovarian Cancer: Recent Advances And Combination Therapeutic Approaches', *OncoTargets and Therapy*, Volume 13, pp. 6109–6129. Available at: https://doi.org/10.2147/OTT.S205950.

96) Peña-Blanco, A. and García-Sáez, A.J. (2018) 'Bax, Bak and beyond — mitochondrial performance in apoptosis', *The FEBS Journal*, 285(3), pp. 416–431. Available at: https://doi.org/10.1111/febs.14186.

97) Peter, M.E. and Krammer, P.H. (2003) 'The CD95(APO-1/Fas) DISC and beyond', *Cell Death & Differentiation*, 10(1), pp. 26–35. Available at: https://doi.org/10.1038/sj.cdd.4401186.

98) Pokhriyal, R. *et al.* (2019) 'Chemotherapy Resistance in Advanced Ovarian Cancer Patients', *Biomarkers in Cancer*, 11, p. 1179299X1986081. Available at: https://doi.org/10.1177/1179299X19860815.

99) Pollmann, M.-A. *et al.* (2005) 'Connexin 43 mediated gap junctional communication enhances breast tumor cell diapedesis in culture', *Breast Cancer Research*, 7(4), p. R522. Available at: https://doi.org/10.1186/bcr1042.

100) Rämer, P.C. *et al.* (2011) 'Mice with human immune system components as *in vivo* models for infections with human pathogens', *Immunology & Cell Biology*, 89(3), pp. 408–416. Available at: https://doi.org/10.1038/icb.2010.151.

101) Ran, F.A. *et al.* (2013) 'Genome engineering using the CRISPR-Cas9 system', *Nature Protocols*, 8(11), pp. 2281–2308. Available at: https://doi.org/10.1038/nprot.2013.143.

102) Raspollini, M.R. *et al.* (2005) 'Correlation of Epidermal Growth Factor Receptor Expression with Tumor Microdensity Vessels and with Vascular Endothelial Growth Factor Expression in Ovarian Carcinoma', *International Journal of Surgical Pathology*, 13(2), pp. 135–142. Available at: https://doi.org/10.1177/106689690501300202.

103) Rodríguez-Sinovas, A. *et al.* (2021) 'Connexins in the Heart: Regulation, Function and Involvement in Cardiac Disease', *International Journal of Molecular Sciences*, 22(9), p. 4413. Available at: https://doi.org/10.3390/ijms22094413.

104) Sáez, J.C. and Leybaert, L. (2014) 'Hunting for connexin hemichannels', *FEBS Letters*, 588(8), pp. 1205–1211. Available at: https://doi.org/10.1016/j.febslet.2014.03.004.

105) Shao, Q. *et al.* (2005) 'Down-regulation of Cx43 by Retroviral Delivery of Small Interfering RNA Promotes an Aggressive Breast Cancer Cell Phenotype', *Cancer Research*, 65(7), pp. 2705–2711. Available at: https://doi.org/10.1158/0008-5472.CAN-04-2367.

106) Sharma, M. *et al.* (2023) 'Connexin 43 mediated collective cell migration is independent of Golgi orientation', *Biology Open*, 12(10), p. bio060006. Available at: https://doi.org/10.1242/bio.060006.

107) Shultz, L.D. *et al.* (2005) 'Human Lymphoid and Myeloid Cell Development in NOD/LtSz- *scid IL2R* γ *null* Mice Engrafted with Mobilized Human Hemopoietic Stem Cells', *The Journal of Immunology*, 174(10), pp. 6477–6489. Available at: https://doi.org/10.4049/jimmunol.174.10.6477.

108) Siminiak, N. *et al.* (2022) 'Immunotherapy in Ovarian Cancer', *Archivum Immunologiae et Therapiae Experimentalis*, 70(1), p. 19. Available at: https://doi.org/10.1007/s00005-022-00655-8.

109) Sirnes, S. *et al.* (2011) 'DNA methylation analyses of the connexin gene family reveal silencing of *GJC1* (Connexin45) by promoter hypermethylation in colorectal cancer', *Epigenetics*, 6(5), pp. 602–609. Available at: https://doi.org/10.4161/epi.6.5.15237.

110) Soung, Y.H. *et al.* (2005) '*CASPASE-8* Gene Is Inactivated by Somatic Mutations in Gastric Carcinomas', *Cancer Research*, 65(3), pp. 815–821. Available at: https://doi.org/10.1158/0008-5472.815.65.3.

111) Stoletov, K. *et al.* (2013) 'Role of connexins in metastatic breast cancer and melanoma brain colonization', *Journal of Cell Science*, p. jcs.112748. Available at: https://doi.org/10.1242/jcs.112748.

112) Sun, Y. *et al.* (2012) 'Connexin 43 interacts with Bax to regulate apoptosis of pancreatic cancer through a gap junction-independent pathway', *International Journal of Oncology*, 41(3), pp. 941–948. Available at: https://doi.org/10.3892/ijo.2012.1524.

113) Telloni, S.M. (2017) 'Tumor Staging and Grading: A Primer', in V. Espina (ed.) *Molecular Profiling: Methods and Protocols*. New York, NY: Springer New York, pp. 1–17. Available at: https://doi.org/10.1007/978-1-4939-6990-6_1.

114) Tseng, J.-C., Vasquez, K. and Peterson, J.D. (no date) 'Optical Imaging on the IVIS SpectrumCT System: General and Technical Considerations for 2D and 3D Imaging'.

115) Varfolomeev, E.E. *et al.* (1998) 'Targeted Disruption of the Mouse Caspase 8 Gene Ablates Cell Death Induction by the TNF Receptors, Fas/Apo1, and DR3 and Is Lethal Prenatally', *Immunity*, 9(2), pp. 267–276. Available at: https://doi.org/10.1016/S1074-7613(00)80609-3.

116) Walker, M., Jacobson, M. and Sobel, M. (2019) 'Management of ovarian cancer risk in women with *BRCA1/2* pathogenic variants', *Canadian Medical*

Association Journal, 191(32), pp. E886–E893. Available at: https://doi.org/10.1503/cmaj.190281.

117) Wang, C.-W. *et al.* (2022) 'Histopathological whole slide image dataset for classification of treatment effectiveness to ovarian cancer', *Scientific Data*, 9(1), p. 25. Available at: https://doi.org/10.1038/s41597-022-01127-6.

118) Wang, D. and Lippard, S.J. (2005) 'Cellular processing of platinum anticancer drugs', *Nature Reviews Drug Discovery*, 4(4), pp. 307–320. Available at: https://doi.org/10.1038/nrd1691.

119) Yang, C. *et al.* (2020) 'Immunotherapy for Ovarian Cancer: Adjuvant, Combination, and Neoadjuvant', *Frontiers in Immunology*, 11, p. 577869. Available at: https://doi.org/10.3389/fimmu.2020.577869.

120) Yang, Y. *et al.* (2021) 'Transforming growth factor-β1-induced N-cadherin drives cell–cell communication through connexin43 in osteoblast lineage', *International Journal of Oral Science*, 13(1), p. 15. Available at: https://doi.org/10.1038/s41368-021-00119-3.

121) Yu, M. *et al.* (2014) 'Cx43 reverses the resistance of A549 lung adenocarcinoma cells to cisplatin by inhibiting EMT', *Oncology Reports*, 31(6), pp. 2751–2758. Available at: https://doi.org/10.3892/or.2014.3163.

122) Zhang, Y.-W. *et al.* (2001) 'Connexin43 suppresses proliferation of osteosarcoma U2OS cells through post-transcriptional regulation of p27', *Oncogene*, 20(31), pp. 4138–4149. Available at: https://doi.org/10.1038/sj.onc.1204563.

123) Zhou, M. *et al.* (2023) 'The roles of connexins and gap junctions in the progression of cancer', *Cell Communication and Signalling*, 21(1), p. 8. Available at: https://doi.org/10.1186/s12964-022-01009-9.

Acknowledgements

First and foremost, I would like to express my deepest gratitude to my supervisor, PD Dr. habil. Mourad Sanhaji, for providing me with the invaluable opportunity to pursue my doctoral research in his laboratory. Throughout my PhD studies, his unwavering support, insightful scientific guidance, and continuous encouragement were instrumental in shaping this thesis. Without his mentorship, this research project could not have been successfully completed.

My sincere thanks extend to my former supervisor, Prof. Dr. Monika Kressin, for her constructive criticism, encouragement, and fresh perspectives, which substantially enhanced the quality of my work. Her complementary expertise was invaluable, particularly in addressing the interdisciplinary aspects of this research and my teaching activities.

I would also like to thank Prof. Dr. Daniela Fietz for her supervision and encouragement throughout my doctoral journey. Her role in establishing and supporting my PhD pathway was essential, and I am grateful for her continuous support. Her contributions significantly improved the scientific quality and depth of my doctoral project.

I am deeply indebted to Prof. Dr. Christine Wrenzycki for her invaluable guidance and assistance during my PhD studies. As a first supervisor in my last year of PhD , her constructive feedback and academic support were crucial in improving this thesis and enabling its successful completion.

I am also sincerely grateful to Prof. Dr. Klaus Strebhardt for giving me the opportunity to initiate my doctoral work in his former laboratory. I greatly appreciate his trust, support, and the stimulating scientific discussions that contributed significantly to my academic development.

Furthermore, I would like to express my sincere appreciation to my co-supervisor, Prof. Dr. Rajkumar Savai, for his highly productive guidance, insightful advice, and scientific input throughout my PhD journey.

I am particularly grateful to Ms. Andrea Krämer for her excellent technical assistance, enlightening discussions, and continuous guidance. Her willingness to share her expertise and provide constructive feedback made this work both intellectually enriching and enjoyable.

I would also like to thank my colleagues from AG Sanhaji, especially Monika, Elisabeth, Samira, Ranadip and Izabela for their practical and technical support throughout my doctoral studies. I further extend my gratitude to the scientific members of Prof. Dr. Juping Yuan's research group (Nina, Andreas, Alexandra, Badi and Babek) at the University Hospital Frankfurt for their support and collaboration.
My sincere thanks also go to AG Fietz/Kressin team (Rashidul, Shashika , Katja, Alexandra, Sigrid) and my friend Mohammad Amin for their support and assistance during my scientific journey.
I am grateful to the Giessen Graduate Centre for the Life Sciences (GGL), particularly Dr. Lorna Lück and Ms. Faiqa Hossain, as well as to the PhD Office of the Faculties of Veterinary Medicine and Medicine, especially Ms. Pia Jürgens, for their invaluable administrative and academic support throughout my doctoral studies.
Finally, I would like to express my deepest gratitude to my mother for her unwavering encouragement, sacrifices, and belief in my abilities. Her constant support and patience gave me the strength to persevere through challenges. Although my father is no longer physically present, his encouragement, values, and belief in the pursuit of knowledge continue to guide me. While he did not live to see the completion of this work, every page of this thesis carries his influence and the lessons he instilled in me about dedication, resilience, and the relentless pursuit of one's dreams.